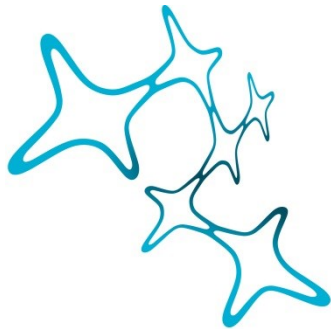


---

# TARGETING MÜLLER CELLS IN DIABETIC RETINOPATHY

---

Anna Monika Pfaller



**Graduate School of  
Systemic Neurosciences**

**LMU Munich**



Dissertation at the  
Graduate School of Systemic Neurosciences  
Ludwig-Maximilians-Universität München

February, 2021

Supervisor  
Prof. Dr. Antje Grosche  
Department of Physiological Genomics  
Ludwig-Maximilians-Universität München

First Reviewer: Prof. Dr. Antje Grosche  
Second Reviewer: Dr. Stefanie Hauck  
External Reviewer: Prof. Dr. Astrid Limb

Date of Submission: 25.02.2021  
Date of Defense : 02.07.2021

**CONTENT**

1. ABSTRACT .....	6
2. INTRODUCTION .....	7
2.1. Retinal structure and cell types .....	7
2.2. The development of diabetic retinopathy .....	8
2.3. The role of Müller cells in diabetic retinopathy .....	10
2.4. Available therapy options for diabetic retinopathy .....	11
2.5. Gene therapeutical approaches .....	13
2.6. The retinal glucocorticoid receptor .....	15
2.7. Animal model: db/db mice .....	16
3. OBJECTIVES .....	18
4. MATERIAL .....	19
4.1. Mice .....	19
4.2. Oligonucleotides .....	19
4.3. Adeno-associated virus .....	20
4.4. Enzymes and proteins .....	20
4.5. Antibodies .....	20
4.6. Probes .....	21
4.7. Chemicals .....	22
4.8. Commercial kits .....	23
4.9. Consumables .....	23
4.10. Buffers and solutions .....	25
4.11. Instruments .....	26
4.12. Software .....	27
5. METHODS .....	28
5.1. DNA extraction .....	28
5.2. Genotyping db/db mice .....	28
5.3. Agarose gel electrophoresis .....	29
5.4. Magnetic activated cell sorting .....	29
5.5. RNA isolation .....	30
5.6. Reverse transcription .....	31
5.7. Probe-based quantitative polymerase chain reaction .....	31
5.8. Immunohistochemistry .....	32
5.8.1. Immunohistochemistry of retinal sections .....	32

5.8.2. Immunohistochemistry of flatmounts .....	33
5.8.3. Immunohistochemistry of clutivated flatmounts .....	33
5.8.4. Quantification of the morphological state .....	34
5.9. Trypsin digest .....	34
5.10. Analysis of vasculature .....	34
5.11. Western blot .....	35
5.12. RNA sequencing.....	36
5.13. Proteomics .....	36
5.14. Comparison of the two OMICS data sets .....	37
5.15. Electroretinogram .....	37
5.16. Measurement corticosterone level .....	38
5.17. Cultivation of retinal explants .....	38
5.18. Adeno-associated virus administration.....	38
5.19. Statistical analysis .....	39
6. RESULTS.....	40
6.1. Characterisation of the animal model.....	40
6.1.1. Unaltered cell numbers of the different retinal layers in diabetic mice .....	40
6.1.2. Unaltered numbers of calretinin-positive cells in diabetic mice.....	41
6.1.3. Onset of cone degeneration in aging diabetic mice .....	42
6.1.4. Defects of the vascular system in db/db mice .....	43
6.1.4.1. Pericyte loss in diabetic mice .....	44
6.1.4.1.1. Vascular hallmarks of diabetic retinopathy in aging diabetic mice .....	44
6.1.5. Onset of microglial activation in diabetic mice .....	46
6.1.6. Reduced light responsiveness of retinae from db/db mice .....	47
6.2. The transcriptome of 12- and 24-week-old diabetic mice .....	49
6.3. The proteome of diabetic mice with an age of 24 weeks .....	51
6.4. Comparison of the two OMICS data sets .....	53
6.5. Search for key regulators of diabetic retinopathy progression.....	54
6.6. The role of the glucocorticoid receptor in DR progression.....	56
6.6.1. Müller cell-specific downregulation of the glucocorticoid receptor target genes in diabetic animals.....	56
6.6.2. Müller cell-specific downregulation of the glucocorticoid receptor in diabetic animals .....	57
6.6.3. Elevated corticosterone level in diabetic mice .....	58
6.6.4. Modulation of the retinal glucocorticoid receptor <i>in vitro</i> .....	59

6.6.4.1. Activation of the retinal glucocorticoid receptor via cortisol treatment <i>in vitro</i> ....	59
6.6.4.2. Effect of the glucocorticoid receptor activation via cortisol treatment <i>in vitro</i> .....	60
6.6.4.3. Long term effect of the glucocorticoid receptor activation via cortisol treatment <i>in vitro</i> .....	63
6.7. Gene therapeutic intervention via Müller cell-specific glucocorticoid receptor overexpression in mice .....	64
6.7.1. Successful adeno-associated virus-induced glucocorticoid receptor overexpression in Müller cells <i>in vivo</i> .....	64
6.7.2. Comparison of different injection systems.....	66
7. DISCUSSION .....	68
7.1. Onset of changes in the retinal morphology of diabetic mice .....	68
7.2. The electroretinogram: a sensitive and suitable readout system.....	70
7.3. Differences on transcript and protein level in diabetic mice.....	70
7.4. Search for a master regulator of the Müller cell phenotype in diabetic retinopathy progression.....	73
7.5. Possible role of the glucocorticoid receptor in diabetic retinopathy progression .....	75
7.6. Modulation of glucocorticoid receptor activity <i>in vitro</i> .....	76
7.7. Modulation of glucocorticoid receptor activity <i>in vivo</i> .....	79
8. CONCLUSION.....	81
9. LIST OF TABLES .....	83
10. LIST OF FIGURES .....	84
11. ABBREVIATIONS.....	85
12. REFERENCES .....	90
13. ACKNOWLEDGEMENTS .....	100
14. PUBLICATION LIST .....	101
15. EIDESSTATTLICHE VERSICHERUNG/ AFFIDAVIT .....	102
16. DECLARATION OF AUTHORS CONTRIBUTION .....	103

## 1. ABSTRACT

Diabetic retinopathy (DR), the leading cause of blindness among working aged adults, is a micro-vascular complication affecting diabetes patients. Müller cells, the major retinal macroglia, are important in maintaining a healthy and functional retina and play a crucial role in various pathological events during DR disease progression. Here, I seek to improve our understanding of Müller cell-specific signaling pathways altered in the course of the disease with the ultimate goal to develop novel gene therapeutic strategies targeting Müller cells in DR.

First, I characterized the retinal phenotype of diabetic mice and showed that db/db mice with an age of 24 and 38 weeks are still in an early DR stage presenting with mild symptoms including the onset of pericyte loss and first signs of microglia activation. Furthermore, I demonstrated that the electroretinogram (ERG) can be used as a highly sensitive readout system, because it shows functional changes clearly before major morphological changes of retinal architecture becomes detectable and is independent from the sex of the mice.

Aiming to identify key regulators that drive Müller cell changes in DR progression, oPOSSUM-3 transcription factor (TF) binding site cluster analysis was performed based on RNA sequencing (seq) expression data, implementing the list of genes specifically regulated in Müller cells of 24-week-old diabetic mice.

I identified the glucocorticoid receptor (GR, gene ID: *Nr3c1*) whose target gene cluster was down-regulated in Müller cells of diabetic animals as most promising candidate. *Nr3c1* transcript was highest expressed in Müller cells and significantly reduced in 24-week-old db/db mice. Importantly, the GR was mainly located in Müller cell nuclei of diabetic and control mice. In addition, I confirmed an elevated blood plasma level of corticosterone, the endogenous ligand of the murine GR, in 24-week-old db/db mice. Although synthetic glucocorticoids are commonly used for therapeutic approaches in ophthalmology with undebatable beneficial effects, the molecular processes of GR signaling and its role in DR progression are largely unknown. Therefore, I investigated the effect of GR modulation in an *in vitro* retinal explant model implementing cortisol stimulation. Constantly high cortisol levels not only influenced the GR phosphorylation level and activity, but also induced expression changes of known downstream GR target genes.

To investigate the effects of a long-term restoration of GR activity in Müller cells of diabetic mice, I set out to develop a gene therapeutic approach in db/db mice. AAV9-Nr3c1-eGFP particles were intravitreally injected into the eyes of 12-week-old mice and the eyes were collected 12 weeks thereafter. I demonstrated a successful glia-specific transduction of the construct and found an optimal injection method in the World Precision Instruments (WPI) system. Due to time constraints, the long-term effect of the GR overexpression in diabetic and control mice is not a part of this thesis and has to be investigated in the future.

## 2. INTRODUCTION

### 2.1. RETINAL STRUCTURE AND CELL TYPES

The vertebrate retina developed in ancestral marine chordates around 500 million years ago. Eyes adapted to the different living areas and ensured that the important visual information from the environment are processed and could be used to increase survivability (Baden et al. 2020). An important part of the eye is the retina which turns light into neuronal signals. Rods and cones, the photoreceptors, capture light and their sensory signals are processed by the brain (Rodieck 1998). Vision loss or impairment is mainly caused by obstruction of the light pathway to the retina or by the inability of the retina to detect, process or transmit sensory signals to the brain. Vision loss in retinal degenerative diseases is mainly due to photoreceptor cells dysfunction or death (Veleri et al. 2015). The different layers and cell types are schematically shown in **Figure 1**. The retina is subdivided into different layers: nerve fiber layer (NFL), ganglion cell layer (GCL), inner plexiform layer (IPL), inner nuclear layer (INL), outer plexiform layer (OPL) and the outer nuclear layer (ONL). It consists of six neuronal cell classes: rods and cones (P), horizontal (HC), bipolar (B), amacrine (AC) and ganglion cells (G) and three types of glial cells (microglia (MG), Müller cells (M) and astrocytes (A)) (Behar-Cohen et al. 2020) (**Figure1**).

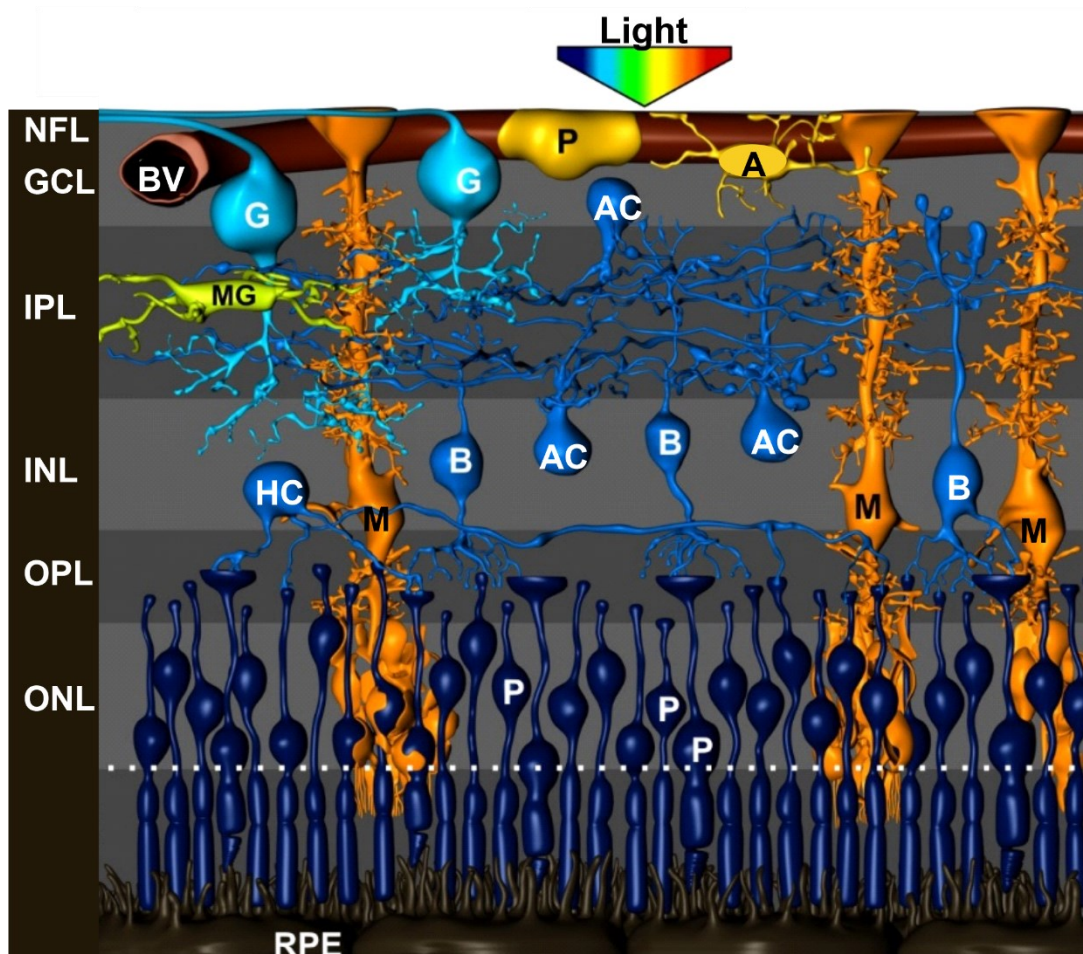


**Figure 1. The cellular architecture of the retina.** The retina can be subdivided in different layers: NFL: Nerve fiber layer, GCL: Ganglion cell layer, IPL: Inner plexiform layer, INL: Inner nuclear layer, OPL: Outer plexiform layer, ONL: Outer nuclear layer. The different retinal cell types are localized in different layers. Astrocytes (A, yellow) and ganglion cells (G, turquoise) are mainly located in the GCL. The somata of Müller cells (M, orange) are located in the INL. Microglia (MG, green) are primarily found in the IPL. The cell bodies of horizontal cells (HC, blue), bipolar cells (B, blue) and amacrine cells (AC, blue) are primarily located in the INL. The somata of cones and rods, the photoreceptors (P, dark blue), in the ONL. A blood vessel (BV, red) and pericyte (P, yellow) are schematically shown. RPE: Retinal pigment epithelium. Original figure by Dr. Jens Grosche.

Furthermore, three layers of retinal vessels (superficial capillary plexus, intermediate capillary plexus and deep capillary plexus) are pervading the retina (Picard et al. 2020). A blood vessel (BV) of the superficial capillary plexus and a pericyte (P), which is sitting on the capillary wall is schematically shown in **Figure 1**.

In the past, most of the studies about vision were performed with humans, primates and cats. However, researchers started to carry out their studies on rodents (e.g. mice and rats) over the last decades (Huberman and Niell 2011). Since a mouse model was used in this study, the similarities and differences of the human and mouse retina are shortly described. In primates and humans, central vision is ensured by the macula, which is a small, specialized area of the retina. The macula contains the fovea, which is the central region of the human retina, responsible for high resolution and a cone-only region with no rods. The mouse retina does not have a distinct fovea or macula. In total, the human retina comprises 120 million rods (95.2%) and 6 million cones (4.8%) (Veleri et al. 2015). In the mouse retina however, the total number of cones is 180,000 and of rods is ~ 6.4 million. Therefore, rods are 97.2% and cones are 2.8% of all the photoreceptors in mice (Jeon et al. 1998). Furthermore, the total retinal thickness of C57BL/6 mice is 204.41  $\mu\text{m}$ . In comparison, the foveal thickness is 212  $\mu\text{m}$  and the central retinal thickness (fovea centralis) is 182  $\mu\text{m}$  in humans (Chan et al. 2006). More anatomical differences could be mentioned. For example, the lens is much larger in mice compared to humans relative to the eye size (Veleri et al. 2015). Although the mouse retina is different from the human retina and mice have relatively poor visual acuity, mice have the greatest variety and sophistication of tools available to label, monitor, and manipulate specific cell types and circuits (Huberman and Niell 2011). In this thesis, I investigated the role of Müller cells, the major macroglia of the retina, in neurodegenerative diseases like DR in a mouse model.

## 2.2. THE DEVELOPMENT OF DIABETIC RETINOPATHY

DR is a common microvascular complication of diabetes and remains the leading cause of blindness in people of working age. About one third of the 246 million people with diabetes have signs of DR, and one third of these may have severe retinopathy or macular oedema (Cheung et al. 2010). Furthermore, DR is associated with an increased risk of life-threatening systemic vascular

complications such as stroke, coronary artery disease and heart failure (Cheung and Wong 2008). DR is classified into non-proliferative diabetic retinopathy (NPDR) and proliferative diabetic retinopathy (PDR). The pathology of DR depends on the respective disease stage, the type and duration of the underlying type of diabetes, blood glucose level and blood pressure (Tarr et al. 2013). Therefore, optimal control of blood glucose, blood pressure, and blood lipids remain the basis for reducing the risk of disease development and progression (Cheung et al. 2010). DR is mostly diagnosed by the detection of microaneurysms as the early symptoms. The screening process is performed in person by ophthalmologists and trained individuals who can determine the degree of disease by appropriate visual inspection of fundus photographs (Joseph et al. 2020). NPDR, which is the early stage of DR, is defined by increased vascular permeability and capillary occlusions in the retinal vasculature. Furthermore, retinal pathologies such as microaneurysms, haemorrhages, cotton wool spots and exudates may occur, even while patients are asymptomatic. PDR is the advanced stage of DR and is characterized by neovascularization, the growth of new abnormal vessels. At this stage, patients may experience severe visual impairment if the new abnormal vessels bleed into the eye and the vitreous (vitreous haemorrhage) (Wang and Lo 2018). Diabetic macular oedema (DME), which can occur at any stage of DR, is the most common reason of vision loss in DR. A breakdown of the blood-retinal barrier (BRB) is taking place, which results in intra-retinal fluid accumulation and a swelling of the macula (Wang and Lo 2018). The differences between a healthy and a DR affected retina are shown in **Figure 2**.

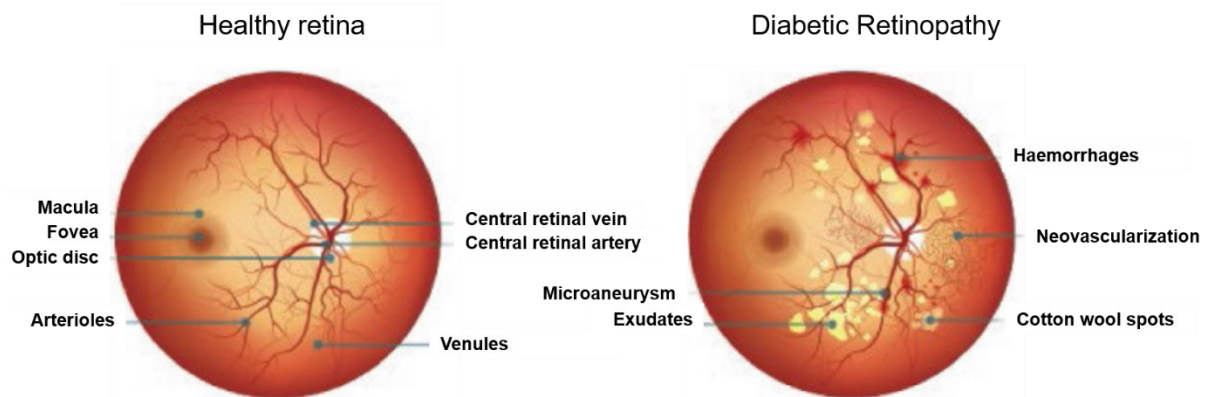


**Figure 2: Differences of a healthy retina and a diabetic retinopathy affected retina.** The retinal pathologies of non-proliferative diabetic retinopathy are microaneurysms, haemorrhages, cotton wool spots and exudates. During proliferative diabetic retinopathy, the patients often suffer from severe vision impairment, which occurs when the new abnormal vessels (neovascularization) bleed into the vitreous, or retinal detachment. The Figure was adopted from Joseph et al. 2020.

Knowledge of the pathophysiologic mechanisms underlying the development of DR continues to improve with new research findings. Several biochemical mechanisms influence the pathogenesis of DR through effects on cellular metabolism, signal transduction, and growth factors. It is known

that pathways involved in the accumulation of sorbitol and advanced glycation end-products, oxidative stress, protein kinase C activation, inflammation, and the regulation of the renin-angiotensin system and the vascular endothelial growth factor (VEGF) are altered in DR (Cheung et al. 2010).

Despite the fact that cellular processes during the development of DR have already been clarified, the interplay of the different cell types of the retina and the exact timing of these interactions have not yet been determined. By understanding how diabetes affects the whole retina, new treatments with neuroprotective potential could be developed.

### 2.3. THE ROLE OF MÜLLER CELLS IN DIABETIC RETINOPATHY

To understand the important role of Müller cells in DR, the unique properties and functions of Müller cells are described. Müller cells are in contact with virtually every cell type as well as blood vessels, vitreous, and subretinal space, since they span the whole thickness of the retina. This unique morphology and location are the reasons that Müller cells perform a wide range of tasks to support correct retinal function. They play a central role in the maintenance of ion- and volume homeostasis by mediating the transport of ions, water and various molecules. Müller cells may also be involved in controlling vascularization and maintaining the BRB (Bringmann et al. 2006). Furthermore, Müller cells have neuroprotective properties via the release of neurotrophic factors, the uptake and degradation of glutamate, and the secretion of the antioxidant glutathione (Bringmann et al. 2006). Another function of Müller cells is their ability to act as living optical fibers by guiding light through the retina and minimizing the intraretinal light scattering and decreasing the signal/noise ratio (Reichenbach and Bringmann 2013). Furthermore, Müller cells are involved in the immune response through several mechanisms including their toll-like receptors, phagocytic function and secretion of cytokines and chemokines. It has also been shown that microglial responses can be mediated by Müller cells (Kumar et al. 2013). Consequences of Müller cell dysfunctions were studied in a transgenic mouse model with conditional Müller cell ablation. It was shown that selective Müller cell ablation leads to early photoreceptor degeneration, vascular abnormalities, BRB breakdown and neovascularization in the retina (Shen et al. 2012).

Altered Müller cell functions during DR progression have been investigated by various studies. It was shown that the function of the glutamate transporter in Müller cells of diabetic rats is decreased (Li and Puro 2002). This leads to a significantly increased glutamate accumulation in the retinae of diabetic rats (Lieth et al. 2000). Furthermore, Pannicke et al. 2006 showed a decreased  $K^+$  (potassium) conductance on the plasma membrane of isolated Müller cells from diabetic rats due to a redistribution of the Kir4.1  $K^+$  channel. These findings are in line with the fact that the  $K^+$  conductance was also decreased in Müller cells of patients with PDR (Bringmann et al. 2002).

The disturbance of the retinal K<sup>+</sup> homeostasis together with the dysfunction of glutamate transporters in diabetic Müller cells may lead to neuronal hyperexcitation and glutamate excitotoxicity (Pannicke et al. 2006). Müller cells get activated and perform a process called gliosis under pathological conditions like diabetes. The extent to which gliotic activation of Müller glia has beneficial and/or detrimental effects on neuronal survival is not yet completely clarified. When Müller cells become gliotic in the course of pathologies, they can release growth factors, cytokines, and chemokines. It was shown that hyperglycaemia promotes the release of VEGF and pigment epithelium-derived factor as well as cytokines and chemokines including interleukin-1 $\beta$ , interleukin-6 (IL-6), tumour necrosis factor- $\alpha$  and chemokine ligand-2 by Müller cells *in vitro* (Coughlin et al. 2017). VEGF stimulates proliferation, migration and tube formation leading to angiogenic growth of new blood vessels (Le 2017). Although VEGF is mainly expressed in Müller cells, endothelial cells, astrocytes and the retinal pigment epithelium (RPE), there are indications that Müller cells are a major source of VEGF in DR and that Müller cell-derived VEGF plays an essential role in retinal inflammation, vascular lesions and leakage in DR (Wang et al. 2010). Although increased VEGF from Müller cells has a negative effect on the vasculature of the diabetic retina, it is possible that Müller cells release growth factors to protect themselves and retinal neurons from hyperglycaemia and ultimately have a beneficial effect (Coughlin et al. 2017). Besides growth factors, Müller cells can release a variety of cytokines and chemokines like IL-6, which is associated with vascular dysfunction and promotion of angiogenesis (Yoshida et al. 2001; Rojas et al. 2010). Furthermore, a correlation between increased IL-6 levels and the development of eye complications in diabetic patients was demonstrated (Koskela et al. 2013). It was shown that IL-6 1) prevents hyperglycaemia-induced Müller cell dysfunction and loss, 2) protects retinal ganglion cells from pressure-induced cell death, 3) maintains proper neuronal function and 4) has neuroprotective effects (Yego et al. 2009; Sappington et al. 2006). Therefore, the gliotic activation of Müller cells can have beneficial or detrimental effects on the survival of retinal cells, particularly neurons.

Although some changes of Müller cell functions and processes in DR are already known, increasing knowledge of Müller cell function and responses in the normal and diseased retina is needed for the development of new therapeutic approaches for retinal diseases. As normal Müller cell functions are important for neuronal survival, the ideal way would be to suppress negative aspects of Müller cell gliosis and promote the positive ones.

#### 2.4. AVAILABLE THERAPY OPTIONS FOR DIABETIC RETINOPATHY

Optimal control of blood glucose, blood pressure, and blood lipids remain the basis for reducing the risk of disease development and progression (Cheung et al. 2010). Furthermore, current treatment strategies for DR target the management of microvascular complications and include intravitreal administration of pharmacologic agents, laser therapy, and vitrectomy. Intravitreal injection

of anti-VEGF agents is currently the gold standard of therapy for early and advanced stages of DR (Wang and Lo 2018).

Laser photocoagulation which has been the standard of treatment in the last decades is a proven method for the treatment of DR. The panretinal photocoagulation is mainly used for the treatment of PDR, and focal or grid laser photocoagulation for DME. In a Diabetic Retinopathy Study, which included more than 1758 patients with proliferative disease, panretinal photocoagulation reduced the risk of severe visual loss by 50% over 5 years in these patients (Cheung et al. 2010). The exact mechanisms involved in panretinal photocoagulation laser therapy treatment are not yet fully understood. It is thought to be an interaction of several factors: direct closure of leaking microaneurysms, improved oxygenation and stimulation of the RPE, as well as reduction of retinal blood flow through the reduced retinal tissue (Wang and Lo 2018). However, because laser therapy is an invasive procedure, it can also result in moderate vision loss as a side effect, noticeable by a reduced visual field, reduced colour vision, and decreased contrast sensitivity (Fong et al. 2007). As laser therapy continues to play an important role as an adjuvant treatment or a rescue therapy alongside anti-VEGF therapy, novel, less invasive laser techniques such as the use of a subthreshold micropulse diode laser, which is a promising new tool for treatment of DME, are being investigated (Vujosevic et al. 2013).

In patients with severe PDR who do not respond to panretinal laser photocoagulation or who have persistent vitreous haemorrhage or retinal detachment, ocular surgery with removal of the vitreous (vitrectomy) is possible (Cheung et al. 2010). Since vitrectomy is also an invasive procedure, this method has harmful effects on the diabetic eye alongside the benefits. Although the risk of retinal neovascularization and macular oedema is reduced, the risk of iris neovascularization and cataract formation is increased (Diabetic Retinopathy Vitrectomy Study Research Group 1985). In recent years, the therapy with intravitreal injections of anti-VEGF has become the first-line treatment for DR. VEGF is a growth factor that plays an important role in retinal neovascularization and in BRB breakdown in DR (Fu et al. 2015). Therefore, treatment with anti-VEGF agents should arrest, or even reverse PDR or DME. A large number of clinical studies have shown beneficial effects of intravitreal anti-VEGF injections for both and it was demonstrated that this therapy improves visual acuity more effectively than laser treatment (Cheung et al. 2010). Nevertheless, anti-VEGF therapy also comes with limitations and adverse effects. Local adverse events are cataract formation, retinal detachment, vitreous haemorrhage, infection and potential loss of neural retinal cells (Wirotko et al. 2008). Furthermore, the effectiveness relies on repeated (monthly) intravitreal injections due to their short half-life time in the eye and the increased incidence of adverse effects like endophthalmitis by frequent injections (Das et al. 2015).

Another therapy which is mainly used for DME is the intraocular administration of corticosteroids, which are potent anti-inflammatory agents efficient in the treatment of DME. These agents become increasingly important when patients prove to be resistant to the gold-standard anti-VEGF therapy. Currently used intravitreal corticosteroids are triamcinolone acetonide, dexamethasone and the fluocinolone acetonide (Wang and Lo 2018). The advantages of corticosteroids are that they require a lower frequency of injections, lower costs and better patient compliance. However, there is a high incidence of adverse effects like cataract and glaucoma. Therefore, corticosteroids are currently only the second-line option for patients who are not responding to other therapeutic treatments (Wong et al. 2016).

In conclusion, the existing treatments are not optimal due to their side effects, partially high costs, and the fact that the progression of DR is slowed only to a limited extent. Hence, there is an urgent need for the development of additional or complementary treatment approaches.

## 2.5. GENE THERAPEUTICAL APPROACHES

Gene therapy has the potential to become a new treatment method for DR. The advantages may be fewer side effects, less injection frequency, ability to intervene at disease onset and a longer therapeutic effect (Wang et al. 2020).

There are several strategies of gene therapy, which goal is to achieve adequate expression of a transgene to decrease or cure a disease condition with minimal adverse effects. Strategies which were developed in the last decades are gene augmentation, gene-specific targeting, and most recently, genome editing (Lee et al. 2019). Gene augmentation therapy introduces a new functional gene into the host cell to compensate a defective gene and therefore, it is mainly used in monogenic diseases. Gene-specific targeted therapy aims to modulate the activity of an existing altered gene or provide an intact copy of a gene for protection or regeneration. Genome editing or corrective therapy transforms a mutated gene into a functional gene and can thus correct mutated genes fundamentally (Wang et al. 2020).

The eye is an ideal target for gene therapy, because the tight BRB prevents viral vectors from entering the systemic circulation. In addition, the eye is a small, defined area and thus has a high accessibility and a relatively immune-privileged state. Vectors that are currently used in ocular gene therapy are adeno-associated viruses (AAV), which are small single-stranded DNA viruses, and lentivirus, RNA viruses of the retrovirus family (Moore et al. 2018). The two classical administration routes of the virus are intravitreal and subretinal injections. Intravitreal injection means that the therapeutic agent is released into the vitreal cavity and therefore, its distribution across the surface of the retina is possible. The therapeutic agent is released into the space between the photoreceptors and the RPE by subretinal injections and therefore, directly targeting these cell

populations (Dauletbekov et al. 2018). In 2017, the FDA approved the first AAV-based gene therapy product for the treatment of Leber congenital amaurosis-2, which is a rare form of blindness caused by variations in the RPE65 gene. The AAV vector, which is subretinally injected, carries a copy of the RPE65 gene. The therapy has been successful and showed improvements in functional vision and an increase in visual field and full-field light sensitivity. Furthermore, it is documented to be a safe and durable treatment (Askou et al. 2020).

Some studies have already investigated gene therapeutically approaches for the treatment of DR. These gene-specific targeted therapies can be divided into two groups according to disease pathophysiology: approaches targeting neovascularization and vascular hyperpermeability and approaches with the goal to protect retinal blood vessels and neurons from damage (Wang et al. 2020). Müller cells are interesting targets for new therapeutic approaches for retinal diseases, due to the fact that their endfeet are located at the inner border of the retina, making them easily accessible. Pellissier et al. 2014 demonstrated that ShH10 and AAV9 were the most powerful capsids to infect mouse Müller glial cells. A scheme of how gene therapeutic targeting of Müller cells by intravitreal virus injection could work is shown in **Figure 3**.

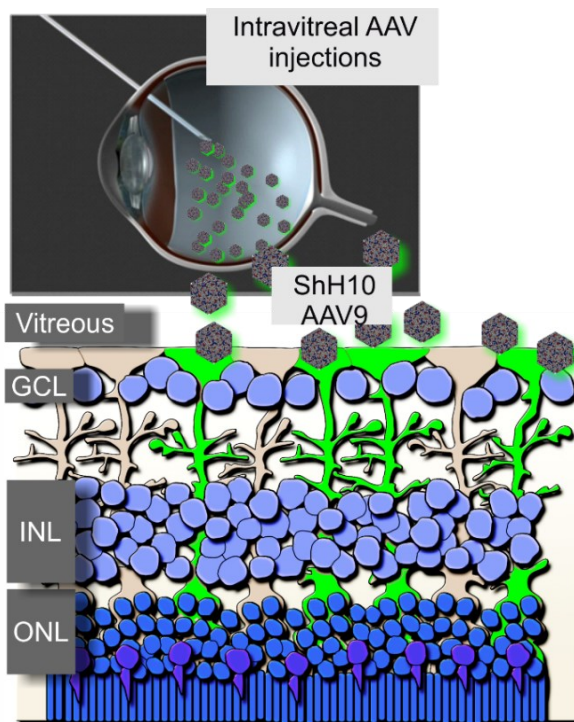


**Figure 3: Gene therapeutic targeting of Müller cells by intravitreal virus injection.** Müller cell endfeet are located at the inner border of the retina and can be targeted by intravitreal adeno-associated virus administration with ShH10 or AAV9. GCL: Ganglion cell layer, INL: Inner nuclear layer, ONL: Outer nuclear layer.

In conclusion, gene therapeutical approaches hold a great potential not only for the treatment of inherited retinal dystrophies, but also multifactorial eye diseases like DR.

## 2.6. THE RETINAL GLUCOCORTICOID RECEPTOR

In ophthalmology glucocorticoids are widely used for the management of diverse diseases with acute and chronic ocular inflammatory conditions. Intravitreal corticosteroids are efficient in the treatment of DME (Wang and Lo 2018). Their therapeutic effects are mediated through genomic actions of the GR (Sulaiman et al. 2018). The GR which is encoded by the gene *Nr3c1* is a nuclear hormone receptor and has broad effects on inflammatory responses, cell proliferation and differentiation in target tissues (Liu et al. 2019). The molecular structure of GR contains four components: an N-terminal transactivation domain, a central DNA binding domain, a hinge region and a C-terminal ligand-binding domain (Vandevyver et al. 2014). The GR is ligand-inducible and can regulate transcription in multiple ways. Without bound ligand, the GR is localized in the cytoplasm and it is bound to a chaperone complex which consists of heat shock proteins as well as immunophilins (Liu et al. 2019). As soon as glucocorticoids bind, the GR undergoes a conformational change by post-translational modifications like phosphorylation. The two nuclear localization signals are exposed by this structural rearrangement and the GR translocates into the nucleus where it can regulate transcription in various ways (Oakley and Cidlowski 2013). The GR signaling pathway and the possible modes of action are shown in **Figure 4**.

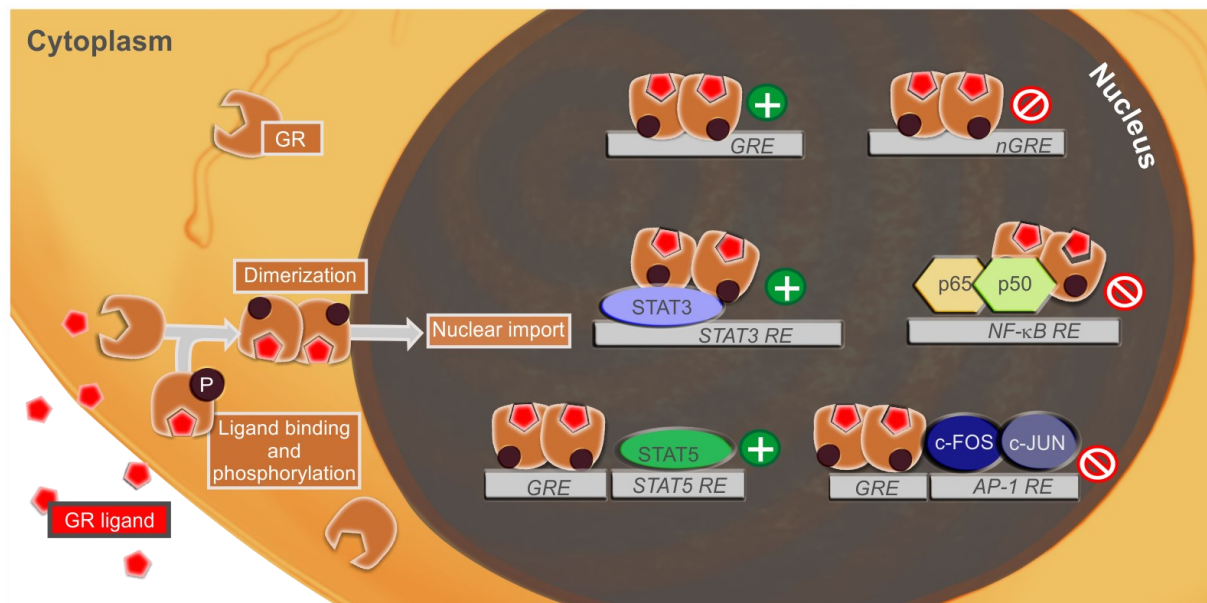


**Figure 4: Glucocorticoid receptor signaling in the retina.** Schematic view on possible modes of action of the glucocorticoid receptor after ligand binding, receptor phosphorylation, dimerization and its translocation into the nucleus. Within the nucleus, the glucocorticoid receptor can regulate transcription in three main ways: direct binding to glucocorticoid-response elements (GREs) or negative GREs (nGREs), interacting with other transcription factors, or by both, direct binding and interaction with others. The expression of respective target genes can be activated or repressed. P: Phosphorylation. The Figure was adopted from Sulaiman et al. 2018 and Liu et al. 2019.

GR activation can lead to transactivation of gene transcription directly by binding to glucocorticoid-response elements (GREs) or transrepression mediated by negative GREs (nGREs) (Liu et al.

2019). Furthermore, the GR can act through protein-protein interactions with other TFs like the nuclear factor kappa-light-chain enhancer of activated B cells (NF- $\kappa$ B) or activating protein-1 (AP-1) (Sulaiman et al. 2018). It is also possible to act via both, direct binding to GREs and interaction with other TFs (Liu et al. 2019).

The main ligand of GR is the glucocorticoid corticosterone in mice and cortisol in humans (Buckingham 2006). Glucocorticoids have a broad range of effects and are involved in metabolic processes, immune system, reproduction, behavior and cognitive functions. Circulating levels of glucocorticoids are regulated by the hypothalamic-pituitary-adrenal (HPA) axis. In case of stress, the HPA axis gets activated and an increase in glucocorticoids helps the body to cope and recover from the stress situation (Gjerstad et al. 2018). Although glucocorticoids are commonly used, the molecular and cellular processes of GR signaling in the diabetic eye are largely unknown.

Gallina et al. 2014 showed that GR is mainly located in nuclei of Müller cells in mouse, guinea pig, dog and human retinae. It was demonstrated that a partial loss of GR in the retina results in a thinner INL and that it plays a critical role in maintaining retinal homeostasis by regulating the inflammatory response (Kadmiel et al. 2015). Furthermore, Gallina et al. 2015 found that activation of GR has a positive effect on the survival of ganglion cells in colchicine-damaged retinae, the survival of amacrine and bipolar cells in excitotoxin-damaged retinae and the survival of photoreceptors in detached retinae.

While several synthetic glucocorticoids are widely used for the treatment of several ocular diseases like DME and the beneficial effect of GR activation was demonstrated in several studies, little is yet known about the molecular mechanism of GR signaling in the eye.

## 2.7. ANIMAL MODEL: DB/DB MICE

Currently, no animal model recapitulates the whole pathophysiology of the multifactorial disease DR. The db/db (Lepr<sup>db</sup>) mice develop type 2 diabetes (T2D) due to a mutation in the leptin receptor gene (Chen et al. 1996) and show a number of abnormalities similar to the characteristics of human DR. The elevations of plasma insulin in homozygous mice begin at 10 to 14 days of age (Coleman and Hummel 1974), they get obese at 4 weeks and hyperglycemic at the age of 4 to 8 weeks (Hummel et al. 1966). The proteome of 10-week-old db/db animals compared to controls was investigated and a change of membrane-associated signaling proteins detected (Ly et al. 2014). Development of the first key features of DR, namely endothelial and pericyte loss, begin at 12 weeks of age in db/db mice (Midena et al. 1989). The total thickness of the retina is decreased in diabetic mice (Tang et al. 2011). The thickness of the INL and ONL in comparison to controls is already decreased at the age of 8 weeks. Furthermore, the number of the retinal ganglion cells was reduced in db/db mice by 8 weeks of age and key features of neurodegeneration, a- and b-wave abnormalities in the ERG and terminal deoxynucleotidyl transferase dUTP nick

end labeling-positive cells, were observed in diabetic animals by 16 and 24 weeks of age. Moreover, a significant overexpression of glial fibrillary acidic protein (GFAP) in Müller cells of diabetic mice (Bogdanov et al. 2014) and the loss of anti-inflammatory defense mainly performed by microglia (Arroba et al. 2016) was observed at 8 weeks. Breakdown of the BRB is visible in 15-month-old diabetic animals. Moreover, apoptosis of neuronal cells, glial reactivation and the proliferation of blood vessels can be detected in the db/db animals by 15 months of age (Cheung et al. 2005). Sataranatarajan et al. 2016 showed that the median survival of male db/db mice was 349 days and of female mice 487 days and reported a reduced life span of males. The main cause of death was suppurative inflammation.

### 3. OBJECTIVES

The focus of this thesis was to gain knowledge about the role of Müller cells in the context of multifactorial diseases such as DR and to target those for therapeutic use. The following objectives, which are schematically summarized in **Figure 5**, should be addressed:

#### Objective 1: Identification of signaling pathways altered in diabetic Müller cells

A transcriptome and proteome analysis of diabetic and non-diabetic mice should be performed to shed light on the molecular pathways and processes during DR progression.

#### Objective 2: Identification of specific master regulator genes driving the Müller cell phenotype in DR

Key regulator genes responsible for the gliotic Müller cell phenotype in T2D affected obese db/db mice should be identified on basis of the Müller cell-specific expression analysis. Genes identified as relevant in Müller cell gliosis in DR should be in-depth characterized.

#### Objective 3: Modulation of a Müller cell-specific gene via AAV-based gene therapy

The expression of a Müller cell-specific regulated gene in DR should be modeled using an AAV-based method in db/db mice with the goal to improve long-term neuronal survival by stabilizing the neuron-supportive phenotype of Müller glia in the diseased retina.

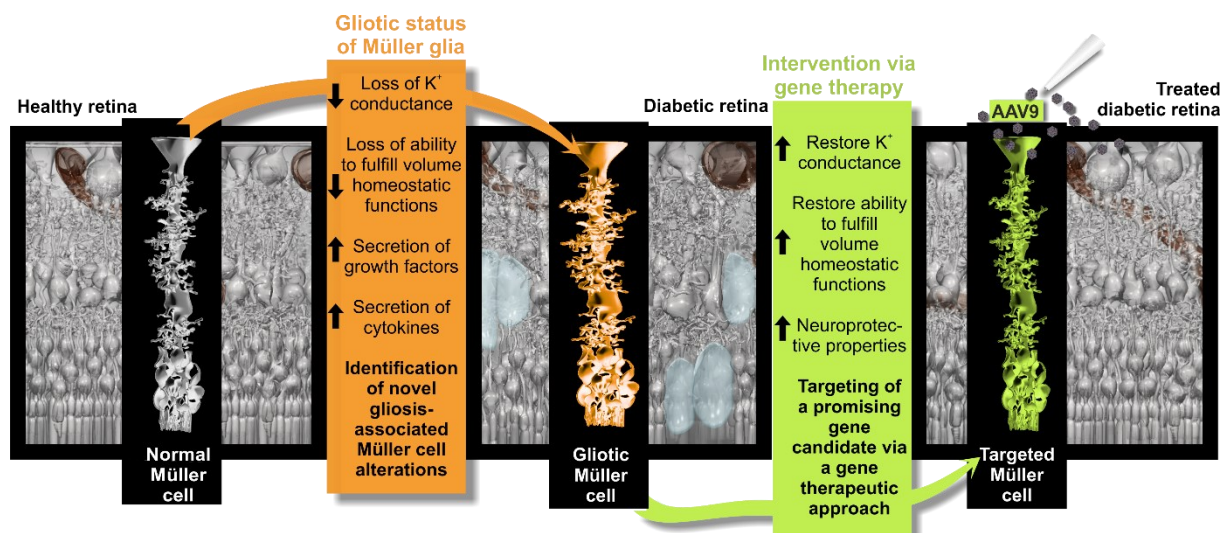


**Figure 5: Scheme of how targeting Müller cells may be of therapeutic use in diabetic retinopathy.** In the diabetic retina Müller cells are getting gliotic and show major alterations of cellular functions being of key relevance for their neuronsupportive, homeostatic functions and thereby might contribute to diabetic retinopathy progression. I wanted to identify novel aspects of Müller cell gliosis beyond known hallmarks of this process (e.g. downregulation of potassium channels, loss of their homeostatic function and upregulation of cytokines and growth factors). A long-term effective gene therapeutic approaches targeting Müller cells via AAV9 should be developed with the goal to promote beneficial Müller cell functions and suppressing negative aspects of Müller cell gliosis.

## 4. MATERIAL

### 4.1. MICE

Db/db heterozygous mice (BKS.Cg-Dock7m +/- Leprdb/J) were obtained from Jackson Laboratories and BKS-Leprdb/db/JOrIRj from Janvier Labs and maintained in the animal facility of the Biomedical Center. All experiments were performed in agreement with the European Communities Council Directive 86/609/EEC and were approved by the local authorities. Animals had free access to water and food in an air-conditioned room on a 12-hour light-dark cycle. Mice of both genders with an age of 12, 24 and 38 weeks were used for the experiments.

### 4.2. OLIGONUCLEOTIDES

Table 1: Oligonucleotides

Name	5'3' Sequence	Usage
Clrn1 fw	TGC TTG TCA ACG CGT CAG	qPCR
Clrn1 rev	GAG TAC CTC TCC TTC ATT GAT CTT G	qPCR
Cryab fw	TGA GCC CCT TCT ACC TTC G	qPCR
Cryab rev	GTC CTT CTC CAA ACG CAT CT	qPCR
Eno1 fw	GCC CTA GAA CTC CGA GAC AA	qPCR
Eno1 rev	CAG AGC AGG CGC AAT AGT T	qPCR
FI	ATT AGA AGA TGT TTA CAT TTT GAT GGA AGG	Genotyping
FO	TTG TTC CCT TGT TCT TAT ACC TAT TCT GA	Genotyping
GFAP fw	TCG AGA TCG CCA CCT ACA G	qPCR
GFAP rev	GTC TGT ACA GGA ATG GTG ATG C	qPCR
Glul fw	GCC CAA GTG TGT GGA AGA G	qPCR
Glul rev	AAG GGG TCT CGA AAC ATG G	qPCR
ldh3b fw	GCT GCG GCA TCT CAA TCT	qPCR Housekeeper
ldh3b rev	CCA TGT CTC GAG TCC GTA CC	qPCR Housekeeper
Nr3c1 fw	TGA CGT GTG GAA GCT GTA AAG T	qPCR
Nr3c1 rev	CAT TTC TTC CAG CAC AAA GGT	qPCR
Pdhb fw	TTA AAT CGG CCA TTC GTG AT	qPCR Housekeeper
Pdhb rev	CAG GAA ATC TTT TGA CTG AGC TT	qPCR Housekeeper
RI	GTC ATT CAA ACC ATA GTT TAG GTT TGT CTA	Genotyping
RO	CTG TAA CAA AAT AGG TTC TGA CAG CAA C	Genotyping
Sfxn5 fw	GCT TCC TCC AAT CGT CAT GT	qPCR
Sfxn5 rev	CAC GAG GCT ATG CAC AGG TA	qPCR

## 4.3. ADENO-ASSOCIATED VIRUS

Table 2: Adeno-associated virus

Name	Characteristics	Supplier
AAV9-GFAP(0.7)-mNR3C1-2A-eGFP	mNR3C1 and eGFP are driven by the same promoter with a 2A linker in between for co-expression Capsid: AAV-9, ITR: AAV-2 Titer: $2.5 \times 10^{13}$ GC/ml Storage Buffer: DPBS 2/5% glycerol	Vector Biolabs AAV-266053

## 4.4. ENZYMES AND PROTEINS

Table 3: Enzymes and proteins

Name	Supplier	Order number
5x reaction buffer	Thermo Scientific™	EP0441
6x DNA gel loading dye	Thermo Scientific™	R0611
DNA ladder 1 kb	Thermo Scientific™	11571595
DNA ladder 100 bp	Invitrogen	15628019
DNase I	Roche	11284932001
dNTP mix 10 mM	Thermo Scientific™	R0192
Low ROX probe 2x mastermix dTTP blue	Takyon	UF-LPMT-B0701
Papain	Roche	10108014001
Prestained protein™ ladder plus	Thermo Scientific™	26620
Random hexamer primer	Thermo Scientific™	SO142
RevertAid reverse transcriptase	Thermo Scientific™	EP0441

## 4.5. ANTIBODIES

Table 4: Antibodies

Name	Supplier	Order number
Anti-Biotin microbeads ultrapure	Miltenyi Biotec	130-105-637
CD11b microbeads, human, mouse	Miltenyi Biotec	130-093-634
CD29-biotin, mouse	Miltenyi Biotec	130-101-943
CD31 microbeads, mouse	Miltenyi Biotec	130-097-418
Donkey anti-rabbit IgG-Alexa Fluor 488	Invitrogen	A21206
Donkey anti-rabbit IgG-Alexa Fluor 555	Invitrogen	A31572

Donkey Fab anti-mouse IgG-Cy3	Dianova	715-167-003
Donkey IgG anti-Goat IgG-Alexa Fluor 647	Dianova	705-605-003
Donkey IgG anti-goat IgG-Cy2	Dianova	705-225-147
Donkey IgG anti-goat IgG-Cy3	Dianova	705-165-003
Donkey IgG anti-mouse IgG-Cy2	Dianova	715-225-150
Donkey IgG anti-rabbit IgG-Cy5	Dianova	711-175-152
Goat anti-Calretinin antibody	Swant	CG1
Goat anti-GFP antibody	Rockland	600-101-215
Goat anti-rabbit IgG, chain specific peroxidase conjugate	Calbiochem	401315
Goat IgG anti-mouse IgG-Cy3	Dianova	115-165-146
Goat IgG anti-rabbit IgG-Alexa Fluor 488	Dianova	111-545-144
Mouse anti-Glutamine synthetase antibody	Millipore	MAB302
Mouse anti-GFAP antibody	Sigma-Aldrich	G3893
Rabbit anti-Pdhb antibody	Abcam	ab155996
Rabbit anti-Cone arrestin antibody	Millipore	AB15282
Rabbit anti-GR antibody	Cell Signaling	12041
Rabbit anti-Iba1 antibody	Wako	019-19741
Rabbit anti-Pde6b antibody	Thermo Fisher	PA1-722
Rabbit anti-PDGFR $\beta$ antibody	Abcam	ab32570
Rabbit anti-Phospho-GR antibody	Thermo Fisher	PA5-17668

## 4.6. PROBES

Table 5: Probes

Probe	Gene	Supplier	Order number
4	<i>Cryab, Pdhb</i>	Merck (original: Roche)	04685016001
17	<i>Cln1</i>	Merck (original: Roche)	04686900001
56	<i>Nr3c1</i>	Merck (original: Roche)	04688538001
58	<i>Glul</i>	Merck (original: Roche)	04688554001
60	<i>Eno1</i>	Merck (original: Roche)	04688589001
67	<i>Gfap, Idh3b, Sfxn5</i>	Merck (original: Roche)	04688660001

## 4.7. CHEMICALS

Table 6: Chemicals

<b>Name</b>	<b>Supplier</b>	<b>Order number</b>
Acetic acid	Sigma-Aldrich	A6283-1L
Agarose	VWR	443666A
Ammoniumpersulfate	Carl Roth	9592.2
Antibiotic-antimycotic (100x)	Gibco™	15240062
Aqua-polymount	Polysciences Europe	18606-20
Bromophenol blue	Merck	1081220005
Bovine serum albumin	Carl Roth	8076.4
Cryomatrix™	Thermo Scientific™	6769006
DAPI	Sigma-Aldrich	D9564
Dimethyl sulfoxide	Sigma-Aldrich	4 1640-100ML
DMEM/F-12, GlutaMAX™	Gibco™	31331028
Donkey serum	Sigma-Aldrich	S30-100ML
Ethanol > 99.8%	Carl Roth	0911.4
Glucose	AppliChem GmbH	A3730
Glycerin	Sigma-Aldrich	G9012-1L
Glycine	Roth	3790.2
Goat serum	Sigma-Aldrich	S26-100ML
HEPES	Millipore	391340-250GM
Hydrocortisone (Cortisol)	Sigma-Aldrich	H0888-1G
Isopropanol	Carl Roth	6752.5
KCl	AppliChem GmbH	A2939
Ketamine 10%	WDT	793-319
KH <sub>2</sub> PO <sub>4</sub>	Roth	3904.2
Methocel® 2% eyedrops	OmniVision GmbH	04682367
MgCl <sub>2</sub> x 6 H <sub>2</sub> O	AppliChem GmbH	A4425
Mydriaticum Stulln® UD eye drops (0.5% tropicamide-phenylephrine 2.5% eye drops)	Pharma Stulln	4647856
Na <sub>2</sub> EDTA	Sigma-Aldrich	E1644-250G
Na <sub>2</sub> HPO <sub>4</sub> x 2 H <sub>2</sub> O	Roth	4984.1
NaCl	Roth	0601.1

Neosynephrin-POS® 10% eye drops	Ursapharm Arzneimittel GmbH	828590
Paraformaldehyde	Carl Roth	0335.2
RNase-free water	Invitrogen	46-6004
Rompun 2% Injections solution (Xylazine)	Bayer	0859-2266-01
Rotophorese® gel 30 (30% Acrylamide solution)	Roth	3029.1
Sodium dodecyl sulfate	Roth	2326.1
β-mercaptoethanol	Merck	444203
SYBR™ Safe DNA Gel Stain	Invitrogen™	S33102
Tetramethylethylenediamine	Roth	2367.1
Tris	Roth	3170.1
Triton™ X-100	Roth	3051.3
Trypsin 1:250	Affymetrix	22710
Tween® 80	Sigma-Aldrich	P4780-100ML

#### 4.8. COMMERCIAL KITS

Table 7: Commercial kits

<b>Name</b>	<b>Supplier</b>	<b>Order number</b>
Clarity Max™ Western ECL Substrate Kit	Bio-Rad	1705062
Corticosterone ELISA kit	Abcam	ab108821
H&E fast staining kit	Roth	9194.1
KAPA Mouse Genotyping Kit	KAPABIOSYSTEMS/ Roche	KK7352
PureLink™ RNA Micro Scale Kit	Invitrogen™	12183016

#### 4.9. CONSUMABLES

Table 8: Consumables

<b>Name</b>	<b>Supplier</b>	<b>Order number</b>
24-well plate	Sarstedt	833.922.005
384-well plate	Thermo Fisher	4483285

48-well plate	Sarstedt	833.923.300
10 µL, Cemented, blunt needle, 33G	Hamilton	80383
Agarose gel electrophoresis system	Biozym	615258
BD Microlance™ 3 (23G)	BD	300800
BD Microlance™ 3 (27G)	BD	302200
Blood collection tubes	Sarstedt	41.1503.015
Cover glasses	Carl Roth	1871
Disposable Scalpel No.11	Feather (Thermo Scientific™)	NC0134996
E1-ClipTip (Multi-channel pipette)	ThermoFisher	4672030BT
Extra Thick Blot Filter Paper	Bio-Rad	1703969
Large cell columns	Miltenyi Biotec	130-042-202
Micro tube 1.3 ml LH	Sarstedt	411.503.105
NANOFIL™	WPI	NANOFIL
NitriL® NextGen® (Cloves)	Meditrade (VWR)	ROES1283A-S
Whatman® nuclepore™ track-etched membranes	Merck	WHA10417101
Omnican® 50 (0.5 ml syringe)	B. Braun	9151117
Omnifix®-F (1 ml syringe)	B. Braun	9161406V
PARAFILM® M	Merck	P7793
Pasteur capillary pipettes (glass pipettes)	neoLab	4-4035
Pipette tips	Tip one (starlab)	S1111-3210, S1110-3710, S1111-0810, S1111-6810
Research® plus (pipette)	Eppendorf	3120000011, 3120000020, 3120000038, 3120000054, 3120000062
SDS-PAGE system	Biozym	615862
Serological pipettes	Sarstedt	86.1253.001, 86.1688.010, 86.1685.020, 86.1256.001
Standard test tube, 1.5 ml	Sarstedt	72.706.200
Standard test tube, 5 ml	Sarstedt	72.201

Stripes of 8 PCR tubes, 0.2 ml	neoLab	7-5209
SuperFrost Plus™ Adhesion slides	Thermo Scientific™	10149870
TC Dish 35, Standard	Sarstedt	833.900
Tube, 15 ml	Sarstedt	62.554.502
Tube, 50 ml	Sarstedt	62.547.004
Transfer membrane ROTI®FluoroPVDF	Carl Roth	2803.1

#### 4.10. BUFFERS AND SOLUTIONS

Table 9: Buffers and solution

Name	Composition
0.1 M Tris buffer (1 l), pH: 7.8	12.1 g Tris solved in distilled water
1.25 M Tris-HCl buffer (100 ml), pH: 6.8	15.1 g Tris solved in distilled water
4% PFA (1 l)	40 g PFA solved in 1x PBS
4x Resolving buffer (500 ml), pH: 8.8	90.75 g Tris, 2 g SDS solved in distilled water
4x Stacking buffer, pH:6.8	30.25 g Tris, 2 g SDS solved in distilled water
5x Extracellular solution (1 l), pH: 7.4 (with Tris)	39.74 g NaCl, 1.12 g KCl, 1.47 g CaCl <sub>2</sub> , 1 g MgCl <sub>2</sub> x 6 H <sub>2</sub> O, 11.91 g HEPES, and 10.9 g glucose solved in distilled water
5x SDS-PAGE sample buffer (50 ml), pH: 6.8	2.5 g SDS, 12.5 ml glycerin, 6.25 ml β-mercaptoethanol, 0.013 g Bromophenol blue solved in Tris-HCl buffer (1.25 M)
10% APS (1.5 ml)	150 mg solved in distilled water
10x PBS (2.5 l), pH: 7.4	36.83 g Na <sub>2</sub> HPO <sub>4</sub> x 2 H <sub>2</sub> O, 5 g KH <sub>2</sub> PO <sub>4</sub> , 200 g NaCl, 5 g KCl solved in distilled water
10x SDS running buffer, pH: 8.45	30.3 g Tris, 144 g glycine, 10 g SDS solved in distilled water
10x TBS buffer (1 l), pH: 7.6	60.6 g Tris, 87.6 g NaCl solved in distilled water
10x Towbin buffer (500 ml), pH: 8.7	15.2 g Tris, 72 g glycine solved in distilled water
30% Sucrose (100 ml)	30 g sucrose solved in 1x PBS

50x TAE buffer (1 l)	242 g Tris, 57.1 ml acetic acid, 37.2 g Na <sub>2</sub> EDTA x 2H <sub>2</sub> O solved in distilled water
PBS/Glucose (1 l), pH: 7.4	2.18 g glucose solved in PBS

## 4.11. INSTRUMENTS

Table 10: Instruments

<b>Name</b>	<b>Supplier</b>
Centrifuge 5910 R	Eppendorf
ChemiDoc XRS+ system	Bio-Rad
Cryostat CM3050 S	Leica
SZ51 (Dissection microscope)	Olympus
DM6 fixed stage fluorescence microscope	Leica
Espion ERG Diagnosys equipment	Diagnosys LLC
Heating mat	Trixie
HPLP-C-P (Hotplate)	Witeg
Galaxy 170 S CO <sub>2</sub> incubator	New Brunswick
Mastercycler® nexus X2	Eppendorf
Titramax 100 (microplate shaker)	Heidolph
pH meter Lab 850	Schott Instruments
Accu-jet® pro (pipetboy)	Brand
Power Supply EV1450	Consort
Q-Exactive HF mass spectrometer	Thermo Scientific™
QuantStudio 6 Flex Real-Time PCR System	Thermo Scientific™
Roll Mixer	Premiere
Sigma 1-14K (benchtop centrifuge)	Sigma
SP8X WLL confocal microscope with STED and digital light extension	Leica
ThermoMixer® C	Eppendorf
Trans blot® Turbo™	Bio-Rad
Ultimate 3000 RSLC nano-HPLC	Dionex
VisiScope CSU-X1 confocal system equipped with a high-resolution sCMOS camera	Microscope: VisiScope, Camera: Visitron Systems
Vortex-Genie 2	Scientific Industries, Inc.

## 4.12. SOFTWARE

Table 11: Software

<b>Name</b>	<b>Supplier</b>
CorelDRAW®	Corel Corporation
Espion V6 software	Diagnosys LLC
GelAnalyzer	Created by Istvan Lazar
GraphPad PRISM 8	GraphPad Software
Fiji (Schindelin et al. 2012)	Open-source Software
Microsoft Office	Microsoft
R (R Core Team 2014)	R Core Team
QuantStudio Software v1.3	Thermo Scientific™

## 5. METHODS

### 5.1. DNA EXTRACTION

Ear punches from the mice were provided for genotyping by the animal facility. The KAPA Mouse Genotyping Kit from KAPABIOSYSTEMS was used for DNA extraction (KAPA Express extract protocol).

Table 12: DNA extraction components

<b>Components</b>	
Nuclease-free water	88 $\mu$ l
10x KAPA Express extract buffer	10 $\mu$ l
1 U/ $\mu$ l KAPA Express extract enzyme	2 $\mu$ l
Mouse tissue	ear punch

The components were mixed, and the lysis performed in the thermocycler using the following protocol.

Table 13: Lysis protocol

<b>Step</b>	<b>Temperature</b>	<b>Duration</b>
Lysis	75 °C	10 min – 2 h
Enzyme inactivation	95 °C	5 min
Storage	4 °C	Hold

Extracts were stored short term at 4 °C and for long term at -20 °C.

### 5.2. GENOTYPING DB/DB MICE

The genotyping of the homozygous db/db, heterozygous db/+ and the wild-type mice of C57BLKS/ J strain was done by polymerase chain reaction (PCR). The protocol is based on the method for genotyping mice with a leptin receptor mutation (Peng et al. 2018). The KAPA Mouse Genotyping Kit provided the necessary reagents for the following reaction:

Table 14: PCR components

<b>Components</b>	
Nuclease-free water	3.25 $\mu$ l
2x KAPA2G Fast (HotStart) genotyping mix with dye	7.25 $\mu$ l
Primer-Mix	2.0 $\mu$ l
Template DNA	2.0 $\mu$ l

The primer mix consists of four primers: forward outside primer (FO), reverse outside primer (RO), forward inner primer (FI) and reverse inner primer (RI). The primers were used in a concentration of 10  $\mu$ M. The ratio of outer to inner primers was 1:2. The components were mixed and the following thermocycling conditions have been used.

Table 15: Thermocycling conditions

Step	Temperature	Duration
Initial denaturation	94 °C	5 min
40 cycles	95 °C	30 sec
	55 °C	30 sec
	68 °C	1 min
Final extension	68 °C	5 min
Storage	4 °C	Hold

PCR products were directly loaded on a 2% (w/v) agarose gel or short term stored at 4 °C. The mice of the db/db breeding can have three different genotypes: wild types (wt), heterozygous (db/+) and homozygous (db/db). The wt mice showed two bands at 610 and 264 bp, db/+ mice three bands at 610, 406 and 264 bp and the db/db mice two bands at 610 and 406 bp.

### 5.3. AGAROSE GEL ELECTROPHORESIS

DNA fragments were separated in a matrix of agarose by length (agarose gel electrophoresis). 2% or 1,5% (w/v) agarose was boiled in 1x TAE buffer. The solution cooled down and SYBR™ Safe DNA Gel Stain, diluted 1:20,000 in the agarose gel buffer mix, was added. Afterwards, the liquid was immediately filled into the agarose gel electrophoresis chamber and the comb put into the gel. The PCR products for which the KAPA Mouse Genotyping Kit from KAPABIOSYSTEMS were used already contained a loading dye. Other DNA samples were mixed with 6x DNA gel loading dye diluted to a 1x concentration. The samples were loaded onto the solid gel. For size determination DNA ladders (100 bp or 1 kb) were used. The electrophoresis was performed in 1x TAE buffer at 1.2 V/cm<sup>2</sup> for 50 min. The gel was photographed by the ChemiDoc XRS+ system.

### 5.4. MAGNETIC ACTIVATED CELL SORTING

Different cell types of the retina were sequentially separated by magnetic activated cell sorting (MACS) as previously described (Grosche et al. 2016). Retinae were isolated and digested with 0.2 mg/ml papain in PBS/Glucose at 37 °C for 30 min. Afterwards, three washing steps with PBS/Glucose were performed and the tissue incubated with 200 U/ml DNase I at room temperature (RT) for 4 min. The retinae were dissociated in extracellular solution (ECS) to get a single

retinal cell solution and centrifuged at 600 xg and 4 °C for 10 min. The supernatant was removed and the cells were resuspended in ECS and incubated with CD11b microbeads which have been developed for the positive isolation of primary mouse CD11b<sup>+</sup> microglia at 4 °C for 15 min. After centrifugation at 600xg and 4 °C for 10 min the cells were resuspended in ECS and transferred onto a large cell column using a fire polished glass pipette. The cells were separated according to the manufacturer's recommendation. The CD11b<sup>+</sup> fraction was centrifuged and the cells stored at -80 °C. The CD11b<sup>-</sup> cells (flow through) were centrifuged, resuspended in ECS and incubated with CD31 (Pecam1)-microbeads for the positive selection of CD31<sup>+</sup> endothelial cells at 4 °C for 15 min. After centrifugation at 4 °C and 600 xg for 10 min the cells were resuspended in ECS, transferred onto large cell columns and eluted according to the manufacturer's recommendation. The CD31<sup>+</sup> fraction was centrifuged and the cells stored at -80 °C. The CD31<sup>-</sup> cells (flow through) were centrifuged, resuspended in ECS and incubated with CD29-biotin at 4 °C for 15 min. The antibody binds to CD29, also known as integrin  $\beta$ 1, which is a cell-surface receptor expressed by Müller cells. Retinal astrocytes are assumed to be found in a small amount in the CD29<sup>+</sup> fraction. The cells were centrifuged at 4 °C and 600 xg for 10 min, resuspended in ECS and incubated with anti-biotin microbeads which enables the positive selection of the CD29<sup>+</sup> Müller cells at 4 °C for 15 min. After centrifugation the cells were resuspended in ECS, transferred onto the columns and separated according to the manufacturer's recommendation. The remaining CD29<sup>-</sup> fraction mostly contained the retinal neurons. The remaining samples were centrifuged at 10000 xg and 4 °C for 15 min and the cell pellet was stored at -80 °C.

## 5.5. RNA ISOLATION

The PureLink™ RNA Micro Scale Kit was used for RNA isolation according to the manufacturer's recommendation. The lysis buffer was freshly prepared via adding 1%  $\beta$ -mercaptoethanol to the provided lysis buffer of the kit. 350  $\mu$ l of this lysis buffer were added to every sample before they were vortexed. Afterwards, the cells were passed 10 times through a 23G needle and a 1 ml syringe, 350  $\mu$ l 70% ethanol was added to the samples, followed by a vortexing step. Everything was transferred to the provided columns and centrifuged at 14000 xg and RT for 1 min. The flow through was discarded and 350  $\mu$ l per sample of the provided wash buffer 1 were added. Afterwards, the columns were centrifuged at RT and 14000 xg for 1 min and the flow through discarded. 10  $\mu$ l of the DNase were mixed with 10  $\mu$ l DNase buffer for every sample and transferred directly onto the middle of the column and incubated at RT for 15 min. After the incubation 350  $\mu$ l per sample of wash buffer 1 were added, the columns were centrifuged at 14000 xg and RT for 15 sec and the flow through discarded. Then, 500  $\mu$ l per sample of the provided wash buffer 2 were added, the columns were centrifuged at 14000 xg and RT for 15 sec and the flow through discarded. Afterwards, a washing step with 500  $\mu$ l of the provided washing buffer 2 followed, the

samples centrifuged at 14000 xg and RT for 15 sec and the flow through discarded. This step was repeated and the membrane dried by centrifuging the columns at 14000 xg and RT for 1 min. The columns were placed in collection tubes, 25 µl RNase-free water were added and incubated for 1 min and centrifugated at 14000 xg and RT for 3 min. Afterwards, the eluate was pipetted on top of the columns and the centrifugation step repeated. The isolated RNA was stored at -80 °C.

## 5.6. REVERSE TRANSCRIPTION

The isolated RNA was transformed into complementary DNA (cDNA) via reverse transcription. The RNA samples with a volume of 25 µl were defrosted on ice and 3.5 µl RNase-free water and 1µl random hexamer primer added. The mix was incubated in the PCR thermocycler at 70 °C for 5 min. Afterwards, the samples were stored on ice and the following components were added:

Table 16: cDNA components

<b>Components</b>	
5x reaction buffer	8.0 µl
dNTP mix 10 µM	2.0 µl
RevertAid reverse transcriptase	0.5 µl

After adding the components to the sample, it was carefully mixed and the following program performed on the PCR thermocycler.

Table 17: Thermocycling conditions

<b>Step</b>	<b>Temperature</b>	<b>Duration</b>
1	25 °C	10 min
2	42 °C	60 min
3	70 °C	5 min
4	4 °C	Hold

The cDNA was short term stored at -20 °C and long term at -80 °C.

## 5.7. PROBE-BASED QUANTITATIVE POLYMERASE CHAIN REACTION

Probe-based quantitative PCR (qPCR) was used for single gene expression analysis. It uses real-time fluorescence from 5'-3' exonuclease cleavage of a target-specific probe to measure DNA amplification at each cycle of a PCR. Primers were designed using the Universal ProbeLibrary Assay Design Center (Roche®). The cDNA samples with a volume of 40 µl were defrosted and 25 µl RNase-free water were added to a total volume of 65 µl. The primers were diluted to a

concentration of 10  $\mu\text{M}$  and mixed. As the probes are light sensitive, the exposure to light was avoided. The following mix was used for the qPCR.

Table 18: qPCR components

<b>Components</b>	
Primer mix	4 $\mu\text{l}$
RNase-free water	0.75 $\mu\text{l}$
Low ROX probe mastermix dTTP blue	10 $\mu\text{l}$
Probe	0.25 $\mu\text{l}$

7.5  $\mu\text{l}$  of this mix and 2.5  $\mu\text{l}$  of the cDNA were added per well of a 384-well plate. The plate was centrifuged and the following running conditions used.

Table 19: qPCR conditions

<b>Step</b>	<b>Temperature</b>	<b>Duration</b>
Initial denaturation	95 °C	10 min
40 cycles	95 °C	15 sec
	60 °C	1 min
Storage	4 °C	Hold

qPCR was performed on QuantStudio 6 Flex Real-Time PCR System and the results manually evaluated via Microsoft Excel.

## 5.8. IMMUNOHISTOCHEMISTRY

Immunohistochemistry with retinal sections, flatmounts and cultured flatmounts was performed to evaluate morphological changes.

### 5.8.1. IMMUNOHISTOCHEMISTRY OF RETINAL SECTIONS

The mice were euthanized and the eyes removed. Afterwards, the eyes were punctured on the anterior segments with a 23G needle and fixed in 4% PFA at RT for 5 min. A dissection microscope was used for the careful removal of the anterior eye segment and the vitreous. Afterwards, the eyes were fixed in 4% PFA at RT for 1 h and washed three times in PBS. After the washing steps the eyes were incubated in 30% sucrose at 4 °C overnight. Then, they were embedded in cryomatrix<sup>TM</sup> and sectioned into 10  $\mu\text{m}$  thick slices using a cryostat. Slices were stored at -20 °C until immunohistochemistry was performed. After thawing, the slices were washed three times with PBS and incubated with blocking solution (3% DMSO, 0.1% Triton X-100, 5% of goat or donkey serum diluted in PBS) at RT for 30 - 60 min. Afterwards, the slices were incubated with

the primary antibody diluted in blocking solution in a wet chamber at 4 °C overnight. The slides were washed three times with 1% BSA in PBS at RT for 10 min and incubated with their respective fluorescent secondary antibodies diluted in 1% BSA/PBS in a wet chamber at 4 °C overnight or at RT for 2 h. Afterwards, the slices were washed three times with PBS for 10 min and mounted using aqua-polymount. Experiments without the primary antibody served as negative controls. The stainings were observed and photographed using confocal microscopy. Stimulated emission depletion (STED) microscopy experiments were performed by Gabriela Jäger (stainings) and Dr. Kirsten Wunderlich (images).

### 5.8.2. IMMUNOHISTOCHEMISTRY OF FLATMOUNTS

The procedure is analogous to the staining of retinal sections with the following changes. The eyes were punctured on the anterior segments with a 23G needle and fixed in 4% PFA at RT for 5 min. After the careful removal of the anterior eye segment and the vitreous, the retina was separated from the sclera and four to six radial cuts were made in direction to the equator under a dissection microscope. Afterwards, the flattened retinae were fixed in 4% PFA at RT for 1 h, washed three times in PBS and transferred to a 48-well plate for staining. The retinae were incubated with blocking solution (2% BSA, 0,5% Triton X-100, 5% of goat or donkey serum diluted in PBS) at RT for 30 - 60 min. Afterwards, the slices were incubated with the primary antibody diluted in blocking solution in the 48-well plate covered with parafilm at 4 °C overnight (volume per well 150 µl). Then the wells were washed three times with 1% BSA in PBS at RT for 10 min and incubated with their respective secondary antibodies diluted in 1% BSA/PBS in the 48-well plate covered with parafilm at 4 °C overnight (volume per well 150 µl). The flatmounts were washed three times with PBS for 10 min and mounted using aqua-polymount. Z-stacks of the stainings were taken by a confocal microscope.

### 5.8.3. IMMUNOHISTOCHEMISTRY OF CLUTIVATED FLATMOUNTS

The culture medium was removed and the retinal explants were fixed directly on the membrane with 4% PFA at RT for 1 h. Afterwards, the wells were washed three times with PBS. During this process the flatmounts detached from the membrane. In the next step, the membranes were removed and the flatmounts incubated in 30% sucrose at 4 °C overnight. Afterwards, they were embedded in cryomatrix™ and sectioned into 10 µm thick slices using a cryostat. Slices were stored at -20 °C until immunohistochemistry was performed. After thawing, the same steps as described for the immunohistochemistry of retinal sections were performed. Z-stacks of the stainings were taken by a confocal microscope.

#### 5.8.4. QUANTIFICATION OF THE MORPHOLOGICAL STATE

For the quantification of cell numbers, pictures of slides or z-stacks of flatmounts of the central retina near the optic nerve were taken and cell numbers quantified using Fiji (Schindelin et al. 2012) and its cell counter and find maxima tool. The measurements of length or area was also done with Fiji (Schindelin et al. 2012).

#### 5.9. TRYPSIN DIGEST

To analyze the vascular architecture of the retina a trypsin digest-based protocol as described in Chou et al. 2013 was used. The eyes of the mice were collected and fixed in 4% PFA at 4 °C for 24 h before the retina was isolated. The cornea and lens were removed and the retina carefully separated from the sclera and choroid. Any debris or remaining tissue was discarded. The retinae were placed in a 24-well plate and washed four to five times slightly shaking with sterile water at RT for 30 min. The retinae were left in water on the shaker at RT overnight. The water was removed and the retinae digested with 3% trypsin in 0.1 M Tris buffer gently shaking at 37 °C for 1.5 h. Trypsin was exchanged by sterile water and the internal limiting membrane removed. Afterwards, the retinal vasculature was separated from the remaining tissue via a series of 5 min water washing steps. When no or only little debris was left, the vasculature was carefully manipulated under a dissection microscope and subsequently moved to a microscope slide via a trypsin coated, fire polished glass pipette. After drying on a heating plate at 37 °C overnight a hematoxylin and eosin (H&E) staining following the instructions of the kit was performed to visualize the vasculature, endothelial cells and pericytes. As a last step it was mounted with aqua-polymount on the slide. After hardening the finalized vasculature was examined using an upright motorized fluorescence microscope.

#### 5.10. ANALYSIS OF VASCULATURE

The cell numbers of endothelial cells, pericytes and acellular capillaries were established via the cell counter plugin of Fiji (Schindelin et al. 2012). Pericytes and endothelial cells were identified by their characteristic morphology. Endothelial cell nuclei are elongated and positioned in the center of the vessel. Pericyte nuclei are more spherical in shape, their staining is denser and they are sitting on the capillary wall. The calculation of the endothelial cell/pericyte ratio is also described by Midena et al. 1989.

## 5.11. WESTERN BLOT

Gels with an acrylamide concentration of 12% were used for sodiumdodecylsulfate-polyacrylamide gel electrophoresis (SDS-PAGE). For two separating gels the following components were mixed:

Table 20: Separating gel solution SDS-PAGE

Components	
Distilled water	7 ml
30% Acrylamide solution	8 ml
4x Resolving buffer	5 ml
10% APS	200 $\mu$ l
TEMED	20 $\mu$ l

The liquid mixture was immediately filled into two gel casting molds and covered with isopropanol. When the gels were solid, the isopropanol was removed and the stacking gel mixed.

Table 21: Stacking gel solution SDS-PAGE

Components	
Distilled water	4.2 ml
30% Acrylamide solution	0.65 ml
4x Stacking buffer	1.6 ml
10% APS	67 $\mu$ l
TEMED	6.7 $\mu$ l

The liquid mixture was immediately filled into the two molds and the comb put into the gel. When the gels were solid, they were directly used or short-term stored in a wet chamber at 4 °C. The samples were mixed with 5x SDS-PAGE sample buffer, incubated at 95 °C for 10 min and loaded onto the gel next to the prestained protein™ ladder plus. The electrophoresis was accomplished at 60 V for 45 min and at 150 V for 70 min. Afterwards, a Western blot was performed with a Trans blot Turbo™ machine transferring the proteins to a 0.22  $\mu$ m PVDF membrane by blotting at 24 V for 35 min. The membrane containing the proteins was blocked in 5% BSA in TBST at RT for 1 h to avoid unspecific binding of the antibodies. The expected size of GR was 95 kDa and of the phosphorylated GR 86 kDa. PDHB was used as a housekeeper because it is represented on a similar level in all retinal cell types. As it expected size was 35 kDa and the molecular weight of the Phospho-/GR was 86/95 kDa, the membranes were cut into two pieces at the 70 kDa band of the standard. The membrane pieces were shaking in the primary antibody at 4 °C overnight.

On the next day they were washed three times in TBST for 10 min and incubated with the secondary antibody in 5% BSA in TBST at RT for 2 h. Next, they were washed three times in TBST for 10 min. The Clarity Max™ Western ECL Substrate Kit was used and the bands visualized using the ChemiDoc XRS+ system. GelAnalyzer was used for the quantification of the bands.

### 5.12. RNA SEQUENCING

The sample preparation for RNA seq of four different retinal cell types of diabetic and control mice was done by Prof. Dr. Antje Grosche and Dirkje Felder. RNA was extracted from enriched microglia, endothelial cells, Müller cells and neurons isolated from three db/db and control mice of 12 or 24 weeks of age. A paired-end RNA seq (coverage depth: 25-45 million reads per sample) was performed. Statistical analysis and bioinformatics were conducted in R (R Core Team 2014). Dr. Felix Grassmann processed and analyzed the received raw data. Furthermore, Lew Kaplan performed principal component analysis (PCA) and identified genes that were differentially expressed between genotypes (t-test  $P < 0.05$ ) and were enriched in Müller cells compared to the flow through. For better visualization each gene value was log-transformed and normalized to its median across all samples from which then a heatmap was generated (Kolde 2019). The principle component analysis was performed on the log-transformed FPKM values and plotted using the factoextra package (Kassambara and Mundt 2020). Pathway enrichment analysis focusing on molecular functions was done via the open-access program PANTHER (Thomas et al. 2003).

### 5.13. PROTEOMICS

Label-free liquid chromatography mass spectrometry was done for proteome analysis. Proteomics was done for two different approaches in this thesis.

First, a proteome analysis of four different retinal cell types of diabetic and control mice was performed. MACS enriched retinal cell types from four control and diabetic mice at 24 weeks of age were collected by Prof. Dr. Antje Grosche and Dirkje Felder. Sample processing, mass spectrometry and data analysis was performed by the Research Unit Protein Science. The detailed method is described in Pauly et al. 2019. Liquid chromatography-tandem mass spectrometry analysis was performed on a Q-Exactive HF mass spectrometer coupled to an Ultimate 3000 RSLC nano-HPLC. Full scan MS spectra (from  $m/z$  300 to 1500) and MS fragment spectra were acquired in the Orbitrap with a resolution of 60,000 or 15,000. Up to ten most intense ions were identified depending on signal intensity (TOP10 method). Spectra were analyzed, exported and used for peptide identification in the UniProtKB/Swiss-Prot taxonomy mouse database. For quantification, the total cumulative normalized abundance was calculated. Statistical analysis was done by Lew Kaplan using R (R Core Team 2014). A principal component analysis of the proteomics data was

performed and a heatmap which was focusing on proteins differentially regulated in Müller cells of diabetic mice generated by filtering  $P < 0.05$  and at least twofold difference (Kolde 2019; Kassambara and Mundt 2020). Pathway enrichment analysis for molecular functions was done via the open-access program PANTHER (Thomas et al. 2003).

Second, the effect of cortisol treatment on retinal explants was investigated by proteome analysis. Six retinae per group (untreated, cortisol treated) were evaluated. Cultivation of retinal explants with and without cortisol is described in **chapter 5.17**. Sample processing, mass spectrometry and data analysis was performed by the Research Unit Protein Science. It was done in the same way as described before. A PCA of the proteomics data was performed and a heatmap generated by filtering  $P < 0.05$  and at least 1,3-fold difference. Pathway enrichment analysis for molecular functions was done via the open-access program PANTHER (Thomas et al. 2003).

#### 5.14. COMPARISON OF THE TWO OMICS DATA SETS

Since proteomic as well as transcriptomic data from 24-week-old db/db and wild-type mice in an analogous manner were acquired, I was interested in investigating how well changes in transcript were translated to changes in protein. The analysis, performed by Lew Kaplan, started with the determination of glia specific genes and proteins. Briefly, FPKM or normalized abundance values were log-transformed, before a t-test between the respective glial and flow through values was calculated. Only genes/proteins with  $P < 0.05$  and a glia:flow through ratio of twofold were considered to be glia-specific. The final comparison encompassed genes/proteins that were glia-specific in at least one of the two datasets and detected in both. Further, the ratios between the respective wild-type and mutant 24-week-old animals for each dataset were calculated to directly compare the inter-genotype differences between datasets. Finally, a spearman correlation coefficient was calculated. This analysis and the corresponding scatter plots were done using the R programming language (R Core Team 2014).

#### 5.15. ELECTRORETINOGRAM

ERG was performed to test the retinal light responsiveness. The recordings were done in cooperation with Prof. Susanne Koch. The mice were dark adapted overnight and the ERG measurements performed in the morning under dim red light illumination. The mice were weighted and anesthetized with 100 mg/kg ketamine and 5 mg/kg xylazine by i.p. injection. The pupils of the mice were fully dilated with 0.5% tropicamide-phenylephrine 2.5% eye drops. The mice were lying on a heating mat with 37 °C and two reference electrodes positioned subcutaneously (on the head and base of the tail). Espion ERG Diagnosys equipment was used for the simultaneously recordings of both eyes. The eyes of the mice were covered with Methocel® 2% eye drops during

the measurement and electrodes placed on the cornea. Rod-driven responses were measured and quantified at scotopic light conditions (0.001 cd/ms<sup>2</sup>). Furthermore, mixed (rod- and cone-driven) responses were analyzed by applying light flashes of 3 cd/ms<sup>2</sup>. Whereas, cone-driven light responses (30 cd/ms<sup>2</sup>) were recorded after 5 min of light adaption. Analysis of the data was done by using the Espion V6 software. The a-wave amplitude was measured from baseline to the trough of the a-wave. The b-wave amplitude was calculated from the trough of the a-wave to the peak of the b-wave.

#### 5.16. MEASUREMENT CORTICOSTERONE LEVEL

The corticosterone ELISA Kit from Abcam was used for the measurement of the corticosterone level of the blood plasma of five 24-week-old diabetic and control mice. The experiment was performed following the protocol of the manufacturer. The blood of the mice was collected in blood collection tubes and centrifuged at 3000 xg and 4 °C for 10 min and stored at -20 °C. The blood plasma samples were used in a 1:100 dilution for the ELISA.

#### 5.17. CULTIVATION OF RETINAL EXPLANTS

Retinal explants of wild-type mice were cultivated for two or five days and cortisol was added twice a day to maintain a constantly high concentration. The experiments were done together with Farhad Ghaseminejad as follows: The mice were euthanized and the eyes removed. Afterwards, the eyes were punctured on the anterior segments with a 23 G needle and the anterior eye segment and the vitreous removed. The retina was separated from the sclera and four to six radial cuts were made in direction to the equator under a dissection microscope. A 24-well plate was used for the cultivation. Each well was filled with 500 µl medium (DMEM/F-12, GlutaMAX™, 1:100 Antibiotic-Antimycotic) and a Whatman® nuclepore™ track-etched membrane placed in each well. The retinae were positioned in the center of the membrane and covered with a drop of medium. The retinal explants were cultivated in an incubator with 37 °C and 5% CO<sub>2</sub>. The medium was changed every day in the evening and supplementary cortisol added every morning to maintain a constantly high concentration of 500 ng/ml. Western blot, qPCR and a proteomic analysis via mass spectrometry were performed with two-day-cultivated explants. To check for effects of a longer-term cortisol stimulation, retinal explants of wild-type mice were cultivated for five days and immunohistochemistry was performed.

#### 5.18. ADENO-ASSOCIATED VIRUS ADMINISTRATION

The mice were weighted and anesthetized with 100 mg/kg ketamine and 5 mg/kg xylazine by i.p. injection. During the anesthesia the mice were lying on a heating mat with 37 °C. After the pupils

of the mice were fully dilated with 0.5% tropicamide-phenylephrine 2.5% eye drops, AAV particles ( $5 \times 10^{13}$  GC/ml) or PBS (sham control) were administered. Two different injection systems from Hamilton and WPI were used. For intravitreal injections with the Hamilton syringe it was necessary to generate a hole with a 27G needle where the Hamilton injection needle was inserted. The NanoFil™ from WPI uses the same needle for entering the eye and injecting the AAV. 1  $\mu$ l was injected in the eyes of 12-week-old control mice with the Hamilton system and 2  $\mu$ l with the WPI system. Methocel® 2% eye drops were applied to the eyes of the mice after injection. The mice were kept on the heating mat until they were completely awake from the anesthesia. 12 weeks post injection, morphometric analysis and ERG measurements were performed.

#### 5.19. STATISTICAL ANALYSIS

The data were analyzed with GraphPad PRISM 8 and reported as mean  $\pm$  standard error (SEM). Differences among groups were determined using the ANOVA or student t-test. Identification of outliers was also performed with GraphPad PRISM 8.

## 6. RESULTS

The db/db (Lepr<sup>db</sup>) mouse, a model for T2D, was used as an animal model for DR. The phenotype of these mice is described in **chapter 2.7**. To validate data from the literature and further characterize this DR mouse model, a morphometric analysis was performed on eyes from db/db and control animals at 12, 24 and 38 weeks of age. Samples for the RNA seq experiment were collected from db/db mice and controls with an age of 12 and 24 weeks. The analysis of the proteome and ERG measurements were done on 24-week-old animals (**Figure 6**).

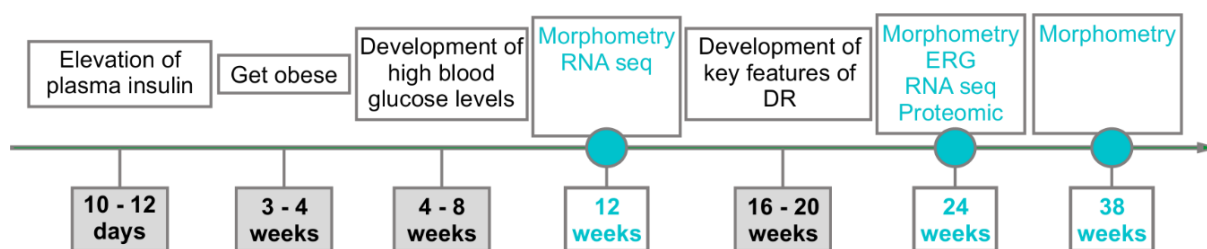


**Figure 6. The db/db mouse as an animal model for diabetic retinopathy.** Timeline of the development of features of type 2 diabetes and diabetic retinopathy in the db/db mouse model. Time points of data collection are highlighted in turquoise.

### 6.1. CHARACTERISATION OF THE ANIMAL MODEL

Although the db/db mouse is a well-established animal model, I wanted to define the status of DR progression in our breeding and define the morphological and functional changes in the retina due to T2D.

#### 6.1.1. UNALTERED CELL NUMBERS OF THE DIFFERENT RETINAL LAYERS IN DIABETIC MICE

First, I analyzed the cell numbers of the GCL, INL and ONL, since Tang et al. 2011 described retinal thinning in diabetic mice. DAPI-staining of eye cryosections from db/db and control animals with different ages were performed and cell numbers were determined for the three nuclear layers of the retina. No significant change of the cell numbers in the GCL, INL and ONL of the retina from db/db and control animals could be detected (**Figure 7**).

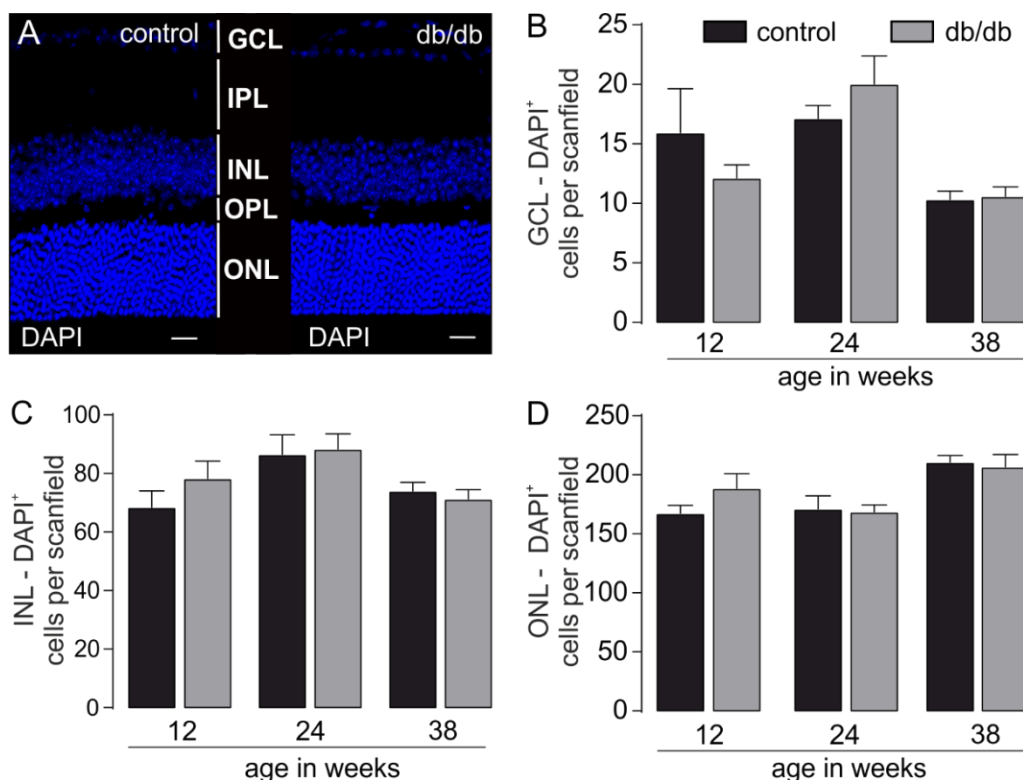


**Figure 7. Unaltered cell numbers of the different retinal layers in diabetic mice.** (A) Representative micrograph of a DAPI-staining of the retina of a diabetic and a control mouse 38 weeks of age. Scale bar, 20  $\mu$ m. Cell counts of the (B) ganglion cell layer, the (C) inner nuclear layer and of the (D) outer nuclear layer of retinæ from db/db (grey bars) and control (black bars) animals are plotted. Bars represent the mean  $\pm$  SEM from n=3-4 animals. Scanfield: 68  $\mu$ m x 200  $\mu$ m (whole thickness of the retina). GCL: Ganglion cell layer, IPL: Inner plexiform layer, INL: Inner nuclear layer, OPL: Outer plexiform layer, ONL: Outer nuclear layer.

### 6.1.2. UNALTERED NUMBERS OF CALRETININ-POSITIVE CELLS IN DIABETIC MICE

Results from DAPI-based cell counts in the inner retina were validated by the quantification of calretinin-positive cells in the GCL and INL in retinæ from diabetic and healthy mice (**Figure 8**). Calretinin is typically expressed by ganglion and displaced amacrine cells in the GCL, while it is specifically localized to amacrine cells in the INL (Lee et al. 2010; Lee et al. 2016) (**Figure 8A**). The number of calretinin-positive cells in both the GCL (**Figure 8B**) and the INL (**Figure 8C**) were not found to be significantly different between the db/db and the non-diabetic animals.

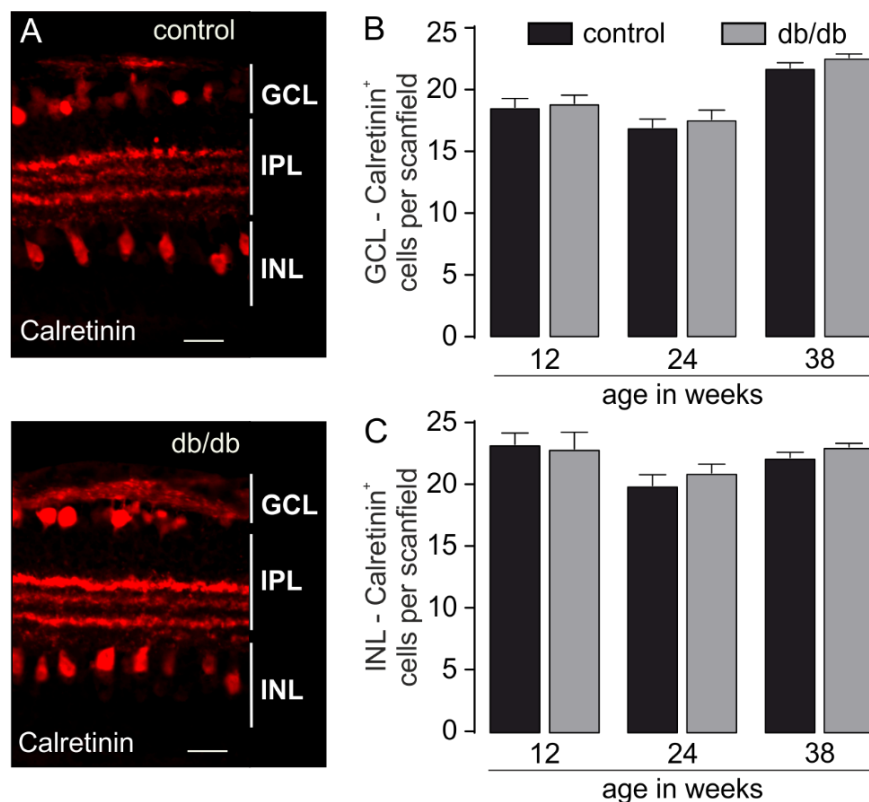


**Figure 8: Unaltered number of calretinin-positive ganglion and amacrine cells in diabetic mice. (A)** Representative micrographs of a calretinin staining of the retinae from a 38-week-old diabetic and a control mouse. Scale bar, 20  $\mu$ m. Numbers of calretinin-positive cells per scanfield of the **(B)** ganglion cell layer and the **(C)** inner nuclear layer of the retinae from db/db and control animals, respectively. Bars represent the mean  $\pm$  SEM from n=3-4 animals per group. Scanfield: 200  $\mu$ m x 200  $\mu$ m (whole thickness of the retina). GCL: Ganglion cell layer, IPL: Inner plexiform layer, INL: Inner nuclear layer.

### 6.1.3. ONSET OF CONE DEGENERATION IN AGING DIABETIC MICE

Rods and cones mediate phototransduction and are prone to degenerative processes in multifactorial diseases like DR (Kern and Berkowitz 2015). Therefore, the number of cones and the outer segment length of both photoreceptor types were analyzed to identify early signs of change. Cone-arrestin (**Figure 9A**) and PDE6B (**Figure 9D**) stainings were used to discriminate cones and rods, respectively. While the outer segment length of rods did not differ between control and diabetic mice (**Figure 9E**), outer segments of cones were significantly shorter in 38-week-old diabetic animals when compared to controls (**Figure 9C**). Furthermore, the total number of cones per scanfield was significantly reduced (**Figure 9B**). These results indicate that the progression of neurodegenerative processes as one hallmark of DR is rather slow in our db/db model, given that significant morphological changes occur late, namely not before 38 weeks of age.

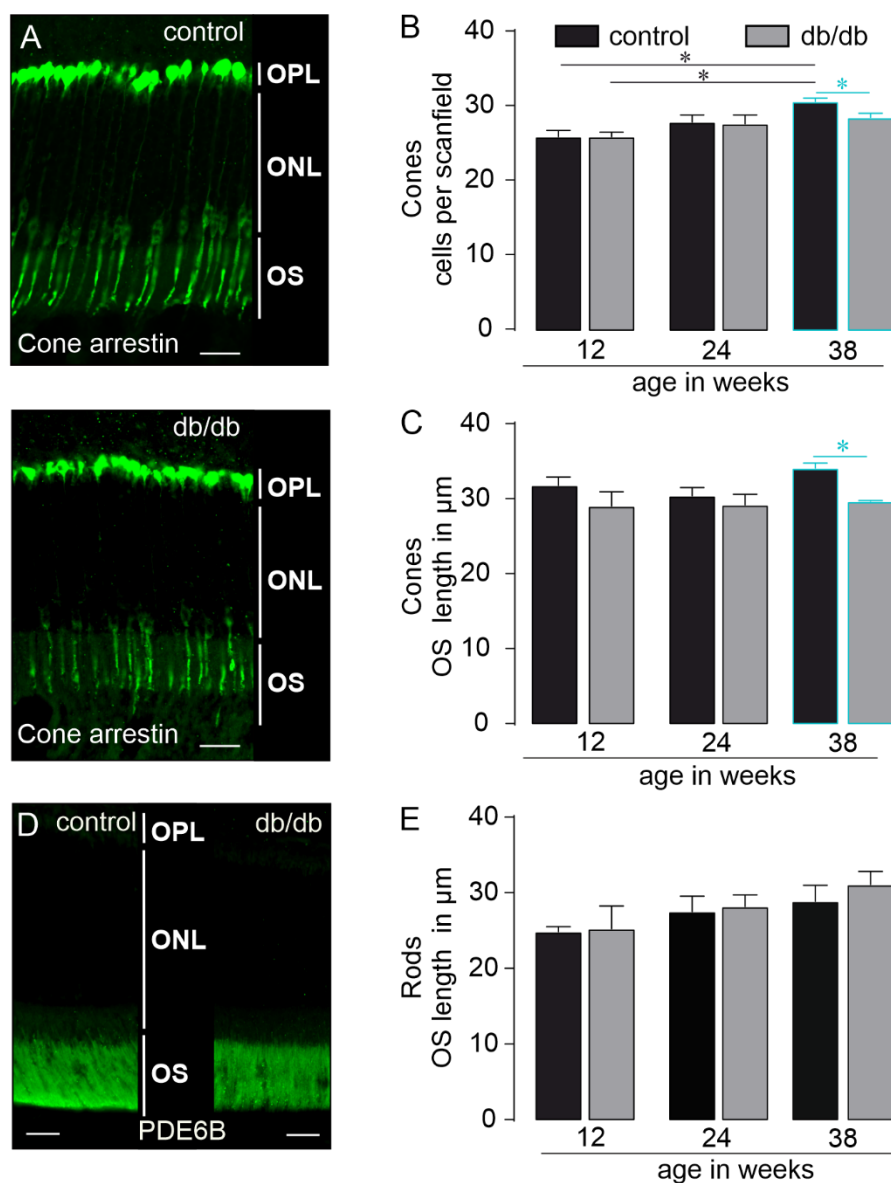


**Figure 9: Onset of cone degeneration in aging diabetic mice.** (A) Representative micrographs of cone-arrestin stainings from 38-week-old diabetic and control mice. Scale bar, 20 µm. (B) Cone numbers were quantified of retinæ from diabetic and control animals. Scanfield: 200 µm x 200 µm (whole thickness of the retina). (C) The length of cone outer segments (OS) of the retinæ from db/db and control animals was measured. (D) Representative micrograph of a PDE6B staining (rods) from 38-week-old old diabetic and control mice. Scale bar, 20 µm. (E) The rod OS length of retinæ from db/db and control animals was measured. Bars represent mean ± SEM and data from n=3-4 animals per age and genotypes. OPL: outer plexiform layer, ONL: Outer nuclear layer, OS: outer segments. \*P<0.05.

#### 6.1.4. DEFECTS OF THE VASCULAR SYSTEM IN DB/DB MICE

As the microvascular system is affected by diabetes and vascular changes are hallmarks of the DR pathogenesis, it was investigated in db/db mice (Shin et al. 2014).

#### 6.1.4.1. PERICYTE LOSS IN DIABETIC MICE

The loss of pericytes is one of the key features of DR which was also detectable in db/db animals starting at the age of 12 weeks (Midena et al. 1989). To validate this feature, the number of platelet-derived growth factor receptor beta (PDGFR $\beta$ )-positive pericytes from db/db and control animals was quantified (**Figure 10**). In diabetic mice, a decreasing number of pericytes was observed starting at 24 weeks of age which was even more pronounced in 38-week-old db/db mice (**Figure 10**). This age-dependent loss of pericytes was not observed in wild-type controls at any age investigated. A significantly lower number of pericytes was observed in db/db mice compared to wild-type controls in 38-week-old animals.

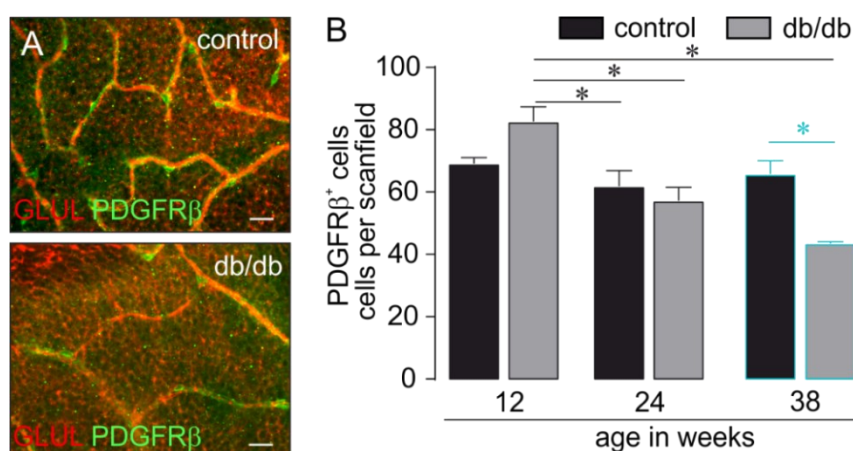


**Figure 10: Loss of pericytes in diabetic mice.** (A) Representative micrograph staining of platelet-derived growth factor receptor beta (PDGFR $\beta$ , green) and glutamine synthetase (GLUL, red) of retinal flatmount preparations of diabetic and control mice with an age of 38 weeks. Scale bar, 20  $\mu$ m. (B) PDGFR $\beta$ -positive cells were counted per scanfield (410  $\mu$ m x 298  $\mu$ m) of the retinae from diabetic and control animals. Bars represent mean  $\pm$  SEM from n=3-6 animals per group. \*P<0.05.

#### 6.1.1.1. VASCULAR HALLMARKS OF DIABETIC RETINOPATHY IN AGING DIABETIC MICE

Utilizing H&E-stained trypsin-digested retinal flatmounts, I further analyzed alterations of the microvascular system and confirmed the findings of vascular changes, such as the observed pericyte loss (**chapter 6.1.4.1**). Confocal scan images from respective flatmounts of 12 and 24-week-old db/db animals and controls (**Figure 11A**) were used to quantify acellular capillaries (devoid of pericytes and endothelial cells) (**Figure 11B**). Subsequently, the endothelial cell/pericyte ratio was calculated (**Figure 11E**). There was no difference in the number of acellular capillaries between diabetic and non-diabetic animals at any age (**Figure 11B**). However, a significant rise in the endothelial cell/pericyte ratio was calculated for 24-week-old diabetic animals compared to controls (**Figure 11E**). This was due to slightly higher endothelial cell numbers in db/db mice with a concomitant decrease in pericytes (**Figure 11C-D**).

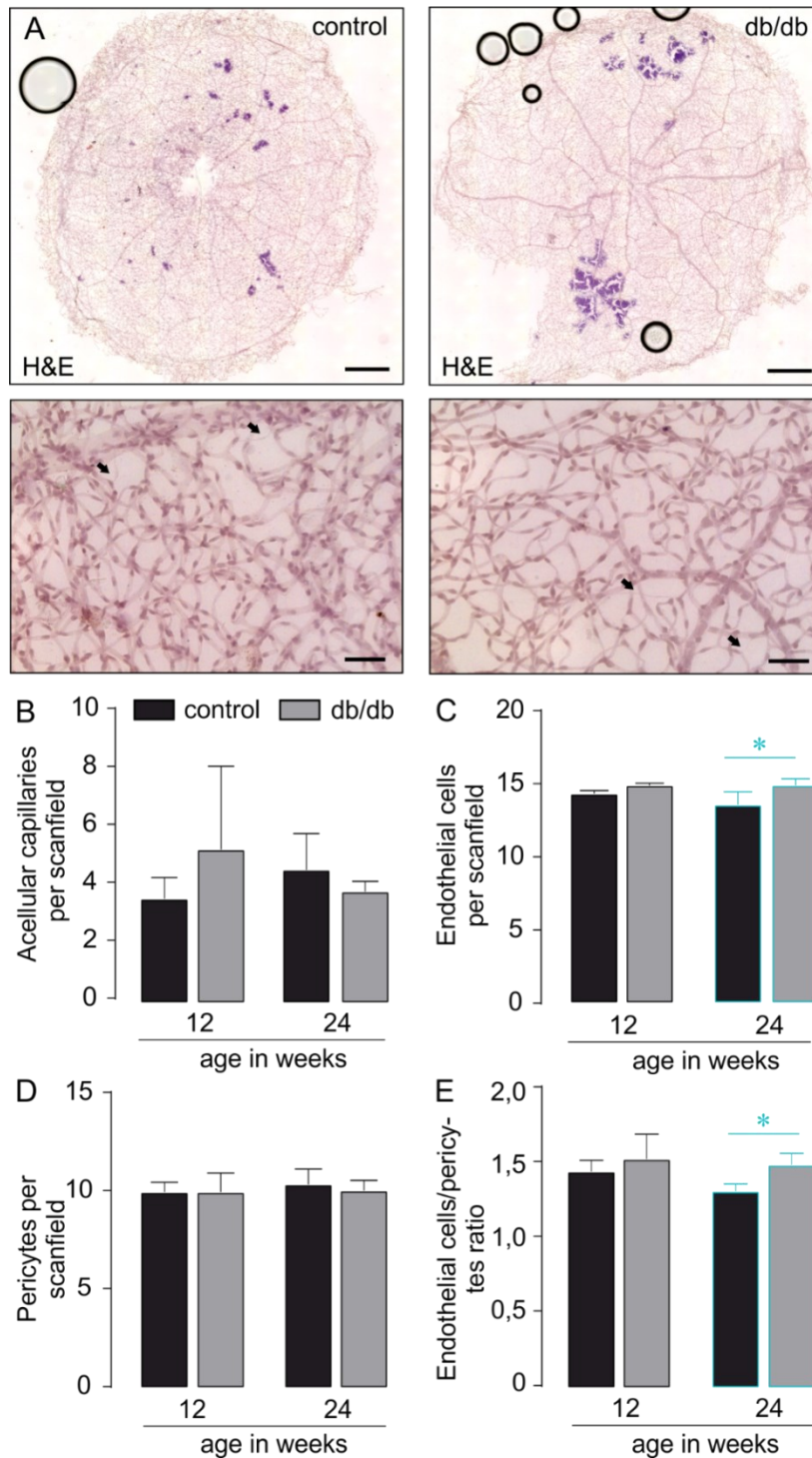


**Figure 11: Recapitulation of vascular hallmarks of diabetic retinopathy in 24-week-old diabetic mice.** (A) Representative images of a hematoxylin and eosin (H&E) staining of trypsin-digested retinæ from diabetic and control mice 24 weeks of age. The arrows point at acellular capillaries. Scale bar: top panel, 500  $\mu$ m; bottom panel, 50  $\mu$ m. (B) Acellular capillaries per scanfield were quantified in trypsin-digested flatmounts of db/db and control animals with an age of 12 and 24 weeks. No differences were detected. (C) The endothelial cell number from db/db and control animals with an age of 12 and 24 weeks was calculated based on cell counts per scanfield. (D) The pericyte cell number from db/db and control animals with an age of 12 and 24 weeks was calculated basing on cell counts per scanfield. (E) The endothelial cells/pericytes ratio of the vasculature from db/db and control animals with an age of 12 and 24 weeks was calculated based on cell counts per scanfield. Scanfield: 100.05  $\mu$ m x 100.05  $\mu$ m. Bars represent the mean  $\pm$  SEM from results of n=3-4 animals per group. \*P<0.05.

## 6.1.5. ONSET OF MICROGLIAL ACTIVATION IN DIABETIC MICE

Microglia are resident immune cells of the retina which are highly sensitive to external factors and morphological changes occur when the cells get activated (Rashid et al. 2019). The number of IBA-positive microglia/macrophages from db/db and control animals was evaluated to explore the role of neuroinflammation in our disease model (**Figure 12**). No significant difference in the number of IBA-positive cells per scanfield was detected at any age investigated between genotypes (**Figure 12C**). Additionally, I determined the area occupied by the finely branched microglial processes, which is typically reduced upon gliotic activation. There was a tendency of smaller microglial ‘territories’ in db/db mice as compared to controls (**Figure 12B**), although it did not reach significance levels. Moreover, the microglial soma area in the 38-week-old diabetic animals was significantly bigger than that of age-matched control mice, suggesting more evidence towards initiation of microglial activation (Gaucher et al. 2007) (**Figure 12D**).

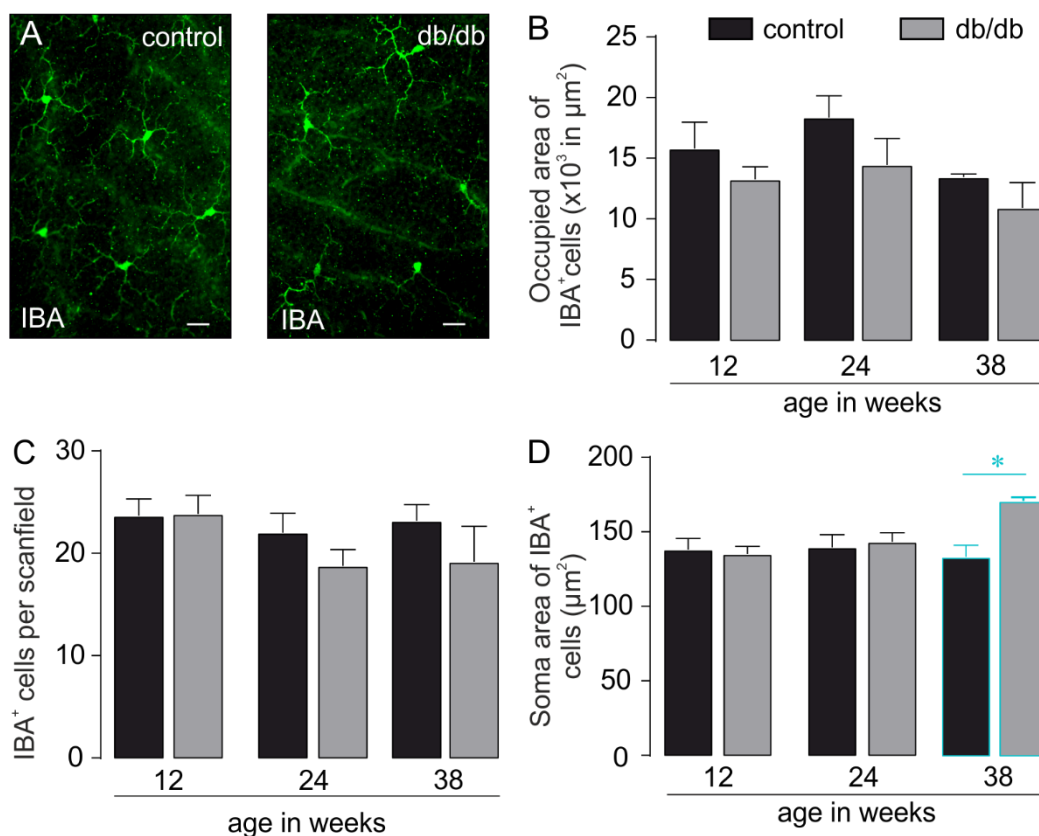


**Figure 12: Mild signs of microglia activation in db/db mice.** (A) Representative micrograph of IBA stainings of retinal flatmounts from 38-weeks-old diabetic and control mice. Scale bar, 20  $\mu\text{m}$ . (B) The area occupied by the fine network of microglial processes from each cell was determined in retinal flatmounts from diabetic and control animals. (C) IBA-positive cells were quantified per scanfield. Z-scans through the whole thickness of the retina were performed and cells across all retinal layers were counted. (D) The soma area of each microglia in a scan field was measured as an indicator of beginning microglial activation. Scanfield: 410  $\mu\text{m}$  x 298  $\mu\text{m}$ . Bars represent mean  $\pm$  SEM and comprise data from 3-6 animals per age and genotype. \*P<0.05.

In conclusion, I detected mild signs of microglial activation that support the assumption that neuroinflammation is ongoing and potentially contributing to disease progression in db/db mice.

#### 6.1.6. REDUCED LIGHT RESPONSIVENESS OF RETINAE FROM DB/DB MICE

Having investigated morphological features of retinæ from db/db mice, I ultimately aimed to address the effects of diabetes-associated alterations on the functional integrity of the retinal tissue. To this end, ERG recordings were conducted to examine retinal light responsiveness. These experiments were performed on 24-week-old animals of both genotypes – a time point where major anatomical changes have not yet been observed, but initial changes of the microvascular system (**Figure 11**) and microglial activity (**Figure 12**) could be detected.

The rod-driven b-wave amplitude measured under scotopic conditions was significantly smaller in diabetic mice than in their control counterparts (**Figure 13A**). Similarly, a significant reduction of the cone-driven b-wave was observed (**Figure 13B**).

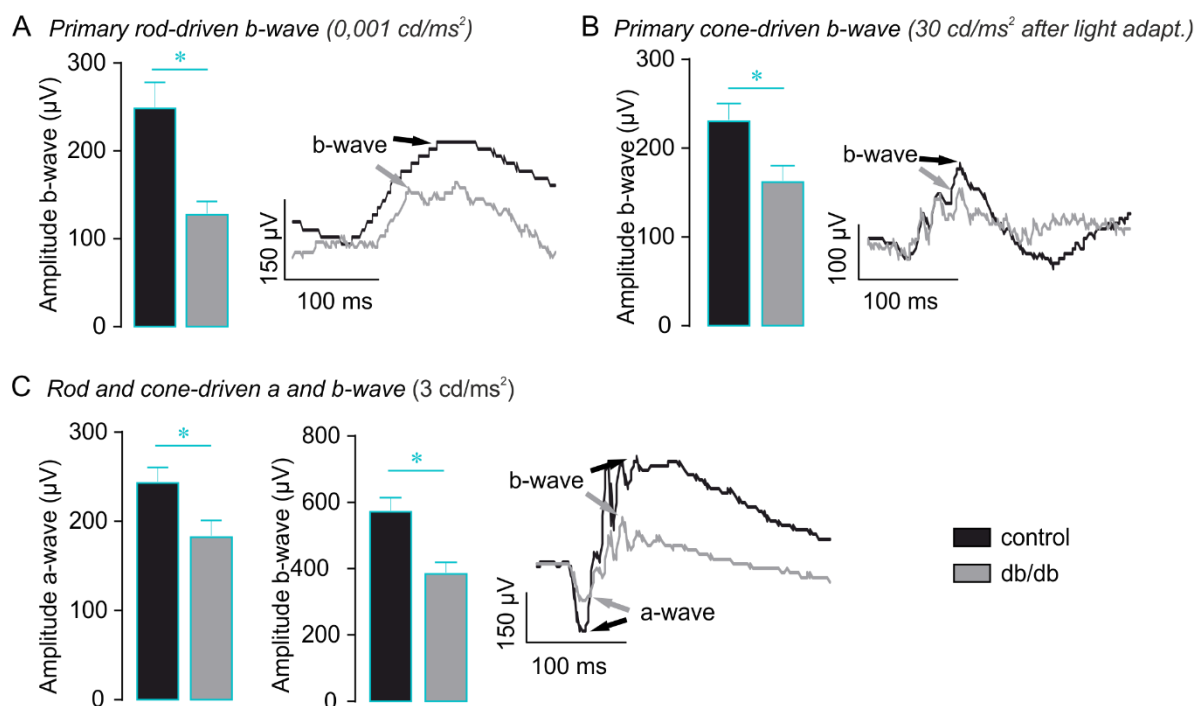


**Figure 13: Reduced light responses in the electroretinogram of retinæ from 24-week-old diabetic mice.** (A) *Left*, rod-driven responses (b-wave) were measured and quantified at scotopic light conditions (0,001 cd/ms<sup>2</sup>) in diabetic and control mice. Note the significant reduction of the b-wave amplitude in db/db mice. *Right*, representative traces of responses measured in mice of the respective genotypes. (B) *Left*, the cone-driven light responses (b-wave, 30 cd/ms<sup>2</sup>) were recorded after 5 min of light adaption. B-wave amplitudes were significantly smaller in db/db mice compared to that of controls. *Right*, representative traces of cone-driven responses measured in mice of the respective genotypes. (C) *Left*, Mixed (rod- and cone-driven) responses were analyzed by applying light flashes of 3 cd/ms<sup>2</sup> to eyes of diabetic and control mice. A- and b-wave amplitudes were significantly smaller in db/db mice compared to that of controls. *Right*, representative traces of cone and rod-driven responses measured in mice of the respective genotypes. Bars represent mean values  $\pm$  SEM n=11 individual mice were measured per group. \*P<0.05.

Accordingly, also the mixed responses (cones and rods) amplitudes were significantly reduced in diabetic mice – for both a- and b-waves (**Figure 13C**).

In conclusion, the ERG measurements confirmed the results reported by Bogdanov et al. 2014, who detected a-wave abnormalities in the ERGs recorded from diabetic animals with an age of 16 and 24 weeks.

Some phenotypes of the diabetes like cognitive deficits and neurovascular dysfunctions are stronger in male animals (Fan et al. 2018) and it is known that the life span of males is reduced compared to female db/db mice (Sataranatarajan et al. 2016). As both sexes suffer from DR, I wanted to identify a readout method that represents the effects of diabetes for both sexes. Therefore, I analyzed the ERG of female and male diabetic and control mice with an age of 24 weeks (**Figure 14**).

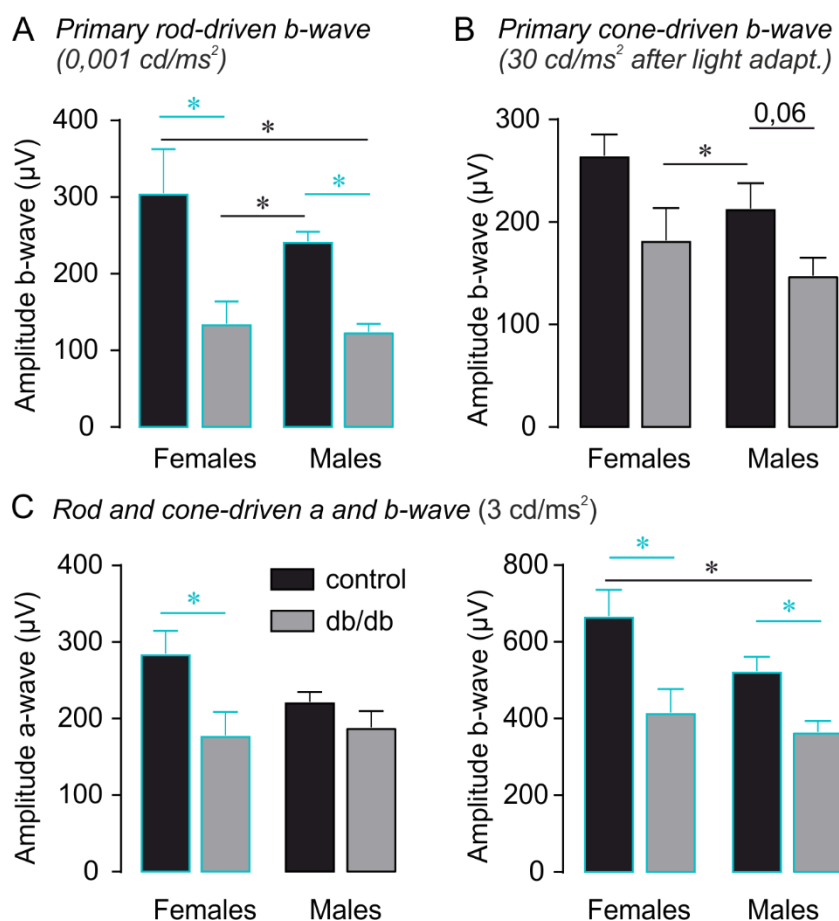


**Figure 14: No major sex-specific differences in the light responses of diabetic mice. (A)** Rod-driven responses (b-wave) were measured and quantified at scotopic light conditions (0,001 cd/ms<sup>2</sup>) in 24-week-old diabetic and control mice. Note the significant reduction of the b-wave amplitude in male and female db/db mice. **(B)** Cone-driven light responses (b-wave, 30 cd/ms<sup>2</sup>) were recorded after 5 min of light adaptation. **(C)** Mixed (rod- and cone-driven) responses were analyzed by applying light flashes of 3 cd/ms<sup>2</sup> to eyes of diabetic and control mice. A- and b-wave amplitudes were significantly smaller in female db/db mice compared to that of controls. Bars represent mean values ± SEM. females n=4-5. males n=6-7. \*P<0.05.

The rod-driven b-wave amplitude measured under scotopic conditions was significantly smaller in female and male diabetic mice than in their control counterparts (**Figure 14A**). Similarly, a decreasing trend of the cone-driven b-wave was observed for both sexes (**Figure 14B**). Accordingly, the mixed responses (cones and rods) b-wave amplitude was significantly reduced in female and male diabetic mice (**Figure 14C**). However, the mixed responses (cones and rods) a-wave amplitude was only significantly reduced in female 24-week-old diabetic mice. Evidently, ERG can be utilized as a highly sensitive readout, because it sensitively delineates functional changes even before major morphological/anatomical signs of retinal degeneration become detectable and is able to identify differences in both sexes.

## 6.2. THE TRANSCRIPTOME OF 12- AND 24-WEEK-OLD DIABETIC MICE

A transcriptome analysis of diabetic and control mice was performed to shed light on the molecular processes in Müller cells during DR progression. Therefore, four different retinal cell types (microglia, vascular cells, Müller cells and neurons) were isolated from three db/db and control mice at 12 and 24 weeks of age, using MACS. RNA was then extracted and sequenced to a depth of 25-45 million reads per sample. The gene expression of marker genes of the four different cell types implicated a successful enrichment of the respective cell population (**Figure 15A**). glutamine synthetase (*Glul*) is a well-established marker for Müller cells, rhodopsin (*Rho*) is a neuronal marker, integrin subunit alpha M (*Itgam*) is a microglia marker and platelet and endothelial cell adhesion molecule 1 (*Pecam1* or *CD31*) is an endothelial marker. Microglia and vascular cells showed a mild contamination with Müller cells considering the rather high *Glul* expression. Moreover, irrespective of sorting out *CD31*-positive cells (primarily endothelial cells), a rather high expression of *Pecam1* was found in the Müller cell fraction indicating its minor contamination with vascular cells. PCA revealed that samples from each of the four different cell types were separated, indicating that the cell identity outweighs expression changes as a result of aging or diabetes-associated changes (**Figure 15B**). Hence, I primarily focus on expression changes of Müller cells after the onset of DR, comparing genes which were regulated specifically in Müller cells in 24-week-old diabetic mice to the control group. The genes which were at least twofold up- or downregulated were identified and plotted in a heatmap (**Figure 15C**). Furthermore, a pathway enrichment analysis on significantly up- or downregulated genes was performed via PANTHER (Thomas et al. 2003) (**Figure 15D-E**). I found 199 genes which were down- and 128 genes that were upregulated in Müller cells of db/db mice. Pathways related to the cytoskeleton, RNA and protein binding and potassium channel activity were found to be enriched if checking for the downregulated candidate gene list (Figure 16D). In contrast, genes associated with pathways related to growth factor signaling and ion binding were upregulated in diabetic mice (**Figure 15E**).

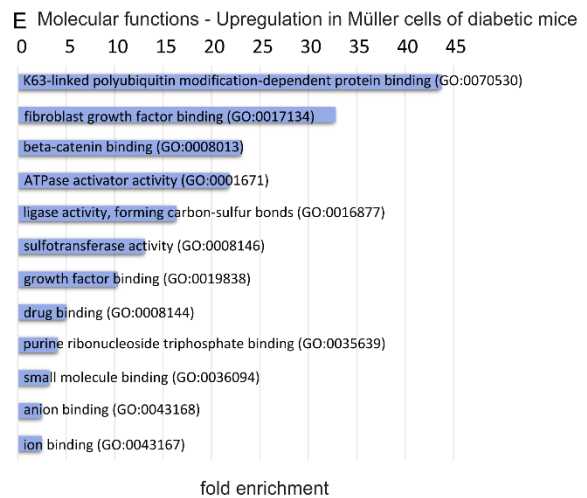
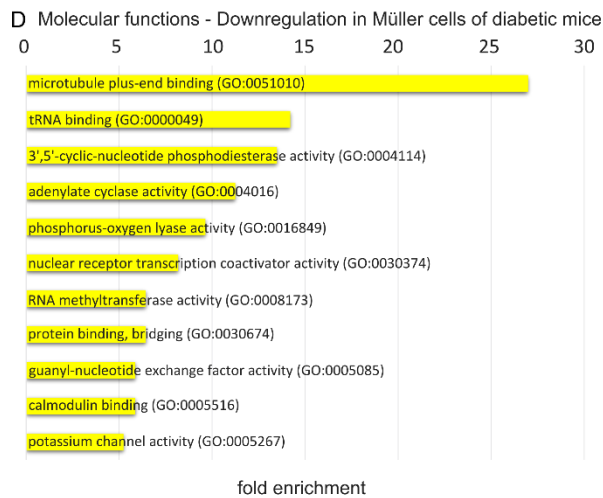
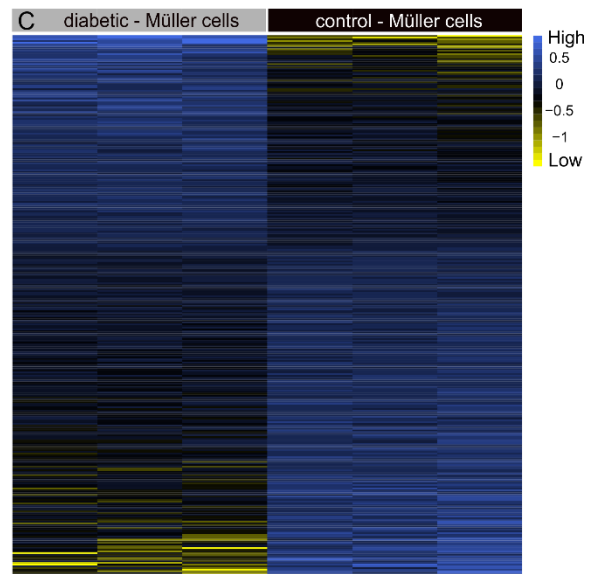
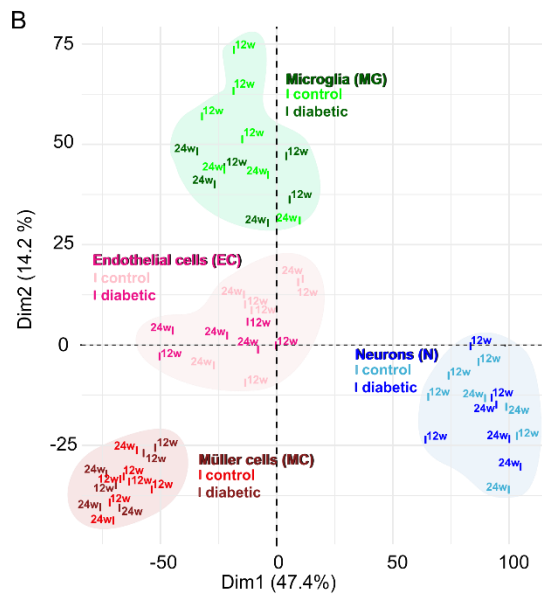
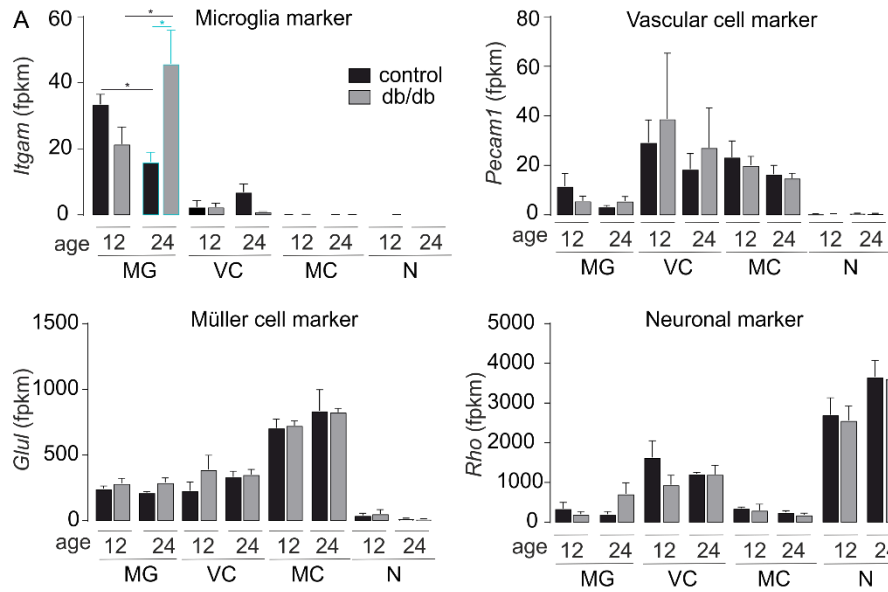


**Figure 15: Cellular marker expression, bioinformatic analysis and pathway enrichment analysis of RNA seq data from purified retinal cell types from diabetic and control animals. (A)** RNA sequencing of magnetic activated cell sorted cells revealed an enrichment of the different retinal cell types in 12 and 24-week-old control and db/db mice. MG: Microglia, VC: Vascular cells, MC: Müller cells, N: Neurons. *Glul*: Glutamine synthetase. *Rho*: Rhodopsin. *Itgam*: Integrin subunit alpha M. *Pecam1*: Platelet and endothelial cell adhesion molecule 1. Age in weeks. Bars represent mean  $\pm$  SEM (n=3-4). \*P<0.05 **(B)** Principal component analysis of the RNA seq data from major retinal cell types enriched from retinæ of control and diabetic mice at 12 and 24 weeks of age, respectively. Distinct clusters are formed by the different cell types implicating a good level of cell enrichment. **(C)** Filtering (P< 0.05, at least twofold difference) was performed to identify genes differentially expressed specifically in Müller cells from 24-week-old animals of the two genotypes. Three biological replicates per genotype are plotted demonstrating a low level of heterogeneity regarding gene expression within each genotype. Molecular functions significantly down- **(D)** or up- **(E)** regulated in Müller cells of 24-week-old db/db mice showed a high representation of pathways related to growth factors, ion binding and channel activity. B-C: Analysis done by Lew Kaplan.

The RNA seq provided key evidence that Müller cell function might be affected by diabetes, while partially confirming findings from earlier studies reporting diminished Müller cell homeostasis function (e.g. via downregulation of potassium channel activity) (Pannicke et al. 2006).

### 6.3. THE PROTEOME OF DIABETIC MICE WITH AN AGE OF 24 WEEKS

Parallel to the transcript analysis, label-free liquid chromatography mass spectrometry was done for proteome analysis on samples collected in the same way as RNA seq. Briefly, MACS enriched retinal cell types from four control and diabetic mice at 24 weeks of age were analyzed and evaluated. The same marker genes of the four different cell types (microglia: *Itgam*, vascular cells: *Pecam1* or *CD31*, Müller cells: *Glul* and neurons: *Rho*) used for RNA seq were chosen to demonstrate cell enrichment. These data very convincingly confirm a successful separation of the different cell population (**Figure 16A**). Similar to RNA seq, the PCA showed that four distinct cell clusters are formed by samples from the respective cell populations (**Figure 16B**). The proteins which were at least twofold up- or downregulated in Müller cells of diabetic mice with an age of 24 weeks were identified and plotted in a heatmap. In most cases a consistent trend of protein expression changes was demonstrated across all biological replicates per genotype (**Figure 16C**). 38 proteins were down- and 137 proteins upregulated in Müller cells of diabetic mice. The selected proteins, analogous to the analysis performed on the RNA seq data set, were then subjected to pathway enrichment analysis via PANTHER (Thomas et al. 2003) (**Figure 1D-E**). Pathways related to the adenosine triphosphatase (ATP) activity and transporter activity were found to be enriched if checking for the downregulated candidate proteins (**Figure 16D**). In contrast, pathways related to RNA, protein binding, ligase and transferase activity were associated with proteins upregulated in Müller cells from diabetic mice (**Figure 16E**).

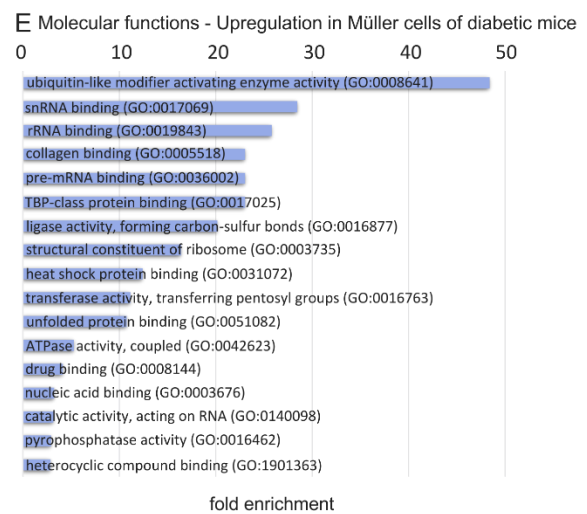
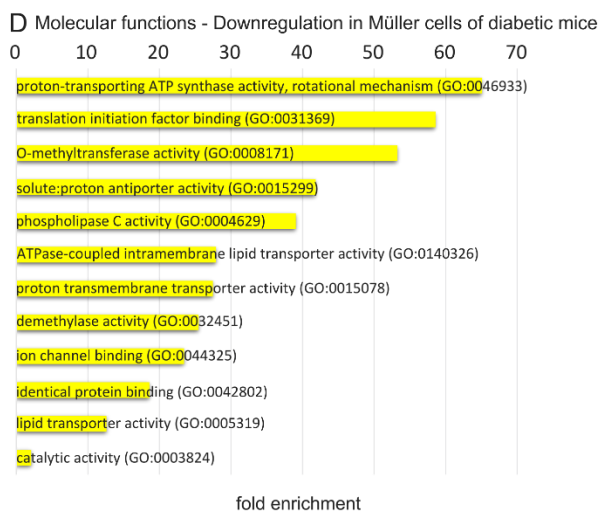
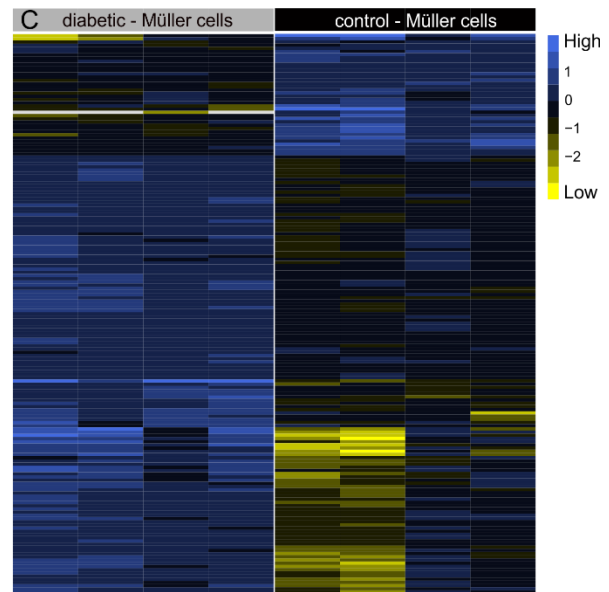
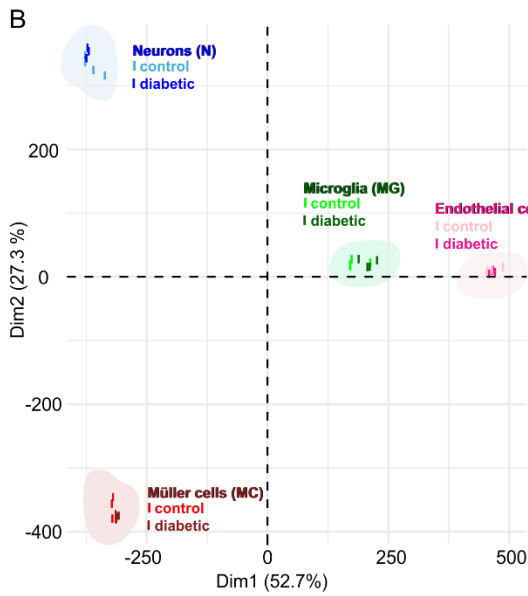
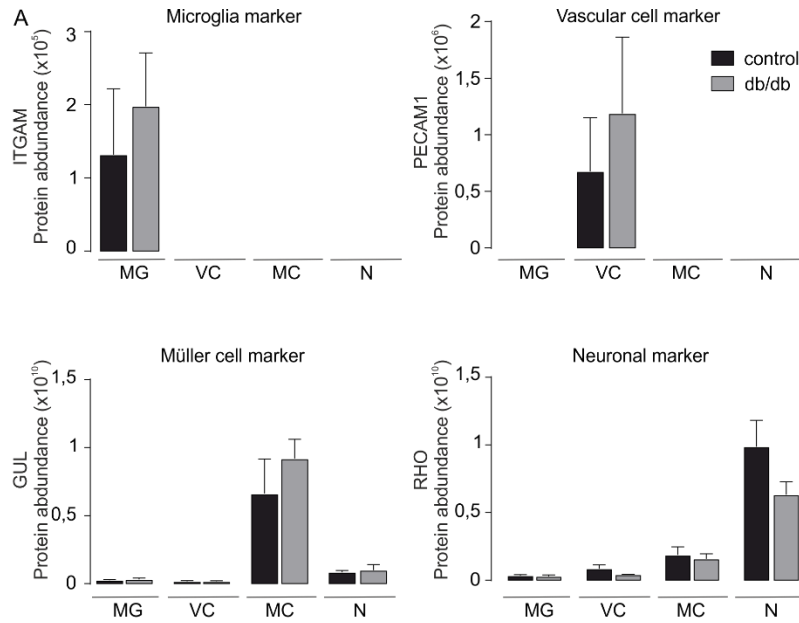


**Figure 16: Cellular marker expression, bioinformatic analysis and pathway enrichment analysis of proteomics data from purified retinal cell types from diabetic and control animals with an age of 24 weeks.** (A) The protein expression of marker genes for the four cell types implicated a successful separation of the different cell population. MG: Microglia, VC: Vascular cells, MC: Müller cells, N: Neurons. GLUL: Glutamine synthetase. RHO: Rhodopsin. ITGAM: Integrin subunit alpha M. PECAM1: Platelet and endothelial cell adhesion molecule 1. Bars represent mean  $\pm$  SEM (n=4). (B) Principal component analysis of the proteomics data from four diabetic and control mice. Distinct clusters are formed by the four cell type groups. (C) Filtering ( $P < 0.05$ , at least twofold difference) was performed to identify proteins differentially regulated in Müller cells of diabetic mice. Molecular functions significantly down- (D) or up- (E) regulated in Müller cells of 24-week-old db/db mice showed a high representation of pathways related to RNA binding and protein binding. B-C: Analysis done by Lew Kaplan.

#### 6.4. COMPARISON OF THE TWO OMICS DATA SETS

In the next step, a comparison of the two OMICS data sets was performed to test for concurrent and/or discrepant regulation patterns of transcript and protein. The regulation pattern of both data sets showed that 56.92% of the 3078 common genes and corresponding proteins were regulated in the same way (Figure 17A). Furthermore, 986 genes and proteins overlapped in the Müller cell-specific regulated data sets and 57.61% were concordantly regulated (Figure 17B).

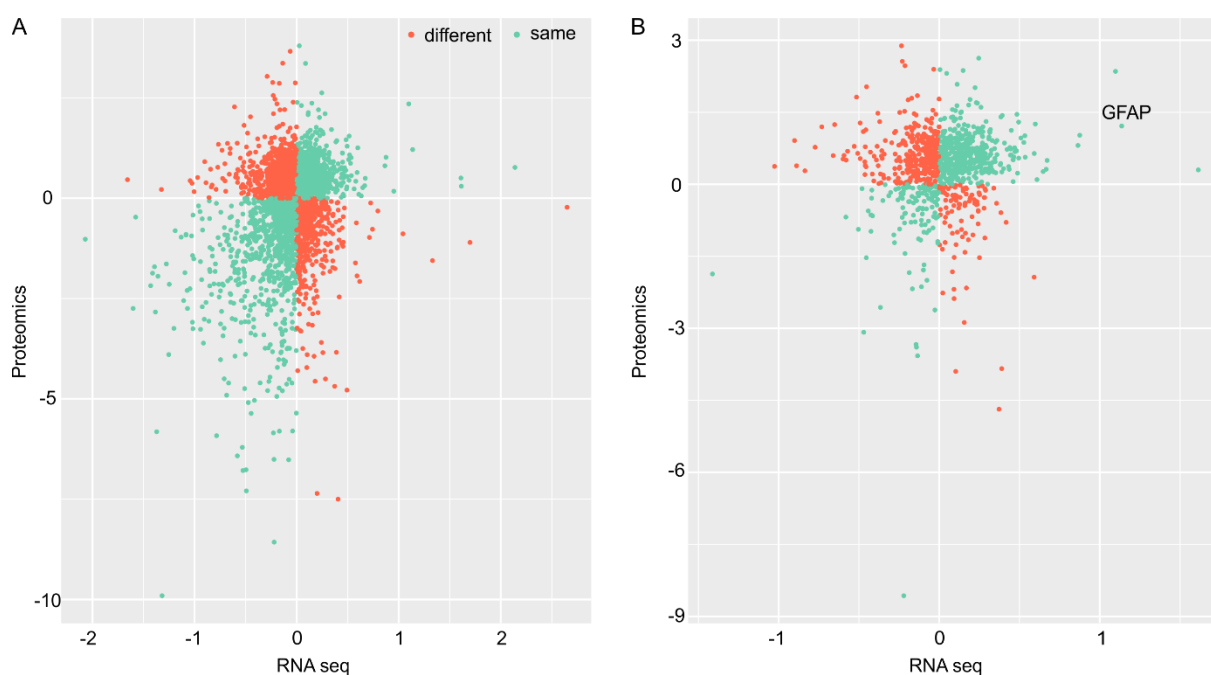


**Figure 17: Comparison of Müller cell-specific transcriptome and proteome profiles of 24-week-old diabetic mice.** (A) The RNA seq and proteomics data sets were compared and showed that out of the 3078 commonly identified genes and proteins 56.92% were concordantly regulated. Spearman correlation factor: 0.24. (B) Focusing on the Müller cell-specific genes and corresponding proteins, 986 common hits were identified and 57.61% were concordantly regulated. Spearman correlation factor: 0.12. GFAP: Glial fibrillary acidic protein. Analysis by Lew Kaplan.

Bogdanov et al. 2014 showed a GFAP upregulation in Müller cells, a sign of gliosis, beginning with an age of 8 weeks in diabetic mice, a finding I could partially confirm. Our RNA seq data showed that *Gfap* was significantly upregulated in Müller cells of diabetic animals at 24 weeks,

but not at 12 weeks of age (**Figure 18A**). These data were confirmed by qPCR from control and diabetic 24-week-old mice (**Figure 18B**). Proteomic analysis of MACS-enriched retinal cell types also revealed a trend of GFAP upregulation in Müller cells in 24-week-old db/db mice (**Figure 18C**). Nevertheless, GFAP-positive Müller cells were not present in stainings from retinal sections of diabetic and control mice 24 weeks of age (**Figure 18D**). In summary, an upregulation was detected on transcript as well as an upregulation trend on protein level in 24-week-old diabetic mice.

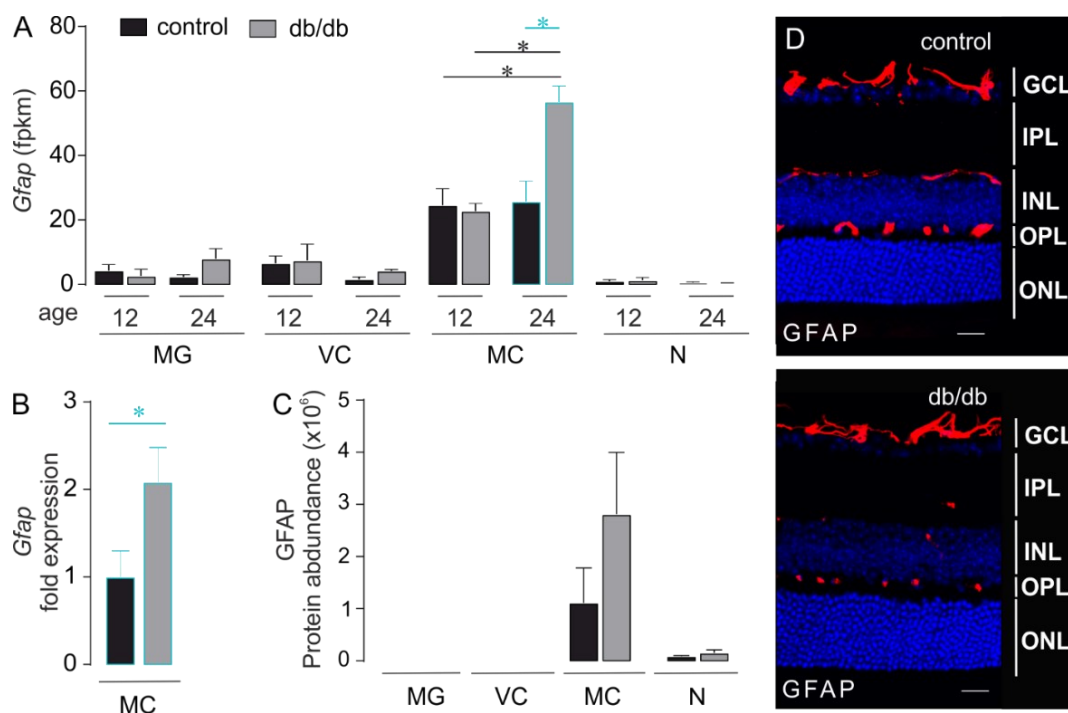


**Figure 18: Glial fibrillary acidic protein upregulation in 24-week-old diabetic mice.** (A) RNA seq of magnetic activated cell sorted (MACS) retinal cell types revealed significant upregulation of glial fibrillary acidic protein (*Gfap*) transcripts in Müller cells in 24-week-old db/db mice, but not earlier. Bars represent mean  $\pm$  SEM (n=3-4). \*P<0.05. (B) qPCR on MACS-sorted retinal cells isolated from 24-week-old mice confirmed the findings from RNA seq. *Gfap* was expressed at a higher level in Müller cells of diabetic mice. Bars represent mean  $\pm$  SEM (n=5-7). \*P<0.05. (C) Proteomic analysis of purified retinal cell types demonstrated a trend of GFAP upregulation in Müller cells of 24-week-old db/db mice. Bars represent mean  $\pm$  SEM (n=4). \*P<0.05. (D) Representative confocal images of a GFAP labeling in retinal sections of a control and diabetic mouse at 24 weeks of age did not show any GFAP-positive Müller cells. GCL: Ganglion cell layer, IPL: Inner plexiform layer, INL: Inner nuclear layer, OPL: Outer plexiform layer, ONL: Outer nuclear layer. MG: Microglia, VC: Vascular cells, MC: Müller cells, N: Neurons. Age in weeks. Scale bar: 20  $\mu$ m.

Since those findings could not be verified by immunostaining, the rise in GFAP levels could possibly also be due to expression changes in contaminating astrocytes or still be sublevel not yet detectable in Müller cells.

## 6.5. SEARCH FOR KEY REGULATORS OF DIABETIC RETINOPATHY PROGRESSION

As the goal of this thesis was to identify key regulators of DR progression, I then focused on

TFs and ran an oPOSSUM-3 TF binding site cluster analysis (Ho Sui et al. 2005) on the basis of the RNA seq expression data, implementing the list of genes specifically regulated in Müller cells of 24-week-old diabetic mice. Only the gene IDs of the top hits with a Z-score and Fisher-score over 5 are named in **Figure 19A and 19B**.

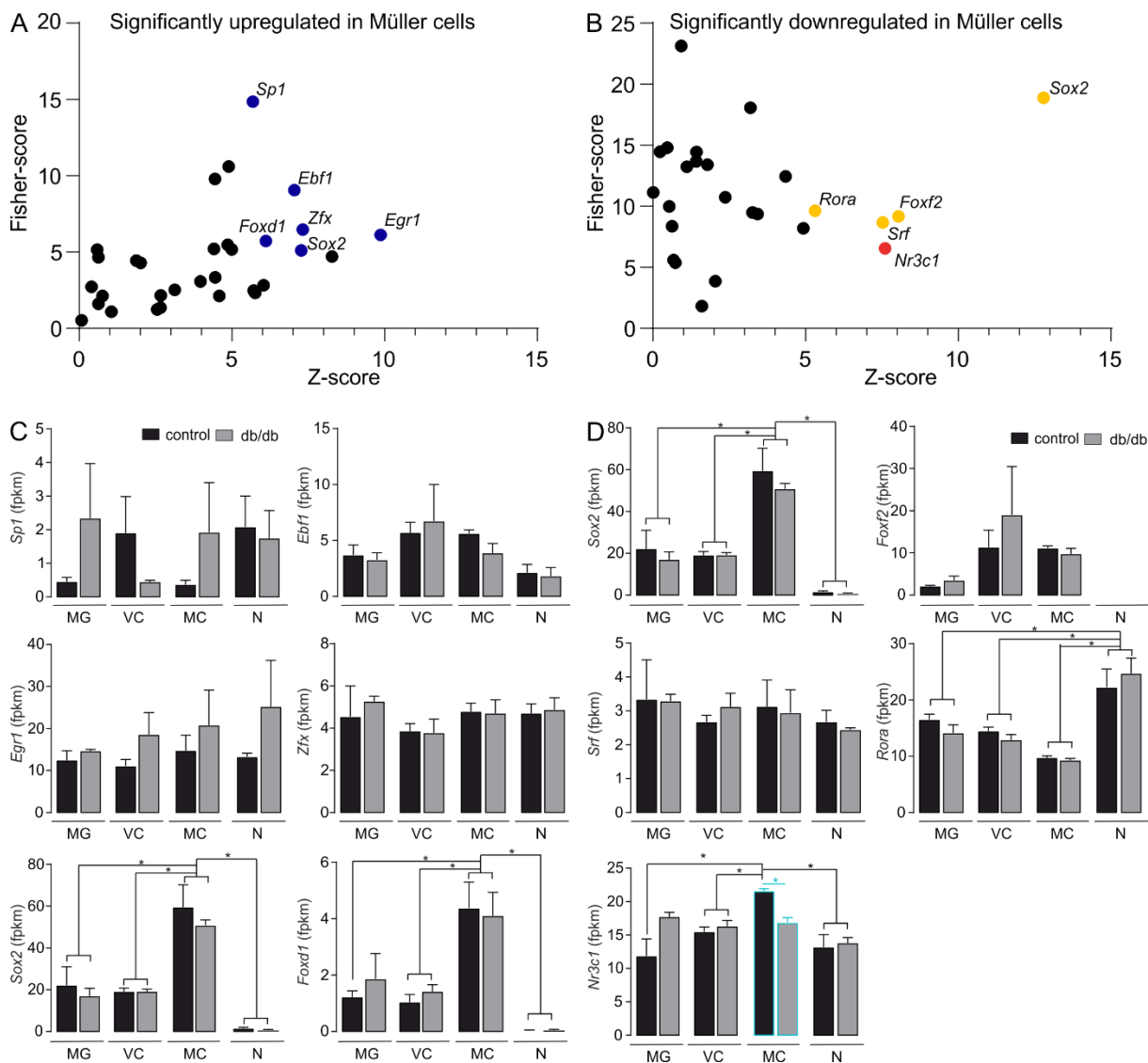


**Figure 19: oPOSSUM-3 transcription factor binding site cluster analysis of Müller cell-specific regulated genes of 24-week-old diabetic animals.** Genes identified by RNA seq to be significantly up- (A) or down- (B) regulated in Müller cells of 24-week-old diabetic mice were submitted to oPOSSUM-3 analysis (Ho Sui et al. 2005). The goal was to search for transcription factors that may act as putative master regulators determining the glial response to stress induced by diabetic conditions. Only those transcription factors that were expressed at transcript level in Müller cells as determined by our RNA seq experiment, are shown in the graphs. Only up- (blue) or downregulated (yellow) gene IDs of the top hits (Z-score and Fisher-score > 5) were added to the graph. The promising gene cluster of *Nr3c1* was labeled in red. (C) RNA seq data (animals with 24 weeks of age) of those transcription factors whose gene cluster was significantly upregulated in Müller cells is shown. (D) Summary of the transcriptome data (24-week-old animals) of those transcription factors whose gene cluster was significantly downregulated in Müller cells. MG : Microglia, VC : Vascular cells, MC : Müller cells, N : Neurons. Bars represent mean  $\pm$  SEM (n=3). \*P<0.05.

The gene cluster of *Sp1*, *Ebf1*, *Egr1*, *Zfx*, *Sox2* and *Foxd1* are upregulated in Müller cells of 24-week-old diabetic mice (**Figure 19A** in blue) and the cluster of the genes *Sox2*, *Rora*, *Foxf2*, *Srf* and *Nr3c1* were downregulated (**Figure 19B** in yellow). Furthermore, cell type specific expressions in 24-week-old diabetic and control mice of these top hits were investigated. For the gene clusters which were significantly upregulated in Müller cells the gene expression of the TF itself is shown in **Figure 19C**. *Sox2* and *Foxd1* are mainly expressed in Müller cells, but the gene expressions were not altered in diabetic mice compared to control mice. The transcriptome data of the TFs which clusters were significantly downregulated in Müller cells are shown in **Figure 19D**. The cluster of *Sox2* is also significantly downregulated in Müller cells, whereby the Fisher-score and Z-score were higher than in the upregulated data set. The TF *Rora* is mainly expressed in neurons and no difference in diabetic mice was detected. *Nr3c1* is mainly expressed in Müller cells and the RNA seq revealed significant reduction of *Nr3c1* transcripts in Müller cells of 24-week-old db/db mice. Therefore, I decided to focus on *Nr3c1* (**Figure 19B** in red), evaluating its potential as a key regulator in DR progression.

## 6.6. THE ROLE OF THE GLUCOCORTICOID RECEPTOR IN DR PROGRESSION

The *Nr3c1* gene codes for the GR. Treatment with GR agonists like dexamethasone were proven to be effective in inflammatory diseases, including DR (Ghaseminejad et al. 2020). Although synthetic glucocorticoids are commonly used for therapeutic approaches in ophthalmology, the molecular processes of GR signaling and its role in DR progression are not known and therefore, investigated in this study.

### 6.6.1. MÜLLER CELL-SPECIFIC DOWNREGULATION OF THE GLUCOCORTICOID RECEPTOR TARGET GENES IN DIABETIC ANIMALS

The oPOSSUM-3 analysis (Ho Sui et al. 2005) showed that the target gene cluster of the GR is downregulated specifically in 24-week-old diabetic animals compared to control mice (**Figure 19B**). A list with potential target genes of the GR was generated using three different databases: JASPER, ENCODE and CHEA (Davis et al. 2018; Mathelier et al. 2014; Rouillard et al. 2016). As the GR gene cluster was downregulated, this list was compared to the genes which were specifically downregulated in Müller cells of 24-week-old diabetic mice identified by the RNA seq. 1363 genes, a quarter of the 7031 Müller cell-specific downregulated genes, were also potential target genes of the GR (**Figure 20A**). The expression of two exemplary Müller cell-specific GR target genes is shown in (**Figure 20B**). Forkhead box o1 (*Foxo1*) is a TF that is the main target of insulin signaling and regulates metabolic homeostasis in response to oxidative stress (Wu et al. 2018). Its transcript is significantly downregulated in 24-week-old diabetic mice compared to control

mice. Carbonic anhydrase 4 (*Ca4*) which is a member of a large family of zinc metallo-enzymes that catalyze the reversible hydration of carbon dioxide was also significantly down-regulated in Müller cells of 24-week-old diabetic mice.

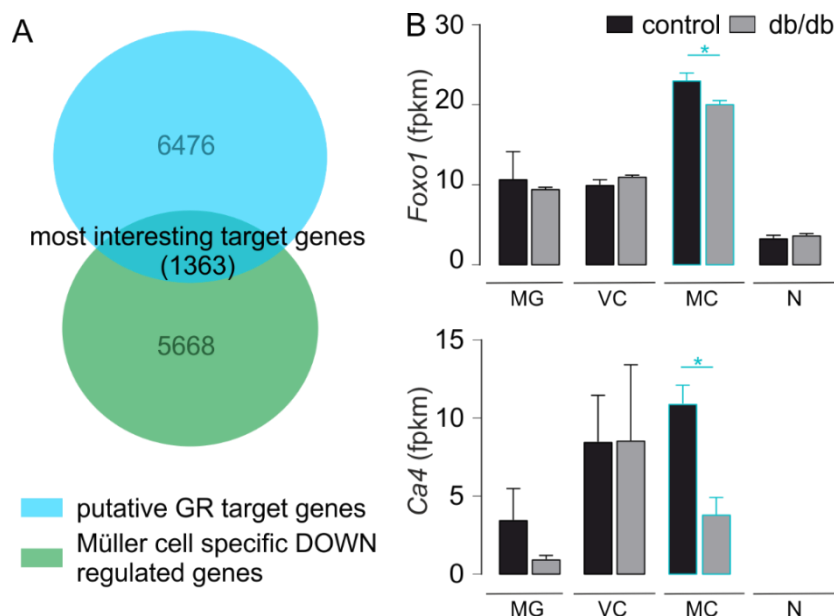


**Figure 20: The broad influence of the glucocorticoid receptor target gene cluster on Müller cell gene expression changes in the diabetic retina. (A)** 1363 of the 7031 genes that were downregulated in Müller cells as determined by RNA seq were predicted as putative direct targets of the GR by at least one of the three databases: CHEA, JASPER, ENCODE (Davis et al. 2018; Mathelier et al. 2014; Rouillard et al. 2016). **(B)** The expression on transcript level of two predicted GR target genes is significantly downregulated in Müller cells of 24-week-old diabetic mice. MG: Microglia, VC: Vascular cells, MC: Müller cells, N: Neurons, Bars represent mean  $\pm$  SEM (n=5). \*P<0.05.

Given the high representation of GR target genes in the list of genes specifically downregulated in Müller cells of diabetic mice, I inferred that the GR might have a major influence on Müller cell function and DR progression.

#### 6.6.2. MÜLLER CELL-SPECIFIC DOWNREGULATION OF THE GLUCOCORTICOID RECEPTOR IN DIABETIC ANIMALS

Accordingly, the regulation of the GR itself was further investigated. RNA seq of MACS enriched retinal cell types revealed significant reduction of *Nr3c1* transcripts in Müller cells in 24-week-old db/db mice (**Figure 19D**). As the GR was not detected in the proteomics, qPCR and Western blot experiments on samples from MACS retinal cells isolated from 24-week-old diabetic and control mice were performed. A GR downregulation trend at transcript and protein level was shown (**Figure 21A-B**). Furthermore, I could confirm earlier findings (Gallina et al. 2014) that the GR is mainly located in the Müller cell nuclei of the vertebrate (and more specifically mouse) retina using standard confocal and super resolution STED microscopy (**Figure 21C-D**).

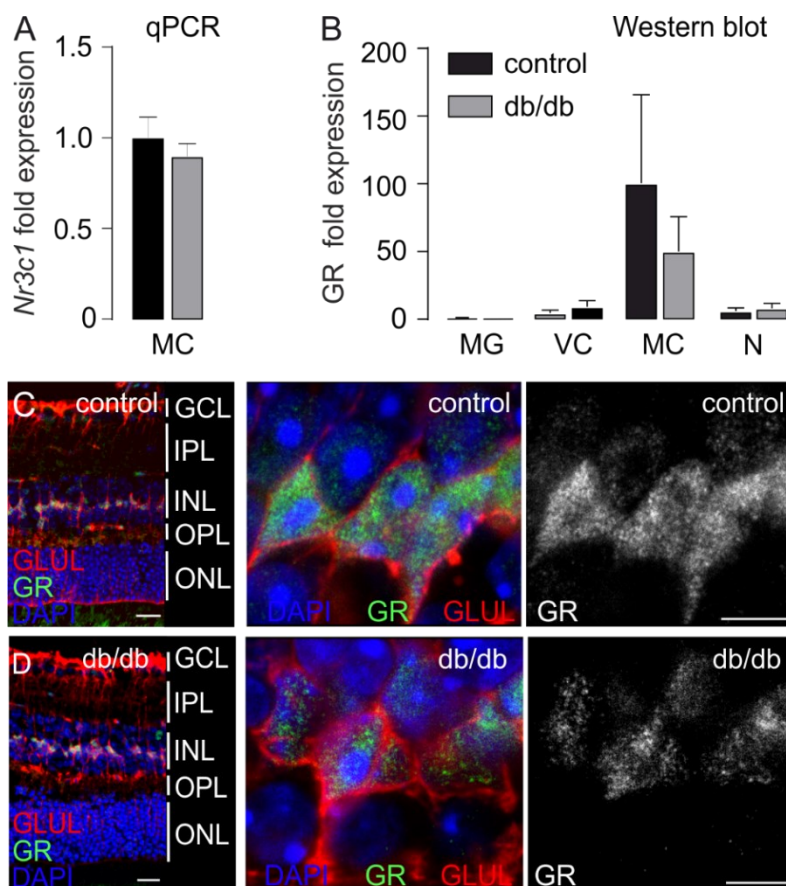


**Figure 21: Downregulation trend of the glucocorticoid receptor in Müller cells of 24-week-old diabetic mice.** (A) Quantitative PCR on magnetic activated cell sorted (MACS) retinal cells isolated from 24-week-old mice could not confirm the findings from RNA seq, but a *Nr3c1* downregulation trend was visible in Müller cells of diabetic mice. Bars represent mean  $\pm$  SEM (n=5-7). (B) Western blot experiments on MACS retinal cell types isolated from 24-week-old mice show a similar trend. Less glucocorticoid receptor (GR) was expressed in Müller cells of diabetic mice. Bars represent mean  $\pm$  SEM (n=6). (C) *Left*, Confocal image of a GR labeling in retinal section of a 24-week-old control mouse. Scale bar, 20  $\mu$ m. *Right*, STED images of a GR staining in the inner nuclear layer. Müller cells were co-stained for glutamine synthetase (GLUL). Scale bar, 5  $\mu$ m. (D) *Left*, Confocal image of a GR labeling in retinal section of a 24-week-old diabetic mouse. Scale bar, 20  $\mu$ m. *Right*, STED images of a GR staining in the inner nuclear layer. Müller cells were co-stained for GLUL. Scale bar, 5  $\mu$ m. C and D: STED images were taken by Dr. Kirsten Wunderlich. GCL: Ganglion cell layer, IPL: Inner plexiform layer, INL: Inner nuclear layer, OPL: Outer plexiform layer, ONL: Outer nuclear layer. MG: Microglia, VC: Vascular cells, MC: Müller cells, N: Neurons.

### 6.6.3. ELEVATED CORTICOSTERONE LEVEL IN DIABETIC MICE

The GR transcript as well as its target gene cluster is Müller cell-specific downregulated in diabetic mice 24 weeks of age. The main ligand of GR is corticosterone in mice and cortisol in humans (Buckingham 2006). It has been demonstrated that the corticosterone levels in mouse models of type 1 and T2D are significantly elevated. It was shown that the serum corticosterone level is increased in db/db animals with an age of 9 weeks (Erickson et al. 2017). Furthermore, diabetic patients have a significantly higher urinary-free cortisol level (Roy et al. 1998). Here, I measured the corticosterone level in blood plasma of 24-week-old diabetic and control mice via ELISA to confirm these earlier findings in our mouse colony (**Figure 22**). In line with the earlier studies,

diabetic animals had a mean concentration of 1281 ng/ml corticosterone in the blood plasma compared to control animals with a mean concentration of 485 ng/ml.

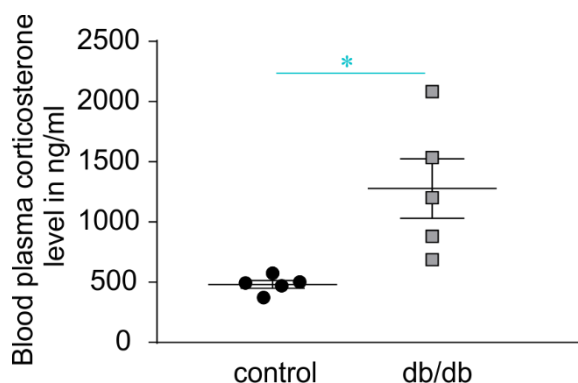


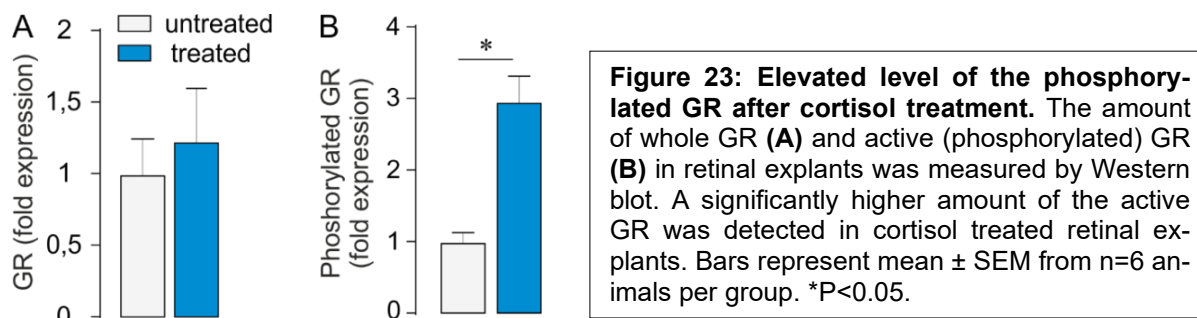
**Figure 22: Elevated corticosterone level in diabetic mice at 24 weeks of age.** The corticosterone level was measured from the blood plasma of diabetic and control animals at an age of 24 weeks via ELISA. The graph represents mean  $\pm$  SEM from n=5 animals per group. \*P<0.05.

#### 6.6.4. MODULATION OF THE RETINAL GLUCOCORTICOID RECEPTOR *IN VITRO*

To investigate the effect of a higher corticosterone level on the retina, I used an *in vitro* model. Cortisol is the primary corticosteroid hormone in humans, whereas corticosterone is the complement in rodents (Buckingham 2006). As cortisol has higher glucocorticoid potency than corticosterone (Gong et al. 2015) and its effect is well known on retinal explants in culture (Gorovits et al. 1997; Toops et al. 2012), I used cortisol for the following experiments: Retinal explants of wild-type mice were cultivated for two days in culture and cortisol was added twice a day to maintain a constantly high concentration of 500 ng/ml. Western blot, qPCR and a proteomic analysis via mass spectrometry was performed on the explants. To check for effects of a more long-term cortisol stimulation, retinal explants of wild-type mice were cultivated for five days and immunohistochemistry was performed.

##### 6.6.4.1. ACTIVATION OF THE RETINAL GLUCOCORTICOID RECEPTOR BY CORTISOL TREATMENT *IN VITRO*

After ligand binding to the inactive cytoplasmic GR, the receptor becomes phosphorylated and changes its conformation (Toops et al. 2012). Therefore, the amount of the phosphorylated active GR and the amount of inactive and active forms of the receptor were measured by Western blot analysis. A higher concentration of the active GR was detected in retinal explants which were constantly incubated with cortisol for 2 days, while the level of whole GR (inactive and active form) is constant in the cortisol treated and untreated retinal cultures (**Figure 23**). Therefore, it was shown that I activated the GR in retinal explants due to cortisol treatment using this *in vitro* approach.



#### 6.6.4.2. EFFECT OF THE GLUCOCORTICOID RECEPTOR ACTIVATION BY CORTISOL TREATMENT *IN VITRO*

Next, the effects of the GR activation at transcript and protein levels were investigated. Proteome profiling was performed by mass spectrometry of six retinæ per group, aiming to evaluate the effect of the cortisol treatment on protein expression levels. The PCA of these data revealed that the untreated and treated groups are clearly separated into two clusters (**Figure 24A**). The proteins which were at least 1.3-fold up- or downregulated in the untreated versus treated group were identified and plotted in a heatmap (**Figure 24B**). Furthermore, a pathway enrichment analysis via PANTHER (Thomas et al. 2003) performed showed significantly up- or down-regulated proteins (**Figure 24C-D**). I found 61 proteins which were at least 1.3-fold down- and 72 proteins that were at least 1.3-fold up-regulated in treated explants. Pathways related to the cytoskeleton, to energy supply and to ATP activity were those found to be enriched, by checking for the downregulated candidate gene list (**Figure 24C**). In contrast, pathways related to RNA binding, transcriptional activity and phosphatase activity were associated with protein up-regulation upon cortisol treatment (**Figure 24D**). In summary, the evaluation of the data set and the pathway enrichment analysis of the proteome profiles clearly illustrate that cortisol treatment induces an activation of the GR in the retina, most likely in Müller cells.

In the following, the effect of this robust GR activation on known GR target genes was evaluated. Immunohistochemistry previously showed in this study that the GR is mainly located in the Müller cell nuclei in mice (**Figure 21C-D**). Therefore, the focus was set on GR target genes which were regulated in Müller cells in the diabetic mice. To do so, potential target genes of the GR were identified using three different databases: JASPER, ENCODE and CHEA (Davis et al. 2018; Mathelier et al. 2014; Rouillard et al. 2016). Next, it was examined whether these genes are also Müller cell-specific using the own bulk RNA seq data from purified retinal cell types (**chapter 6.2**). Finally, these Müller cell-specific putative GR targets were compared to the mass spectrometric profiling data of retinal explants after cortisol treatment over 48 h.

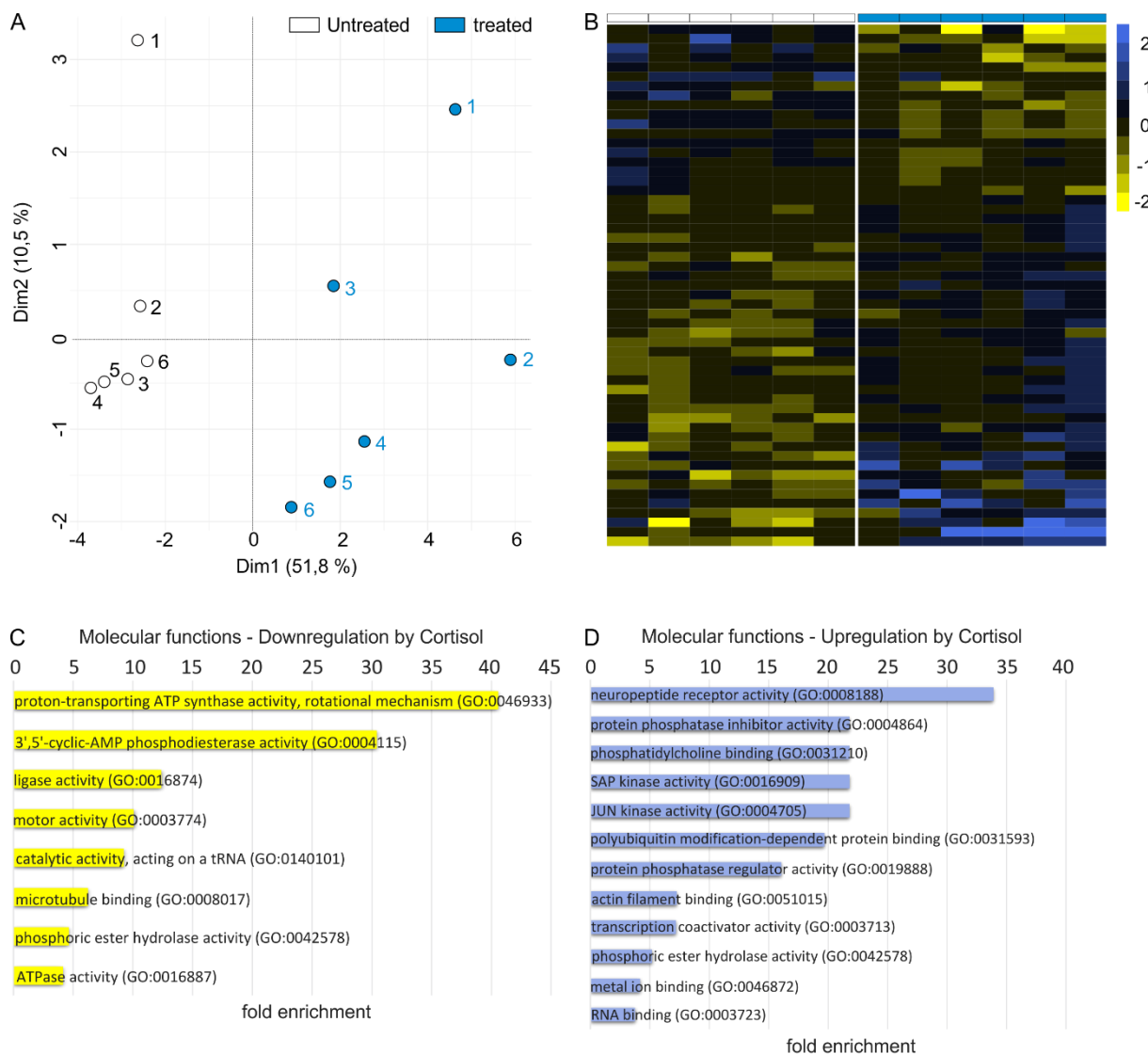


**Figure 24: Bioinformatic analysis and pathway enrichment analysis of proteomics from cortisol treated and untreated retinal explants.** (A) Principal component analysis of the proteomics data from six cortisol treated and untreated retinal explants. Distinct clusters are formed by the two groups implicating a change in the treated explants on protein level. (B) Filtering ( $P < 0.05$ , at least 1.3-fold difference) was performed to identify proteins differentially regulated in the treated explants. Molecular functions significantly down- (C) or up- (D) regulated in the cortisol treated samples represent the cellular process following the activation of the GR in the cell.

Eleven of the 72 up-regulated proteins were reported as predicted targets of GR and were expressed at high levels in Müller cells as determined by our RNA seq experiment. None of down-regulated proteins in the cortisol treated explants were neither Müller cell-specific nor a putative target gene of the GR (Figure 25A). Therefore, I focused on those 11 most interesting candidates. The Müller cell-specificity of these 11 candidates was cross-validated and compared to published single cell (sc) RNA seq resource data from mouse retina (Macosko et al. 2015). For five of these candidate genes, an exclusive expression in Müller cells could be confirmed by this approach (Figure 25B). The protein abundance of the untreated and treated explants of these five target

genes is shown in **Figure 25C**. A literature research for the target genes in relation to diabetes and neurodegeneration, which also takes place in DR, was performed and the proteins crystallin alpha B (CRYAB) and enolase1 (ENO1) were identified as the two most interesting candidates. Expression changes upon cortisol treatment were cross-validated for both genes via qPCR on MACS Müller cells from retinal explants cultured according to the same protocol as performed for the initial proteome profiling. In line with the protein data, a trend towards upregulation of both genes at transcript level in purified Müller cells of cortisol treated versus untreated retinal explants was detected (**Figure 25D**).

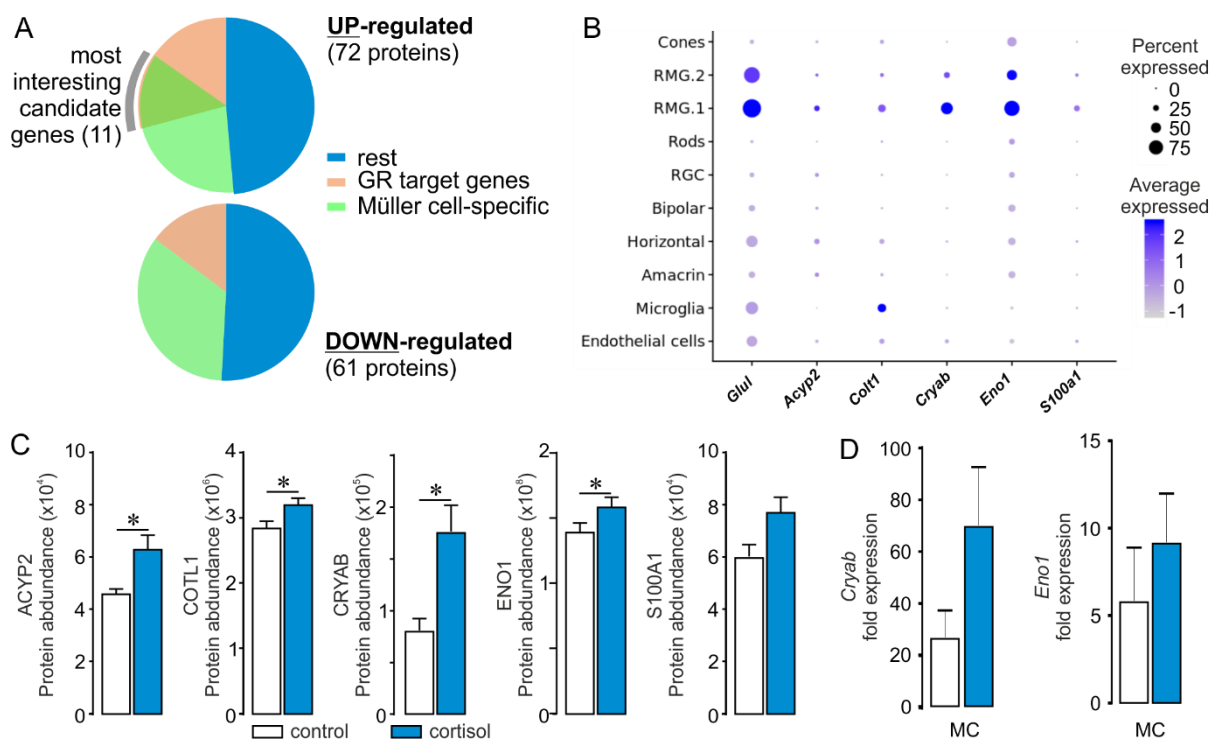


**Figure 25: Expression changes of putative glucocorticoid receptor target genes due to enhanced GR signaling in retinal explants.** (A) Eleven of the up-regulated proteins were predicted targets of the GR and were expressed at high transcript levels in Müller cells as determined by our RNA seq experiment on magnetic activated cell sorted retinal cell populations. (B) Cross-validation of the Müller cell-specificity of these 11 candidates with published single cell RNA seq data from mouse retina (Macosko et al. 2015) (reanalyzed by Lew Kaplan) showed that five candidate genes were exclusively expressed in Müller cells (C) Protein expression of these candidates in the cortisol untreated and treated samples. Bars represent mean  $\pm$  SEM from n=6 animals per group. \*P<0.05 (D) The gene expression of the two most interesting candidates was investigated and the upregulated trend was confirmed. Bars represent mean  $\pm$  SEM from n=3 animals per group. \*P<0.05.

Overall, the *in vitro* data from retinal explants demonstrate that GR stimulation via cortisol administration had an effect on its conformation and activity, and also on the expression of known downstream GR target genes with clear modulation of those specifically expressed by Müller cells.

#### 6.6.4.3. LONG TERM EFFECT OF THE GLUCOCORTICOID RECEPTOR ACTIVATION VIA CORTISOL TREATMENT *IN VITRO*

In order to evaluate long term effects of permanent stimulation by cortisol administration, four retinal explants from wild-type mice were cultivated for five days, while cortisol was added twice a day to maintain high concentration levels. The same experiment was performed with four control retinae which were cultivated without adding cortisol. Explants were then prepared for immunofluorescence staining for various cell markers to assess cell survival and Müller cell gliosis induction. After five days in culture, the different nuclear layers of the retina were well maintained (**Figure 26**). Even though only few calretinin-positive neuronal cell bodies were observed in the treated and untreated explant cryosections, the three distinct layers of the calretinin-stained layers of the IPL were clearly visible, implying that synaptic connections are still present. Furthermore, IBA-positive microglia remained present in both cultivation conditions. As indicated by a moderate rise of GFAP expression, Müller cells were becoming gliotic irrespective of the absence or presence of cortisol. Apart from this, staining for GLUL, an established Müller cell marker (Roesch et al. 2008), demonstrated that the overall morphology of Müller cells was well preserved. The main difference observed due to cortisol treatment over 5 days in culture was found regarding the GR itself. While a cytoplasmic diffusion of the GR was detected in the untreated explants, it stayed in the Müller cell nuclei when the explants were stimulated with cortisol (**Figure 26**).

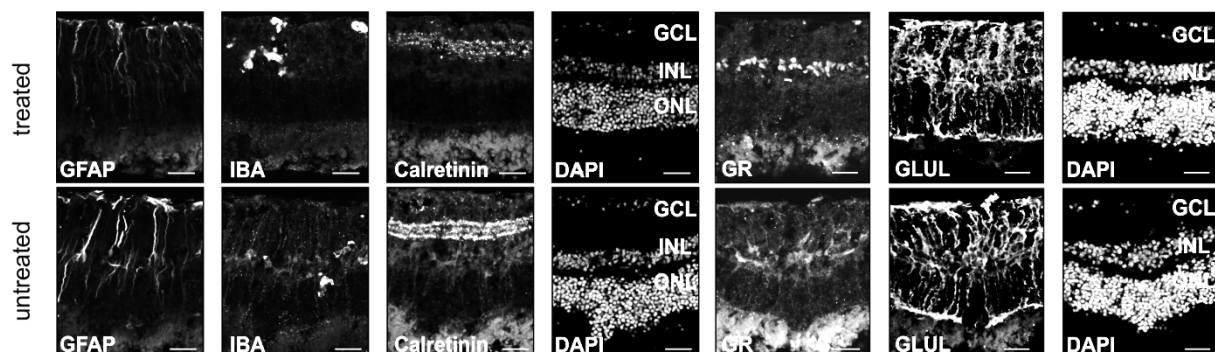


**Figure 26: Cortisol treatment reduces cytoplasmic diffusion of the glucocorticoid receptor *in vitro* (5-day culture).** Representative micrographs of stainings of cortisol treated and untreated explant cryosections. No major differences were detected for the layering of the retina (DAPI-staining), microglia (IBA-staining) and calretinin-staining. Müller cells keep their elongated structure and express their cell marker glutamine synthetase (GLUL) under both cultivation conditions. A moderate gliotic activation was shown (glial fibrillary acidic protein (GFAP) staining) due to the long-term cultivation. The main difference was that the cortisol treatment reduced the cytoplasmic diffusion of the GR and it is still localized in the nuclei of Müller cells. Scale bar, 50  $\mu$ m. GCL: Ganglion cell layer, INL: Inner nuclear layer, ONL: Outer nuclear layer.

In sum, the data emphasize the central role of GR signaling in the retina and in Müller cells specifically, since robust effects of the cortisol treatment of the retinal explants were detected. These consistently high cortisol levels mimic the elevated corticosterone level in diabetic mice, reflecting the early tissue response at the onset of DR. Nevertheless, the cultivation for 5 days also showed

the limitation of the *in vitro* model. As a result of the long-term cultivation, Müller cells were becoming gliotic indicated by GFAP upregulation. Therefore, a gene therapeutic approach was developed to investigate the role of long-term GR modulation in mice.

## 6.7. GENE THERAPEUTIC INTERVENTION VIA MÜLLER CELL-SPECIFIC GLUCOCORTICOID RECEPTOR OVEREXPRESSION IN MICE

Multifactorial retinal diseases such as DR develop slowly and treatment over years or even decades is needed. Current available treatments for DR typically require repetitive application. Common methods are laser photocoagulation, injection of anti-VEGF agents or intravitreal corticosteroids such as dexamethasone (Das et al. 2015). In contrast, gene therapy requires a single injection in the patient's eye, significantly reducing the risk of procedure-related complications.

### 6.7.1. SUCCESSFUL ADENO-ASSOCIATED VIRUS-INDUCED GLUCOCORTICOID RECEPTOR OVEREXPRESSION IN MÜLLER CELLS *IN VIVO*

The results presented in **chapter 6.6.** point to GR as a promising candidate gene that could be targeted in Müller glia to treat DR. Therefore, the goal of this study was to develop a gene therapeutic approach to achieve long-term efficient stimulation of GR signaling in Müller cells. I performed experiments using an AAV9-construct for GR overexpression. The intravitreal injection was applied using a Hamilton injection system. I demonstrated a successful glia-specific expression of the AAV construct on basis of the reporter eGFP co-expressed with GR and moderate upregulation of GR as determined by immunostainings (**Figure 27A**). 12 weeks post injection, expression analysis on MACS retinal cells was performed. Given that GR immunoreactivity was mainly located in the nuclei of Müller cells (**Figure 21C-D**), only Müller cell-specific gene expression is shown in **Figure 27B**. A significant upregulation of *Nr3c1* in AAV-injected controls and a trend of upregulation in db/db mice was detected. However, a slight *Gfap* upregulation due to AAV injection was also visible in control and db/db mice, while *Glul* gene expression was not affected. Furthermore, the gene expression of four putative GR target genes enolase1 (*Eno1*), clarin 1 (*Clrn1*), crystallin alpha B (*Cryab*) and siderflexin 5 (*Sfxn5*) were investigated. Most of these genes were expressed at higher levels in treated eyes compared to untreated controls irrespective of the genotype (**Figure 27B**). Thus, one may deduce that changes in expression levels are consequences of downstream effects of the AAV-induced GR upregulation. Having shown that ERG is a highly sensitive and valuable readout which delineates functional changes even before major morphological signs (**chapter 6.1.6.**) are detectable, ERG measurements were performed 12 weeks post-injection.

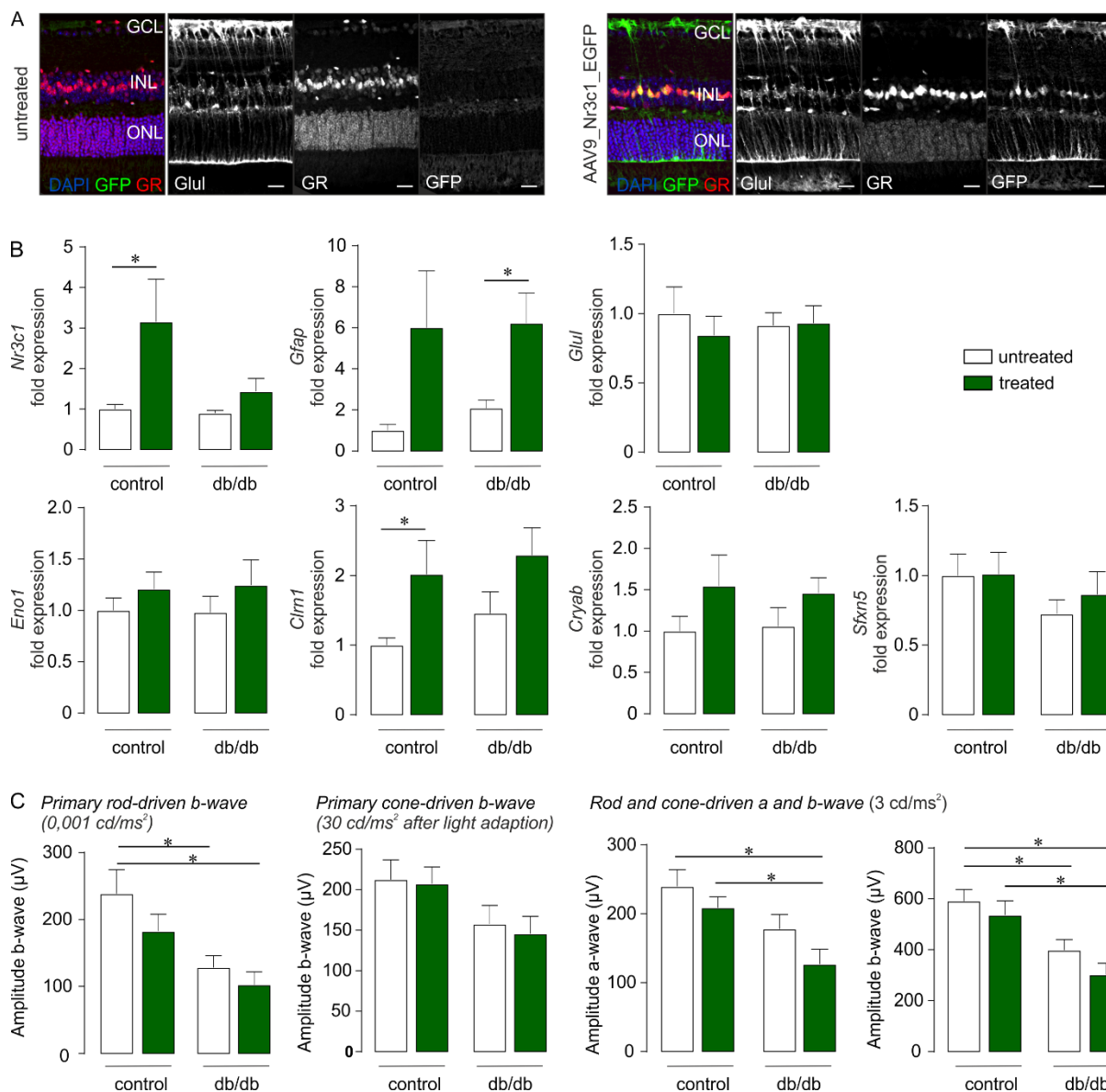


**Figure 27: Overexpressing the glucocorticoid receptor (gene ID: Nr3c1) in Müller cells of the mouse retina *in vivo*.** (A)  $2.5 \times 10^{13}$  GC/ml AAV9-Nr3c1-eGFP particles were injected intravitreally (Hamilton system) in 12-week-old diabetic and control mice. Tissue was collected 12 weeks thereafter and stained for the Müller cell marker glutamine synthetase (GLUL). EGFP indicated successful viral transduction. GCL: Ganglion cell layer; INL: Inner nuclear layer; ONL: Outer nuclear layer. Scale bar, 20  $\mu$ m. (B) Quantitative PCR on magnetic activated cell sorted retinal cells isolated from 24-week-old mice, 12 weeks after single adeno-associated virus injection, was performed. Only Müller cell-specific gene expression is shown. I could detect a significant upregulation of *Nr3c1* in control mice and an upregulation trend in db/db mice. *Gfap* was upregulated in both (control and db/db mice), while the gene expression of *Glul* was not affected by the single adeno-associated virus injection. Additionally, the gene expression of four putative target genes (*Eno1*, *Cln1*, *Cryab* and *Sfxn5*) of GR was investigated. Bars represent mean values  $\pm$  SEM. control n=6-7. Db/db n=4-5. \*P<0.05 (C) A reduced light response in the ERG of retinæ of adeno-associated virus injected mice was detected. Rod-driven responses (b-wave) were measured and quantified at scotopic light conditions (0,001 cd/ms<sup>2</sup>) in diabetic and control mice. Cone-driven light responses (30 cd/ms<sup>2</sup>) were recorded after 5 min of light adaption. Mixed (rod- and cone-driven) responses were analyzed by applying light flashes of 3 cd/ms<sup>2</sup> to eyes of diabetic and control mice. Bars represent mean values  $\pm$  SEM. n=8-9. \*P<0.05.

A reduced light response of retinæ of AAV injected mice was detected, independent of the genotype. This significant effect occurred in rod (0.001 cd/ms) as well as in mixed (rod- and cone-driven, 3 cd/ms<sup>2</sup>) responses (**Figure 27C**). GFAP upregulation remained present up to 12 weeks after injection and the outcome of the ERG measurements led to the conclusion that the injection had a noticeable detrimental effect. For this reason, I set out for an optimization of the injection protocol to overcome the described problems.

### 6.7.2. COMPARISON OF DIFFERENT INJECTION SYSTEMS

In order to optimize the intravitreal AAV-injection method, two different injection systems were tested: one from Hamilton and one from WPI. The Hamilton syringe had a 33G blunt-end needle and a loading capacity of 10 µl. However, a hole generated by use of a bigger needle (27G) was needed to then enter the eye with this fine Hamilton syringe. This commonly used injection technique (Giove et al. 2010) comes with the disadvantage that the tissue around the injection side could be damaged by these two insertion/retraction cycles. In contrast, the NanoFil™ (10 µl filling volume) from WPI allows penetration and injection in a single step. The beveled needle is extremely fine (34G) and causes less severe tissue damage at the site of injection. One eye of 12-week-old control mice was injected with the vehicle control (PBS, sham control), while the contralateral eye received the AAV9-Nr3c1-eGFP construct. At 12 weeks post-injection, morphometric analysis (**Figure 28A-B**) and ERG measurements were performed (**Figure 28C**). The morphometric analysis showed that Müller cells in the retinæ of mice which were injected with the Hamilton system stayed in a gliotic state even weeks after the initial injection, as indicated by a rise of their GFAP expression (**Figure 28A**). This response was also detected outside the injection side (**Figure 28A''**) and showed that the injection induced a very wide-spread Müller cell gliosis affecting almost the whole retina. In contrast, Müller cell-specific GFAP expression was not detected in retinæ of mice which were injected with the WPI system (**Figure 28B**). This was neither visible at the injection side (**Figure 28B'**) nor offside the injection (**Figure 28B''**). Finally, ERG measurements were performed 12 weeks post-injection. Light responses of mice injected with the WPI system were better maintained compared to animals treated with the Hamilton system (**Figure 28C**). Considering the results regarding the GFAP expression and ERG recordings, I conclude that the WPI system is the better choice for intravitreal AAV injection.

In sum, I showed a successful glia-specific transduction of the AAV9-Nr3c1-eGFP construct and demonstrated that intravitreal injections via the WPI system are superior to that performed with the Hamilton syringe. In the end, all preliminary experiments are successfully completed. In a next step, the long-term effect of the GR overexpression in diabetic and control mice should be tested. For time reasons these experiments cannot be part of this thesis.

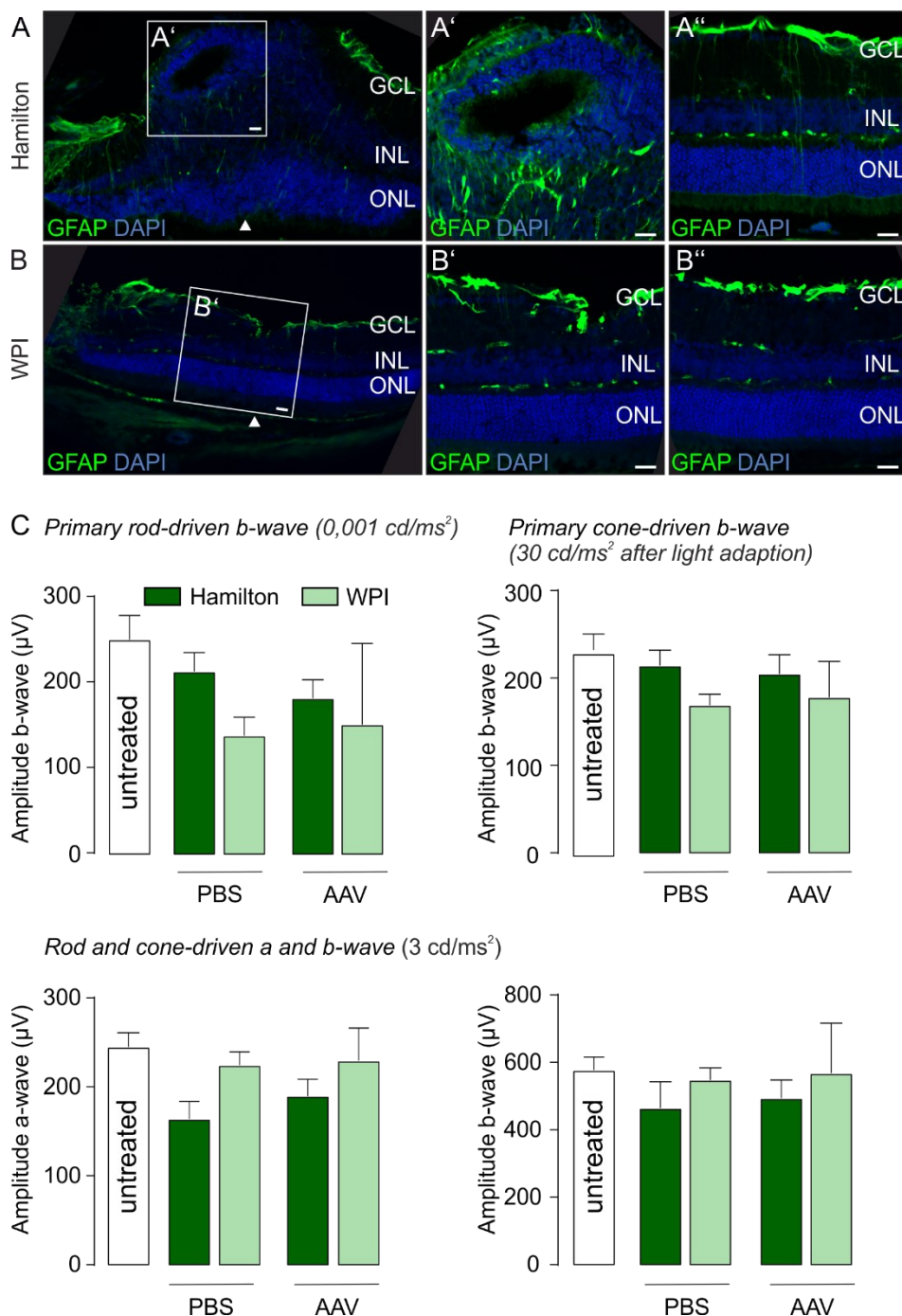


**Figure 28: Suitable intravitreal injection system (World precision instruments) for intravitreal adeno-associated virus injection.**  $2.5 \times 10^{13}$  GC/ml AAV9-Nr3c1-eGFP particles and PBS were injected intravitreally via the Hamilton (**A**) or the WPI system (**B**) into the eyes of 12-week-old control mice. Tissue was collected 12 weeks thereafter and stained for glial fibrillary acidic protein (GFAP). (**A**) A strong gliotic response of Müller cells was indicated by GFAP upregulation upon injection with the Hamilton system. (**B**) No visible gliosis of Müller cells in eyes that were injected with the WPI system. **A'** and **B'**: injection side. **A''** and **B''**: offside the injection side. GCL: Ganglion cell layer; INL: Inner nuclear layer; ONL: Outer nuclear layer. Scale bar, 20  $\mu$ m. (**C**) In contrast to animals injected with the Hamilton syringe, no major change in the light responses measured via electroretinogram recordings of mice which were injected with the WPI system were observed. Rod-driven responses (b-wave) were measured and quantified at scotopic light conditions (0,001 cd/ms<sup>2</sup>). Cone-driven light responses (30 cd/ms<sup>2</sup>) were recorded after 5 min of light adaption. Mixed (rod- and cone-driven) responses were analyzed by applying light flashes of 3 cd/ms<sup>2</sup> to eyes. Bars represent mean values  $\pm$  SEM. Untreated n=11. Hamilton n=4-13. WPI n=2.

## 7. DISCUSSION

### 7.1. ONSET OF CHANGES IN THE RETINAL MORPHOLOGY OF DIABETIC MICE

I performed an initial re-characterization of our db/db mouse breed to cross-validate their phenotype with that published in the literature.

Bogdanov et al. 2014 described that the total retinal thickness and thickness of the INL and ONL of the db/db mice in comparison to controls is already decreased in the central part of the retina at an age of 8 weeks. I could not confirm this finding. In mice from our db/db breed no significant change was detected in GCL, INL and ONL cell counts of retinae from 12-, 24- or 38-week-old diabetic mice compared to controls. This may be due to the fact that different analysis methods were used. Bogdanov et al. 2014 measured the thickness of the total retina, the INL and the ONL in  $\mu\text{m}$ . Here, I quantified single cell numbers in the different layers to achieve a more detailed insight into changes of the cellular tissue composition. Since retinal sections are not always 100% planar, I consider cell counts to be more precise for the quantification of cell loss than simple measurements of the overall thickness of retinal sections. Furthermore, a reduced number of cells in the GCL of db/db mice at an age of 8 weeks was previously reported (Bogdanov et al. 2014). To address this more specifically, I evaluated the number of calretinin-positive cells in the GCL and INL. Again, there was no significant difference in the number of calretinin-positive cells between control and diabetic mice at any age or retinal layer investigated. Bogdanov et al. 2014 used as many as 15 mice per age group to detect the differences in retinal thickness, while I analyzed 3 to 4 animals per genotype. Given that the mean difference in numbers of the cells in GCL per 100  $\mu\text{m}$  (24-week-old db/+ mice: 14.5 cells, 24-week-old db/db mice: 12 cells) and also the mean total thickness of the central retina (24-week-old db/+ mice: 240  $\mu\text{m}$ , 24-week-old db/db mice: 220  $\mu\text{m}$ ) were minor (Bogdanov et al. 2014), it is possible that analysis of a higher number of animals is necessary for the detection of such minor differences.

Additionally, morphological changes of photoreceptors were investigated. The outer segment length of rods did not differ between 12-, 24- and 38-week-old control and diabetic mice, but the outer segments of cones were significantly shorter and the total number of cones per scanfield was reduced in 38-week-old diabetic animals. Predominant cone photoreceptor dysfunction in early-stage DR has previously been shown in zebrafish (Alvarez et al. 2010) and humans (Cho et al. 2000; McAnany and Park 2019). Therefore, our results in mice support these findings and illustrate that neural cells in the retina (photoreceptors) are affected in early stages of DR.

The loss of pericytes is a DR key feature, which was detectable in db/db animals starting at an age of 12 weeks (Midea et al. 1989). In line with this, I observed a decreasing trend in cell number of PDGFR $\beta$ -positive pericytes in our db/db mouse strain, but not in animals younger than 24 weeks of age. Even though I did not find significant differences in the number of acellular

capillaries in our db/db mice, I could confirm a significant rise in the endothelial cell/pericyte ratio in 24-week-old diabetic animals due to slightly higher endothelial cell numbers with a concomitant decrease in pericytes. Therefore, I could detect initial stages of morphological changes in the vasculature of diabetic mice, beginning with an age of 24 weeks.

Reactivation of microglia and an elevation of pro-inflammatory chemokines and cytokines are key features of the DR pathology (Kinuthia et al. 2020). Arroba et al. 2016 described that activated microglia are present in two status of polarization during DR progression in db/db mice. Diabetic mice at the age of 5 weeks showed a M2 anti-inflammatory phenotype, whereas 8-week-old diabetic mice displayed a M1 pro-inflammatory response. Therefore, the microglia morphologies of 12-, 24- and 38-week-old diabetic and control mice were investigated. No significant difference in the number of IBA-positive cells was detected at any age investigated between genotypes. Furthermore, I determined the area occupied by the finely branched microglial processes, which is typically reduced upon gliotic activation. There was the tendency of smaller microglial 'territories' in db/db mice as compared to controls. Moreover, the soma area of the microglia of the 38-week-old diabetic animals was significantly larger than that of age-matched control mice, which provides another indication of microglial activation. In conclusion, I detected mild signs of microglial activation that support the assumption that neuroinflammation is ongoing and potentially contributing to disease progression in db/db mice.

I could confirm a beginning pericyte loss and microglia reactivity in the db/db animals. As the breakdown of the BRB is visible in 15-month-old diabetic animals (Cheung et al. 2005), db/db mice with an age of 24 and 38 weeks are still in an early DR stage and mild symptoms are visible. Evidently, the DR phenotype in our db/db mouse breed develops later than what was already published. Some reasons for that could be slight deviations due to the mouse strain background or different conditions present in the animal facilities regarding stress level of the animals that potentially add to the already triggered hormonal corticosterone stress axis. Since some of the published morphological differences are very small (Bogdanov et al. 2014), an increase of the animal number could show these minor changes in the diabetic mice compared to the controls. Furthermore, the diabetes phenotype is more prominent in male animals. Fan et al. 2018 showed that db/db males develop a greater extent of cognitive deficits and neurovascular dysfunctions than female diabetic mice. Sataranatarajan et al. 2016 showed that the life span of males was reduced compared to female db/db mice. The median survival of males was 349 days compared to 487 days in female mice. Since Midea et al. 1989 and Bogdanov et al. 2014 only used male mice in their experiments, it is possible that the manifestation of the retinal morphological changes are stronger in males than in females. In T2D, unlike type 1 diabetes, there does not appear to be an association between sex and DR in human patients. It is possible that the sex has an influence on the development and progression of DR, but the effect of biological sex becomes

less significant in advanced levels of DR (Ozawa et al. 2015). Given that both sexes are affected and suffering from DR, I followed the overarching goal to develop treatment options that work irrespective of sex effects. Accordingly, I included male and female mice, which might have led to these slightly inconsistent findings.

## 7.2. THE ELECTRORETINOGRAM: A SENSITIVE AND SUITABLE READOUT SYSTEM

I wanted to find a suitable and sensitive readout method for the gene therapeutic approach in diabetic animals. ERG recordings, which measure retinal light responsiveness, are sensitive to subtle alterations in functional integrity. Bogdanov et al. 2014 detected a- and b-wave abnormalities in ERG recordings from diabetic animals with an age of 16 and 24 weeks. Furthermore, Arroba et al. 2016 described a difference in the rod-driven and mixed responses of 5-, 8- and 20-week-old db/db mice compared to controls. In line with these findings, I could detect a significantly smaller rod-driven and cone-driven b-wave amplitude in 24-week-old diabetic mice. Accordingly, the mixed response (cones and rods) amplitudes were also reduced in diabetic mice, in both a- and b-wave amplitudes. Changes of those parameters detected by the ERG were independent from the sex of the mice. Therefore, the ERG can be used as a highly sensitive readout system, because it shows functional changes clearly before major morphological changes of retinal degeneration become detectable.

## 7.3. DIFFERENCES ON TRANSCRIPT AND PROTEIN LEVEL IN DIABETIC MICE

Although the causal link between chronic hyperglycaemia and the development and progression of DR is confirmed, the underlying mechanism remains unclear (Tarr et al. 2013). Therefore, transcriptome and proteome analysis of diabetic and non-diabetic model animals are commonly used techniques to shed light on the processes during DR progression.

In my thesis, transcriptome profiles of purified Müller cells from 12- and 24-week-old diabetic and control mice were generated. Since I was interested in processes during DR progression, the primary focus was on 24-week-old mice, which already showed the first key features of DR. Transcriptional changes on total retinal RNA have been investigated by various experts. Bogdanov et al. 2014 performed a genome-wide expression profiling analysis on total RNA isolated from retinæ of 8-week-old db/db and control mice. They found that gene ontology (GO) terms related to synaptic transmission, glutamate transport and metabolism were enriched in the down-regulated gene panel. GO terms that were over-represented among the up-regulated genes were related to mitochondrial respiration and oxidative stress. Kandpal et al. 2012 performed an RNA seq to characterize the retinal transcriptome from non-diabetic and streptozotocin-treated mice 32

weeks after induction of diabetes. They found that genes involved in disease-associated pathways such as inflammation, microvasculature formation, apoptosis, glucose metabolism, Wnt signaling, xenobiotic metabolism, photoreceptor biology and crystallin transcripts were differentially regulated. Since these studies focused on the whole retina, the differences in metabolism, homeostasis and inflammation could be due to a reaction of all retinal cell types. They provide a first insight in the retinal process, but are not focusing on altered Müller cell processes.

In contrast, van Hove et al. 2020 performed a single-cell RNA seq on retinal tissue from 12-week-old wild-type and Akimba mice, which is a type 1 diabetes model for early stage DR. The retinae of 12-week-old Akimba mice showed vascular defects including leaky spots, reduction of retinal thickness and oedema. An analysis of differentially expressed genes in rods, cones, bipolar cells and macroglia was performed. As Müller cells and astrocytes are the retinal macroglia, I compared our Müller cell-specific regulated genes to the single-cell RNA seq data from macroglia. van Hove et al. 2020 found that networks related to ribosome, cytoskeleton, immune system processes, S100 proteins, glutathione metabolism, iron ion homeostasis, cell cycle regulation/apoptosis and oxidative phosphorylation (OXPHOS) were upregulated in Akimba macroglia (van Hove et al. 2020). In our data set from 24-week-old db/db mice, pathways related to growth factor signaling and ion binding were upregulated in Müller cells of diabetic mice. Genes involved in glutathione metabolism like *Gpx1*, *Gpx3*, *Gpx4*, *Gstm1*, and *Mgst1* were upregulated in the macroglia of Akimba mice. The glutathione s-transferase m1 (*Gstm1*) is also one of the genes which was significantly upregulated in Müller cells of 24-week-old db/db mice. Furthermore, van Hove et al. 2020 showed that genes involved in cell cycle regulation and apoptosis like *Ccnd2*, *Cdkn1a*, *Gadd45g*, *Id3* and *Phlda3* are upregulated in the macroglia of Akimba mice. I found that the cyclin dependent kinase inhibitor 1c (*Cdkn1c*) gene is Müller cell-specific and significantly upregulated in diabetic mice. Another gene which was significantly upregulated in both data sets is metallothionein-2 (*Mt2*). It is known that *Mt2* is an antioxidant, protects against retinal neuron damage (Suemori et al. 2006) and that its expression is regulated by glucocorticoids (Martinho et al. 2013). I showed that corticosterone levels in 24-week-old db/db mice are significantly elevated. Therefore, the change in *Mt2* expression may be due to the high corticosterone level. This finding is confirmed by the fact that proteomics data on 2-days cortisol treated explants showed a significantly higher protein level of *Mt2* than explants which were cultivated without corticosterone (data not shown). Furthermore, van Hove et al. 2020 showed that markers of reactive gliosis like *Gfap* and *Lcn2* were upregulated in the macroglia of Akimba mice. Our RNA seq data showed that *Gfap* was significantly upregulated in Müller cells of diabetic mice with an age of 24 weeks, confirmed by qPCR data from 24-week-old control and diabetic mice. As retinal astrocytes are assumed to be found in a small amount in the MACS Müller cell fraction, this could be also due to

an altered *Gfap* expression in astrocytes. In sum, networks related to gliosis, glutathione metabolism and cell proliferation seem to be upregulated in both diabetes models. Furthermore, Grant et al. 2004 showed that ischemia-mediated overexpression of growth factors like VEGF, insulin-like growth factor-1, angiopoietin-1 and -2, stromal-derived factor-1, fibroblast growth factor-2 and tumor necrosis factor occurs in DR. These are in line with our finding that pathways related to growth factor signaling were upregulated in Müller cells. The angiopoietin like 4 (*Angptl4*) gene is for example upregulated in Müller cells of db/db mice (data not shown).

In addition, pathway enrichment analysis via PANTHER (Thomas et al. 2003) pinpoints pathways related to the cytoskeleton, RNA and protein binding as well as potassium channel activity in the set of downregulated Müller cell-specific genes of the diabetic retina. Van Hove et al. 2020 showed that genes involved in glycolysis, central nervous system (CNS) development and OXPHOS were downregulated in Akimba macroglia. 5 genes were found to be overlapping between our data set and the data set of the Akimba macroglia: *Cers4*, *Fgfbp3*, *Ndr3*, *Pid1* and *Guf1*. Ceramide synthetase 4 (*Cers4*) and GUF1 homolog, GTPase (*Guf1*) are involved in organonitrogen compound metabolic processes and NDRG family member 3 (*Ndr3*) in cellular responses to stimuli (van Hove et al. 2020). Fibroblast growth factor binding protein 3 (*Fgfbp3*) and phosphotyrosine interaction domain containing 1 (*Pid1*) contribute to the regulation of phosphate metabolic processes (van Hove et al. 2020, ESM Table 9: Enrichment.Process). In sum, the genes involved in general cellular functions like metabolic processes are consistently regulated in both data sets. Furthermore, Pannicke et al. 2006 showed that glial cells in diabetic rat retina are more sensitive to osmotic stress, partially associated with decreased potassium conductance mediated by Kir4.1 channels. In support of that, I found that the potassium channel activity was specifically downregulated in Müller cells of 24-week-old db/db mice.

In sum, the pathways which were differentially expressed in Müller cells of diabetic mice give first insights into the disease progression.

In addition to changes at transcript levels, the proteome of 24-week-old diabetic mice was investigated in this thesis. 986 genes and proteins overlapped in the Müller cell-specific regulated proteome and transcriptome data and 57.61% were concordantly regulated. The explanation why protein levels do not necessarily reflect transcript expression is complex. There are manifold mechanisms controlling the process and efficiency of protein translation (Liu et al. 2016b). In a simplistic view, the DNA is copied to a single strand messenger-RNA (mRNA) (transcription) and thereafter the mRNA is used as matrix to produce the respective protein (translation). Thus, mRNA levels would determine the amount of protein generated in a linear fashion. However, from a single gene, different transcript isoforms can be formed via alternative splicing which do not all contain the respective protein-coding sequence. Furthermore, the mRNA can be degraded before it gets translated which could contribute to a discrepancy between transcript and protein levels.

For instance, a delayed protein synthesis from its mRNA template during the cell cycle via the regulation of the translation rate is possible. This ensures that proteins are available at high amounts only in response to specific signals. Furthermore, proteins could have a way higher half-life than mRNA, whereby the half-life of different proteins is also variable and needs to be considered (Liu et al. 2016b). Therefore, the protein and transcript levels of identified gene candidates have to be further validated with additional methods like qPCR, Western blot, ELISA or immunohistochemistry to get detailed insights into the actual function of the gene of interest.

Here, I found that pathways related to the ATP and transporter activity were enriched in the set of downregulated proteins and pathways related to RNA and protein binding, ligase and transferase activity were upregulated in Müller cells from 24-week-old diabetic mice. Other publications already focused on the retinal proteome of diabetic mice. Ly et al. 2014 studied alterations in the retinal membrane proteome of 10-week-old db/db mice by label-free mass spectrometry. They found that pathways related to synaptic transmission and cell signaling were decreased, while pathways related to cell death/survival and metabolism were increased in protein levels (Ly et al. 2014). van Hove et al. 2020 studied the differential protein expression in retinæ from 12-week-old wild-type and Akimba mice. They showed a metabolic shift from glycolysis to OXPHOS, activation of microglia/macrophages, metal ion and oxidative stress response and reactive macroglia in the diabetic retina. Even though I could not detect GFAP staining of Müller cells in 24-week-old db/db mice, I detected an onset of microglia activation in 38-week-old db/db mice. This could be due to the fact that the db/db mice with an age of 24 and 38 weeks seem to be still in an early DR stage as only minor morphological and functional changes could be observed. In contrast 12-week-old Akimba mice already showed a stronger phenotype including vascular defects, reduction of retinal thickness and oedema (van Hove et al. 2020).

In conclusion, the transcriptome and proteome of our db/db mouse breeding showed that macroglia, together with other retinal cell types, may play a key role in retinal neurodegenerative diseases like DR.

#### 7.4. SEARCH FOR A MASTER REGULATOR OF THE MÜLLER CELL PHENOTYPE IN DIABETIC RETINOPATHY PROGRESSION

To identify key regulators that drive Müller cell changes in DR progression, I performed an oPOS-SUM-3 TF binding site cluster analysis (Ho Sui et al. 2005) on the basis of the RNA seq expression data implementing the list of genes specifically regulated in Müller cells of 24-week-old diabetic mice. Gene clusters of *Sp1*, *Ebf1*, *Egr1*, *Zfx*, *Foxd1* and *Sox2* are upregulated and gene clusters targeted by *Sox2*, *Rora*, *Foxf2*, *Srf* and *Nr3c1* were downregulated.

For the gene clusters which were significantly upregulated in Müller cells, the gene expression of the TF itself was investigated. Although it is known that insulin stimulates the biosynthesis of Sp1

Transcription Factor (*Sp1*) and its O-linked N-acetylglucosaminylation (Majumdar et al. 2004) and that db/db mice have elevated circulating insulin levels (Burke et al. 2017), the expression of *Sp1* was not altered in 24-week-old db/db mice. EBF transcription factor 1 (*Ebf1*) plays a crucial role in early adipogenesis and it is assumed that many components of metabolic and inflammatory pathways are positively and directly regulated by *Ebf1* (Griffin et al. 2013). As db/db mice are obese and have a higher amount of fat tissue, this could explain the transcriptional change of this TF cluster. The transcript of *Ebf1* is not regulated in diabetic mice with an age of 24 weeks. Several studies showed that the expression of early growth response 1 (*Egr1*) is triggered by hyperglycaemia in diabetes and, indeed, *Egr1* was found to be upregulated in the retinae of diabetic rats (Ao et al. 2019). Of note, in our analysis of 24-week-old db/db mice, *Egr1* expression seemed to be upregulated in all retinal cell types investigated, even though this trend did not reach significance level. Optic nerve injury which in a secondary response also leads to Müller cell gliosis (Wang et al. 2002), goes along with an upregulation of the zinc finger protein x-linked (*Zfx*). The *Zfx* transcript is not altered in db/db mice with an age of 24 weeks. The family of forkhead TFs stimulates the transcription of target genes involved in many fundamental cell processes like cell cycle progression, DNA repair, cell survival and insulin sensitivity. The activity of these proteins is regulated by insulin and other cytokines (Tsai et al. 2003). Therefore, the altered expression of forkhead box d1 (*Foxd1*) and forkhead box f2 (*Foxf2*) gene clusters in db/db mice could be due to the elevated circulating insulin levels (Burke et al. 2017). The TF *Foxd1* was mainly expressed in Müller cells, but the gene expression was not altered in diabetic mice compared to control mice. Furthermore, the gene expression of TFs which target gene clusters were significantly downregulated in Müller cells of 24-week-old db/db mice was investigated. *Foxf2* expression was not Müller cell-specific and did not change in 24-week-old db/db mice. The cluster of SRY-box transcription factor 2 (*Sox2*) was significantly up- and downregulated in Müller cells, whereby the Fisher-score and Z-Score was higher in the upregulated data set. *Sox2* plays an essential role in progenitor cell maintenance in the developing and adult CNS and has shown to be specifically expressed by Müller glia of C57/BL6 mice (Roesch et al. 2008). I was able to demonstrate that *Sox2* expression is Müller cell-specific, but gene expression was not altered in diabetic mice compared to control mice. Serum response factor (*Srf*) interacts with over 60 cofactors and, thus, is involved in the modulation of many cellular processes. Two prominent examples are its role in coordinating growth factor-mediated stimulation of cells and mitogen-activated protein kinase signalling as well as the effects which are mediated through rho-dependent changes in actin dynamics (Miano 2010). The expression of the TF *Srf* was not altered in db/db mice with an age of 24 weeks. RAR related orphan receptor a (*Rora*) expression was significantly increased in retinae of an oxygen-induced retinopathy mouse model and it is involved in retinal inflammation and pathologic neovascularization in proliferative retinopathy (Liu et al. 2016a). I found that the TF *Rora* is mainly

expressed in neurons, but there was no difference in diabetic mice. *Nr3c1* transcript which codes for the GR was Müller cell-specific and was significantly reduced in 24-week-old db/db mice. In the end, I identified potential key regulators that could have the potential to determine the functional changes in the diabetic retina. In the following, I decided to focus on the GR. The treatment with GR agonists like dexamethasone has proven to be an effective therapy in DR as it counterbalances typical changes associated with DR such as breakdown of the BRB or onset of neuroinflammation (Ghaseminejad et al. 2020). Furthermore, previous studies have shown that the selective GR agonist triamcinolone acetonide reduces vascular leakage (Brooks et al. 2004), inhibits the secretion of VEGF (Itakura et al. 2006) and prevents osmotic swelling of Müller cells (Pazdro and Burgess 2010). Although synthetic glucocorticoids are commonly used for therapeutic approaches in ophthalmology, the molecular processes of GR signaling and its role in DR progression are not known and are investigated in this study.

#### 7.5. POSSIBLE ROLE OF THE GLUCOCORTICOID RECEPTOR IN DIABETIC RETINOPATHY PROGRESSION

The GR is a nuclear hormone receptor with broad effect on inflammatory responses, cell proliferation and differentiation in target tissues. Gallina et al. 2014 showed that the GR is mainly located in Sox2-positive nuclei of Müller cells in mouse, guinea pig, dog and human retinae. It was confirmed that a partial loss of GR in the retina results in a thinner INL and that it plays a critical role in maintaining retinal homeostasis by regulating the inflammatory response (Kadmiel et al. 2015). Furthermore, Gallina et al. 2015 found that activation of GR inhibited the reactivity of microglia and the loss of retinal neurons upon excitotoxic tissue damage. The activated GR can regulate the expression of target genes through multiple ways. It can lead to transactivation or transrepression of gene transcription directly by binding to GREs in regulatory regions of specific target genes. Furthermore, the GR can act through protein-protein interactions with other TFs like NF- $\kappa$ B and AP-1 (Sulaiman et al. 2018). The oPOSSUM-3 analysis showed that the target gene cluster of the GR is downregulated specifically in 24-week-old diabetic animals compared to control mice. Furthermore, I showed that 1363 genes, a fourth of the Müller cell-specific downregulated genes, were also potential target genes of the GR. I studied the expression of two exemplary Müller cell-specific GR target genes. The transcript of *Foxo1* is significantly downregulated in 24-week-old diabetic mice compared to control mice. It is involved in multiple signaling processes and the control of insulin sensitivity, hepatic glucose production and blood glucose levels (Wu et al. 2018). Furthermore, *Ca4* which is a member of a large family of zinc metallo-enzymes that catalyze the reversible hydration of carbon dioxide was significantly down-regulated in Müller cells of 24-week-old diabetic mice. *Ca4* is essential for acid removal from the retina and RPE-driven acid release towards the choroid, and it has been shown that mutant *Ca4* impairs pH regulation

and causes retinal photoreceptor degeneration (Yang et al. 2005). Therefore, the major impact of correct function of the two putative GR target genes on retinal integrity demonstrate that the regulation of the GR target gene cluster in the diabetic retina could in turn have a great influence on the progression of the disease.

RNA seq of MACS enriched retinal cell types revealed significant and specific reduction of *Nr3c1* transcripts in Müller cells of 24-week-old db/db mice. A similar trend on protein level was shown by qPCR and Western blot. I could confirm the Müller cell-specific location of the GR in Müller cell nuclei in diabetic and control mice. It is known that GR mRNA levels increase above the pre-damage levels within 4 h after NMDA-induced damage and remained elevated for one day in chicken retinae. The GR level decreased to pre-damage levels by day 2 and below pre-damage levels by day 3 (Gallina et al. 2014). Therefore, it could well be that the retinal damage during DR progression has an influence on GR expression.

The main ligand of the GR in mice is the glucocorticoid corticosterone. Glucocorticoids have a broad range of effects and are involved in metabolic processes, immune system, reproduction, behaviour and cognitive functions. Circulating levels of glucocorticoids are regulated by the HPA axis. In case of stress, the HPA axis gets activated and an increase in glucocorticoids helps the body to cope and recover from the stress situation (Gjerstad et al. 2018). It has been shown that the corticosterone levels in mouse models of type 1 and type 2 diabetes are significantly elevated. Serum corticosterone level is increased in db/db animals at an age of 9 weeks (Erickson et al. 2017). Furthermore, diabetic patients have a significantly higher urinary-free cortisol level (Roy et al. 1998). I also confirmed an elevated blood plasma corticosterone level in 24-week-old mice. It is known that chronic administration of glucocorticoids can constitutively downregulate GR expression via an auto-regulatory loop (Vandevyver et al. 2014). Therefore, it is possible that the expression of the GR is negatively regulated in diabetic mice due to elevated corticosterone levels.

Given that it has been shown that GR activation has a beneficial effect on the retina, I decided to check whether an upregulation of GR *in vitro* with retinal explants and *in vivo* in diabetic mice via gene therapeutic tools is indeed protective and slows down disease progression.

## 7.6. MODULATION OF GLUCOCORTICOID RECEPTOR ACTIVITY *IN VITRO*

In ophthalmology, glucocorticoids are widely used for management of diverse diseases with acute and chronic ocular inflammatory conditions. For that purpose, the glucocorticoids triamcinolone acetonoid, dexamethasone, prednisolone and flucinolone acetonoid are commonly used. Therapeutic effects are mediated through genomic actions of the GR (Sulaiman et al. 2018). Without bound ligand, the GR is localized in the cytoplasm forming inactive oligomeric complexes in association with molecular chaperones. As soon as glucocorticoids bind, the GR dissociates from

those regulatory complexes and gets phosphorylated at multiple sites. Forming phosphorylated dimers, it then translocates to the nucleus influencing transcription in multiple ways (Sulaiman et al. 2018). Although glucocorticoids are commonly used, the molecular and cellular processes of GR signaling in the diabetic eye are largely unknown.

To address this under controlled conditions, I investigated the effect of GR modulation in an *in vitro* cell culture model. Since cortisol has higher glucocorticoid potency on the GR than corticosterone (Gong et al. 2015) and it is well-established in culture experiments using murine retinal explants (Gorovits et al. 1997; Toops et al. 2012), I used cortisol in the present study. As expected, a higher concentration of the active, phosphorylated GR was detected in retinal explants treated with cortisol by Western blot analysis, while the overall level of whole GR (inactive and active form) was unchanged. Proteome profiling revealed that pathways related to the organization of the cytoskeleton, energy supply and ATP activity were those that were downregulated upon cortisol treatment, while proteins associated with pathways related to RNA binding, transcriptional activity and phosphatase activity were upregulated. The unbound GR, which is bound to a chaperone complex, is located in the cytoplasm of the cell. Ligand binding induces conformational changes in the GR, involving phosphorylation (Liu et al. 2019). This phosphorylation process needs energy in form of ATP (Bennett et al. 2009) and therefore, falls in line with the fact that the ATP pathway is also regulated in the proteome data. Given that phosphorylation of GR leads to its translocation into the nucleus where it can function as a repressing and activating TF (Sulaiman et al. 2018), the upregulation of the transcriptional activity and the RNA binding pathways could be a consequence of this enhanced nuclear localization of the GR. It can act as a TF itself or modulate the binding affinity of other TFs to their DNA binding domains and thereby, it can also indirectly change gene expression profiles. As an example, the GR binds to the JUN subunit of AP-1 which is involved in a variety of cellular processes including proliferation, differentiation, apoptosis and pro-inflammatory responses (Ameyar et al. 2003; Ramamoorthy and Cidowski 2016). Our group showed earlier that Müller cells express high levels of *Fos* and *Jun*, potentially due to the fact that the GR is acting by modulating transcriptional activity at AP-1 sites (Ghaseminejad et al. 2020). In line with this assumption, the pathway of JUN kinase activity was also enriched in the proteome of cortisol treated retinae. As the interaction partners of GR play an important role in inflammation, I evaluated the effects of GR activation on known GR target genes that may play a role in this context. Since the GR is specifically localized in Müller cell nuclei, I focused on GR target genes which were significantly regulated in Müller cells of diabetic mice. Eleven of the 72 up-regulated proteins were reported as predicted GR targets and were expressed at high levels in Müller cells, as determined by our RNA seq experiment. None of those downregulated proteins in cortisol-treated retinal explants were also Müller cell-specific and a putative GR target gene. The Müller cell-specificity of the 11 up-regulated candidates was cross-

validated and compared to published scRNA seq resource data from mouse retina (Macosko et al. 2015). For five of these candidate genes, an exclusive expression in Müller cells could be confirmed. *Cryab* and *Eno1* were identified as the two most interesting candidates. *Eno1* is a component of the glycolytic pathway and strongly expressed in the INL of the retina, supposedly in Müller cells. *Eno1* was found to be reduced in the macula and increased in the vitreous of patients with Macular Telangiectasia type 2 (Len et al. 2012). Furthermore, it was altered in the diabetic rat retina (Quin et al. 2007) and in tear proteomic analysis of patients with T2D with dry eye syndrome (Li et al. 2014). *Cryab* has chaperone-like activity and is involved in the prevention of detrimental protein aggregations under cell stress conditions. It was shown that retinal neurodegeneration in animal models of diabetes was associated with increased levels of the crystalline protein family (Ruebsam et al. 2018). In support of those recent studies, I found a moderate up-regulation of mRNA from both genes in purified Müller cells of cortisol treated versus untreated retinal explants.

Testing whether the cortisol treatment had an impact on the cellular response in retinal explants, I did not find major morphological differences after 5 days *in vitro*. The main difference I could detect was regarding the GR itself. While an enhanced cytoplasmic GR level could be detected in the untreated explants compared to the *in vivo* situation, the GR stayed in the Müller cell nuclei as long as explants were stimulated with cortisol. This demonstrates that constantly high levels of glucocorticoids are needed to maintain the nuclear localization of the GR in Müller cells. Of note, due to the cultivation, Müller cells turned on their typical gliotic response pattern that includes a moderate rise of their GFAP expression. This aspect of Müller cell gliosis did not seem to be affected by GR stimulation, since GFAP immunoreactivity was comparable between treatment groups.

In sum, the *in vitro* data from retinal explants demonstrate that GR stimulation via cortisol administration had an effect not only on its conformation and activity, but also on the expression of known downstream GR target genes with clear modulation of those specifically expressed by Müller cells. These constantly high cortisol levels could mimic the elevated corticosterone level in diabetic mice. However, given the pitfalls of retinal explant cultures that include persistent unspecific neurodegeneration as a consequence of culturing, I did not perform further follow up experiments in this model. Instead, I set out to develop a gene therapeutic approach to enable the investigation of the long-term restoration of GR activity in Müller cells of diabetic mice.

### 7.7. MODULATION OF GLUCOCORTICOID RECEPTOR ACTIVITY *IN VIVO*

DR is the leading cause of vision loss in adults aged 20-64 years in developed countries. As it is a multifactorial retinal disease, it develops slowly and requires a treatment over years or even decades. In addition to the control of systemic factors, laser photocoagulation therapy has been mainly used as management therapy. However, there are notable side effects associated with this mode of treatment including the worsening of existing macular edema as well as impairment of night vision and peripheral retina function. In recent years, the use of injections of intravitreal corticosteroids like dexamethasone or of anti-VEGF agents have revolutionized the management of DR. Although anti-VEGF therapy showed remarkable clinical benefits in DR patients, it also comes with limitations and adverse effects. Moreover, the effectiveness of the before-mentioned therapeutics relies on repeated (monthly) intravitreal injections due to their short half-life in the eye. The incidence of adverse effect like endophthalmitis increases by frequent injections (Das et al. 2015). Intravitreal corticosteroids are efficient in the treatment of DME and they become increasingly important especially when patients prove to be resistant to the gold-standard anti-VEGF therapy. The advantages of corticosteroids are that they require a lower frequency of injections, lower costs and better patient compliance, but they are also associated with a high incidence of adverse effects. Therefore, corticosteroids are currently only the second-line option for patients who are not responding to other therapeutic treatments (Wang and Lo 2018). In conclusion, there is an urgent need for the development of additional or complementary treatment approaches.

In contrast to monthly intravitreal substrate injections, a gene therapeutical approach ideally should only require a single injection into the patient's eye, thereby significantly reducing the risk of procedure-related complications. In 2017, the food and drug administration (FDA) approved the first AAV-based gene therapy product for the treatment of Leber congenital amaurosis-2 which is a rare form of blindness caused by variations in the RPE65 gene. The AAV vector, which is subretinally injected, carries a copy of the RPE65 gene. The therapy is successful and shows improvement in functional vision as well as increase in visual field and full-field light sensitivity. Furthermore, it is documented to be a safe and durable treatment. Therefore, this underscores the great potential of gene therapeutical approaches, not only for the treatment of inherited retinal dystrophies, but also for multifactorial eye diseases like DR (Askou et al. 2020).

I identified the GR as a promising candidate that could be targeted in Müller glia to treat DR-associated changes of the cells and therewith potentially to improve the overall retinal integrity. Accordingly, my goal was to develop a gene therapeutical approach to achieve long-term efficient stimulation of GR signaling in Müller cells. I demonstrated a successful glia-specific expression of the GR expression cassette on basis of the reporter eGFP co-expressed with GR and a moderate up-regulation of GR determined by immunostainings following the intravitreal injection of an

AAV 9-construct for GR overexpression. A significant upregulation of the *Nr3c1* transcript in AAV-injected control and db/db mice was validated by qPCR. Furthermore, a *Gfap* upregulation trend due to AAV injection was visible in control and db/db mice, while the gene expression of *Glul* was not affected. The transcripts of the four putative GR target genes *Eno1*, *Cln1*, *Cryab* and *Sfxn5* were in most cases upregulated in db/db and control mice. Therefore, a downstream effect of AAV induced GR upregulation on predicted target genes could be shown in this study. In ERG recordings, a reduced light response of retinae in AAV injected mice independent of the genotype was detected. As GFAP upregulation was still present 12 weeks after injection and the ERG curves of AAV injected eyes were still reduced, the injection had a noticeable effect and an optimization of the injection method was performed. I compared two different injection systems from Hamilton and WPI with the goal to identify the appropriate injection system. In one eye of 12-week-old control mice PBS (sham control) was injected and in the other eye the AAV9-Nr3c1-eGFP construct. Single animals were injected either with the Hamilton or WPI system. 12 weeks post injection morphometric analysis and ERG measurements were conducted. The morphometric analysis showed that Müller cells in the retinae of mice, which were injected with the Hamilton system, were becoming gliotic as indicated by a rise of their GFAP expression due to the injection. However, I could not detect Müller cell-specific GFAP expression as a sign for gliosis in the retinae of mice which were injected with the WPI system. Furthermore, ERG measurements showed a trend to better light responses of retinae of mice which were injected with the WPI system detected. Therefore, the WPI system is the better choice for intravitreal AAV injection.

In conclusion, I showed a successful glia-specific transduction of the AAV9-Nr3c1-eGFP construct and I found an optimal injection method using the WPI system. Due to time constraints, the long-term effect of the GR overexpression in diabetic and control mice is not a part of this thesis.

## 8. CONCLUSION

I characterized the retinal phenotype of db/db mice and showed that db/db mice with an age of 24 and 38 weeks are still in an early DR stage presenting mild symptoms including the onset of pericyte loss and first signs of microglia activation. However, I could demonstrate that the ERG can be used as a highly sensitive readout system, because it shows functional changes clearly before major morphological changes of retinal degeneration become detectable. Importantly, changes of those parameters detected by the ERG were independent from the sex of the mice. Aiming to identify key regulators that drive Müller cell changes in DR progression, an oPOSSUM-3 TF binding site cluster analysis (Ho Sui et al. 2005) was performed based on the RNA seq expression data, implementing the list of genes specifically regulated in Müller cells of 24-week-old diabetic mice. This identified the GR (gene ID: *Nr3c1*) whose target gene cluster was downregulated in Müller cells of diabetic animals as a promising candidate. *Nr3c1* transcript was highest expressed in Müller cells and significantly reduced in 24-week-old db/db mice. Importantly, the GR was mainly located in Müller cell nuclei of diabetic and control mice. In addition, I confirmed an elevated blood plasma level of corticosterone, the endogenous ligand of the murine GR, in 24-week-old db/db mice. **Figure 29** summarizes the results concerning the GR in diabetic mice which were obtained in this study and asks the question if the long-term restoration of GR has a beneficial effect on Müller cell function.

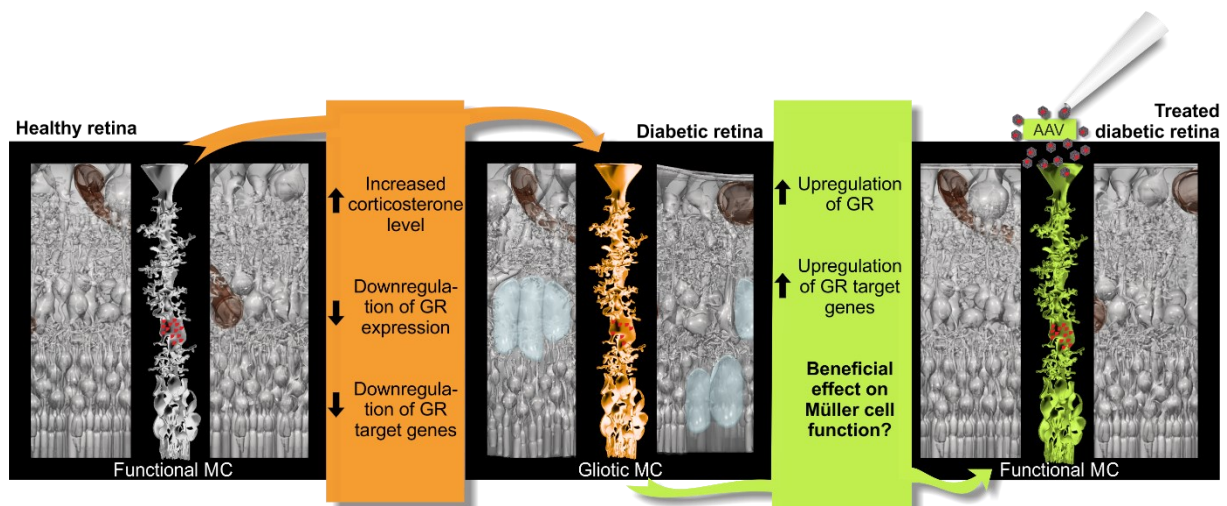


**Figure 29: Possible role of the glucocorticoid receptor in disease progression.** I confirmed that the glucocorticoid receptor (GR) (red dots) is mainly located in Müller cell nuclei of the healthy retina. I showed that 24-week-old db/db mice have an increased corticosterone level. In contrast, the expression of the GR and its target gene cluster is downregulated in Müller cells of db/db mice with an age of 24 weeks. To investigate the long-term restoration of GR activity and the question if a beneficial effect on Müller cell function occurs in diabetic mice, a gene therapeutic approach using an adeno-associated virus (AAV) construct was developed.

As it is known that chronic administration of glucocorticoids can constitutively downregulate GR expression via an auto-regulatory loop (Vandevyver et al. 2014), it could well be that the expression of the GR is negatively regulated in diabetic mice due to elevated corticosterone level. Although synthetic glucocorticoids are commonly used for therapeutic approaches in ophthalmology with undebatable beneficial effects, the molecular processes of GR signaling and its role in DR progression are largely not known. Therefore, I investigated the effect of GR modulation in an *in vitro* retinal explant model implementing cortisol stimulation. Constantly high cortisol levels not only influenced the GR phosphorylation level and activity, but also induced expression changes of known downstream GR target genes with specific modulation of those candidates I showed to be specifically expressed by Müller cells. To investigate the long-term restoration of GR activity in diabetic Müller cells which is not possible in the *in vitro* model, I set out to develop a gene therapeutic approach in db/db mice. This strategy comes with the advantage that it ideally requires only a single injection into the patient's eye and thereby significantly reduces the risk of procedure-related complications. AAV9-Nr3c1-eGFP particles were intravitreally injected into the eyes of 12-week-old mice and the eyes were collected 12 weeks thereafter. I could demonstrate a successful glia-specific transduction of the construct and I found an optimal injection method in the WPI system. Due to time constraints, the long-term effect of the GR overexpression in diabetic and control mice is not a part of this thesis and has to be investigated in the future.

In this thesis, I identified further potential key regulators that may underly the functional changes in the diabetic retina. The TF *Foxd1* whose gene cluster was significantly upregulated in Müller cells of 24-week-old diabetic mice was also mainly expressed in Müller cells. Furthermore, I could show that *Sox2* is specifically expressed in Müller cells and that its gene cluster was significantly up- and downregulated in Müller cells of 24-week-old diabetic mice. As both genes are Müller cell-specific expressed, they should be subject of further investigations. Finally, *Eno1*, a putative target gene of GR, is strongly expressed in the INL of the retina, supposedly in Müller cells, and was found to be reduced in the macula and increased in the vitreous of patients with Macular Telangiectasia type 2 (Len et al. 2012). Given that it was altered in the diabetic rat retina (Quin et al. 2007) and in patients with T2D with dry eye syndrome (Li et al. 2014), *Eno1* may also serve as an interesting candidate to be investigated in future studies.

## 9. LIST OF TABLES

Table 1: Oligonucleotides .....	19
Table 2: Adeno-associated virus .....	20
Table 3: Enzymes and proteins .....	20
Table 4: Antibodies.....	20
Table 5: Probes.....	21
Table 6: Chemicals.....	22
Table 7: Commercial kits .....	23
Table 8: Consumables.....	23
Table 9: Buffers and solution .....	25
Table 10: Instruments.....	26
Table 11: Software .....	27
Table 12: DNA extraction components .....	28
Table 13: Lysis protocol.....	28
Table 14: PCR components .....	28
Table 15: Thermocycling conditions .....	29
Table 16: cDNA components.....	31
Table 17: Thermocycling conditions .....	31
Table 18: qPCR components.....	32
Table 19: qPCR conditions.....	32
Table 20: Separating gel solution SDS-PAGE .....	35
Table 21: Stacking gel solution SDS-PAGE.....	35
Table 22: Abbreviations.....	85

## 10. LIST OF FIGURES

Figure 1. The cellular architecture of the retina.....	8
Figure 2: Differences of a healthy retina and a diabetic retinopathy affected retina .....	9
Figure 3: Gene therapeutic targeting of Müller cells by intravitreal virus injection .....	14
Figure 4: Glucocorticoid receptor signaling in the retina.....	15
Figure 5: Scheme of how targeting Müller cells may be of therapeutic use in diabetic retinopathy .....	18
Figure 6. The db/db mouse as an animal model for diabetic retinopathy .....	40
Figure 7. Unaltered cell numbers of the different retinal layers in diabetic mice.....	41
Figure 8: Unaltered number of calretinin-positive ganglion and amacrine cells in diabetic mice..	42
Figure 9: Onset of cone degeneration in aging diabetic mice.....	43
Figure 10: Loss of pericytes in diabetic mice .....	44
Figure 11: Recapitulation of vascular hallmarks of diabetic retinopathy in 24-week-old diabetic mice .....	45
Figure 12: Mild signs of microglia activation in db/db mice.....	46
Figure 13: Reduced light responses in the electroretinogram of retinae from 24-week-old diabetic mice .....	47
Figure 14: No major sex-specific differences in the light responses of diabetic mice.....	48
Figure 15: Cellular marker expression, bioinformatic analysis and pathway enrichment analysis of RNA seq data from purified retinal cell types from diabetic and control animals .....	51
Figure 16: Cellular marker expression, bioinformatic analysis and pathway enrichment analysis of proteomics data from purified retinal cell types from diabetic and control animals with an age of 24 weeks .....	53
Figure 17: Comparison of Müller cell-specific transcriptome and proteome profiles of 24-week-old diabetic mice.....	53
Figure 18: Glial fibrillary acidic protein upregulation in 24-week-old diabetic mice.....	54
Figure 19: oPOSSUM-3 transcription factor binding site cluster analysis of Müller cell- specific regulated genes of 24-week-old diabetic animals.....	55
Figure 20: The broad influence of the glucocorticoid receptor target gene cluster on Müller cell gene expression changes in the diabetic retina.....	57
Figure 21: Downregulation trend of the glucocorticoid receptor in Müller cells of 24-week-old diabetic mice .....	58
Figure 22: Elevated corticosterone level in diabetic mice at 24 weeks of age.....	59
Figure 23: Elevated level of the phosphorylated GR after cortisol treatment.....	60
Figure 24: Bioinformatic analysis and pathway enrichment analysis of proteomics from cortisol treated and untreated retinal explants .....	61
Figure 25: Expression changes of putative glucocorticoid receptor target genes due to enhanced GR signaling in retinal explants.....	62
Figure 26: Cortisol treatment reduces cytoplasmic diffusion of the glucocorticoid receptor <i>in vitro</i> (5-day culture) .....	63
Figure 27: Overexpressing the glucocorticoid receptor (gene ID: Nr3c1) in Müller cells of the mouse retina <i>in vivo</i> .....	65
Figure 28: Suitable intravitreal injection system (World precision instruments) for intravitreal adeno-associated virus injection.....	67
Figure 29: Possible role of the glucocorticoid receptor in disease progression .....	81

## 11. ABBREVIATIONS

Table 22: Abbreviations

<b>Abbreviation</b>	<b>Word</b>
AAV	Adeno-associated virus
Angptl4	Angiopoietin like 4
AP-1	Activating protein-1
APS	Ammonium persulfate
ATP	Adenosine triphosphatase
bp	Base pairs
BRB	Blood-retinal barrier
BSA	Bovine serum albumin
cm	Centimeter
°C	Degree celsius
Cdkn1c	Cyclin dependent kinase inhibitor 1c
Ca4	Carbonic anhydrase 4
cd/ms <sup>2</sup>	Candela per square meter
cDNA	Complementary DNA
Cers4	Ceramide synthetase 4
Clrn1	Clarin 1
cm	Centimeter
CNS	Central nervous system
CO <sub>2</sub>	Carbon dioxide
Cryab	Crystallin alpha B
DAPI	4',6-diamidino-2-phenylindole
DME	Diabetic macular oedema
DMSO	Dimethyl sulfoxide
DNA	Deoxyribonucleic acid
dNTP	Deoxyribonucleotide triphosphate
DR	Diabetic retinopathy
dTTP	Deoxythymidine triphosphate
Ebf1	EBF transcription factor 1
ECL	Enhanced chemiluminescence
ECS	Extracellular solution
EDTA	Ethylenediaminetetraacetic acid

e.g.	Exempli gratia
eGFP	Enhanced green fluorescent protein
Egr1	Early growth response 1
ELISA	Enzyme-linked immunosorbent assay
Eno1	Enolase1
ERG	Electroretinogram
E/P	Endothelial cell/Pericyte ratio
FDA	Food and drug administration
Fgfbp3	Fibroblast growth factor binding protein 3
FI	Forward inner
FO	Forward outer
Foxd1	Forkhead box d1
Foxf2	Forkhead box f2
Foxo1	Forkhead box o1
FPKM	Fragments per kilobase million
fw	Forward
g	Gram
G	Gauge
GC	Genome copies
GCL	Ganglion cell layer
GFAP	Glial fibrillary acidic protein
Glul	Glutamine synthetase
GO	Gene ontology
Gstm1	Glutathione s-transferase m1
GR	Glucocorticoid receptor
GREs	Glucocorticoid-response elements
Guf1	GUF1 homolog, GTPase
h	Hours
H <sub>2</sub> O	Water
HCl	Hydrochloric acid
H&E	Hematoxylin and Eosin
HPA	Hypothalamic–pituitary–adrenal
ID	Identity
IL-6	Interleukin-6
INL	Inner nuclear layer

i.p.	Intraperitoneal
IPL	Inner plexiform layer
K <sup>+</sup>	Potassium
kb	Kilo base pairs
KCl	Potassium chloride
kDa	Kilodaltons
KH <sub>2</sub> PO <sub>4</sub>	Monopotassium phosphate
kg	Kilogram
l	Liter
Iba	Ionized calcium-binding adaptor molecule 1
Itgam	Integrin subunit alpha M
M	Molar
MACS	Magnetic activated cell sorting/sorted
MC	Müller cells
MG	Microglia
MgCl <sub>2</sub>	Magnesium chloride
mg	Milligram
µg	Microgram
min	Minutes
ml	Milliliter
µl	Microliter
mM	Milli-Molar
µm	Micrometer
mRNA	Messenger-RNA
MS	Mass spectrometry
Mt2	Metallothionein-2
n	Numbers
N	Neurons
Na	Sodium
Na <sub>2</sub> HPO <sub>4</sub>	Disodium phosphate
NaCl	Sodium chloride
Ndr3	NDRG family member 3
NF-κB	Nuclear factor kappa-light-chain enhancer of activated B cells
ng	Nanogram
NFL	Nerve fiber layer

nm	Nanometer
No.	Number
NPDR	Non-proliferative diabetic retinopathy
ONL	Outer nuclear layer
OPL	Outer plexiform layer
OS	Outer segments
OXPPOS	Oxidative phosphorylation
P	Probability value
PAGE	Polyacrylamide gel electrophoresis
PBS	Phosphate-buffered saline
PCA	Principal component analysis
PCR	Polymerase chain reaction
PDE6B	Phosphodiesterase 6B
PDGFR $\beta$	Platelet-derived growth factor receptor beta
PDR	Proliferative diabetic retinopathy
Pecam1/ CD31	Platelet and endothelial cell adhesion molecule 1
PFA	Paraformaldehyde
pH	Power of hydrogen
Pid1	Phosphotyrosine interaction domain containing 1
PVDF	Polyvinylidene fluoride
qPCR	Quantitative PCR
Rev	Reverse
Rho	Rhodopsin
RI	Reverse inner
RNA	Ribonucleic acid
Rora	RAR related orphan receptor a
RO	Reverse outer
RPE	Retinal pigment epithelium
RT	Room temperature
sc	Single cell
SDS	Sodium dodecyl sulfate
sec	Seconds
SEM	Mean $\pm$ standard error
seq	Sequencing
Sfxn5	Siderflexin 5

ABBREVIATIONS

Sox2	SRY-box transcription factor 2
Sp1	Sp1 transcription factor
Srf	Serum response factor
STED	Stimulated emission depletion
T2D	Type 2 diabetes
TAE	Tris-Acetate-EDTA
TBS	Tris-buffered saline
TBST	Tris-buffered saline with 0.1% Tween 80
TEMED	Tetramethyl ethylenediamine
TF	Transcription factor
U	Units
V	Volt
VC	Vascular cells
WPI	World precision instruments
wt	Wild type, wild-type
w/v	Weight per volume
VEGF	Vascular endothelial growth factor
xg	Times gravity
Zfx	Zinc finger protein x-linked
%	Percentage

## 12. REFERENCES

- Alvarez, Yolanda; Chen, Kenneth; Reynolds, Alison L.; Waghorne, Nora; O'Connor, John J.; Kennedy, Breandán N. (2010): Predominant cone photoreceptor dysfunction in a hyperglycaemic model of non-proliferative diabetic retinopathy. In: *Disease models & mechanisms* 3 (3-4), p. 236–245. DOI: 10.1242/dmm.003772.
- Ameyar, M.; Wisniewska, M.; Weitzman, J. B. (2003): A role for AP-1 in apoptosis: the case for and against. In: *Biochimie* 85 (8), p. 747–752. DOI: 10.1016/j.biochi.2003.09.006.
- Ao, Haocheng; Liu, Bingqian; Li, Haichun; Lu, Lin (2019): Egr1 mediates retinal vascular dysfunction in diabetes mellitus via promoting p53 transcription. In: *Journal of cellular and molecular medicine* 23 (5), p. 3345–3356. DOI: 10.1111/jcmm.14225.
- Arroba, Ana I.; Alcalde-Estevez, Elena; García-Ramírez, Marta; Cazzoni, Daniele; La Villa, Pedro de; Sánchez-Fernández, Elena M. et al. (2016): Modulation of microglia polarization dynamics during diabetic retinopathy in db / db mice. In: *Biochimica et Biophysica Acta (BBA) - Molecular Basis of Disease* 1862 (9), p. 1663–1674. DOI: 10.1016/j.bbadis.2016.05.024.
- Askou, Anne Louise; Jakobsen, Thomas Stax; Corydon, Thomas J. (2020): Retinal gene therapy: an eye-opener of the 21st century. In: *Gene therapy*. DOI: 10.1038/s41434-020-0168-2.
- Baden, Tom; Euler, Thomas; Berens, Philipp (2020): Understanding the retinal basis of vision across species. In: *Nature reviews. Neuroscience* 21 (1), p. 5–20. DOI: 10.1038/s41583-019-0242-1.
- Behar-Cohen, Francine; Gelizé, Emmanuelle; Jonet, Laurent; Lassiaz, Patricia (2020): Anatomie de la rétine. In: *Medecine sciences : M/S* 36 (6-7), p. 594–599. DOI: 10.1051/medsci/2020094.
- Bennett, Nigel; Hooper, John D.; Lee, C. Soon; Gobe, Glenda C. (2009): Androgen receptor and caveolin-1 in prostate cancer. In: *IUBMB life* 61 (10), p. 961–970. DOI: 10.1002/iub.244.
- Bogdanov, Patricia; Corraliza, Lidia; Villena, Josep A.; Carvalho, Andrea R.; Garcia-Arumí, José; Ramos, David et al. (2014): The db/db mouse: a useful model for the study of diabetic retinal neurodegeneration. In: *PloS one* 9 (5), e97302. DOI: 10.1371/journal.pone.0097302.
- Bringmann, Andreas; Pannicke, Thomas; Grosche, Jens; Francke, Mike; Wiedemann, Peter; Skatchkov, Serguei N. et al. (2006): Müller cells in the healthy and diseased retina. In: *Progress in retinal and eye research* 25 (4), p. 397–424. DOI: 10.1016/j.preteyeres.2006.05.003.
- Bringmann, Andreas; Pannicke, Thomas; Uhlmann, Susanne; Kohen, Leon; Wiedemann, Peter; Reichenbach, Andreas (2002): Membrane conductance of Müller glial cells in proliferative diabetic retinopathy. In: *Canadian journal of ophthalmology. Journal canadien d'ophtalmologie* 37 (4), p. 221–227. DOI: 10.1016/s0008-4182(02)80113-2.
- Brooks, H. Logan; Caballero, Sergio; Newell, Charles K.; Steinmetz, Robert L.; Watson, Debbie; Segal, Mark S. et al. (2004): Vitreous levels of vascular endothelial growth factor and stromal-derived factor 1 in patients with diabetic retinopathy and cystoid macular edema before and after intraocular injection of triamcinolone. In: *Archives of ophthalmology (Chicago, Ill. : 1960)* 122 (12), p. 1801–1807. DOI: 10.1001/archophth.122.12.1801.
- Buckingham, Julia C. (2006): Glucocorticoids: exemplars of multi-tasking. In: *British journal of pharmacology* 147 Suppl 1, S258-268. DOI: 10.1038/sj.bjp.0706456.

- Burke, Susan J.; Batdorf, Heidi M.; Burk, David H.; Noland, Robert C.; Eder, Adrianna E.; Boulos, Matthew S. et al. (2017): db/db Mice Exhibit Features of Human Type 2 Diabetes That Are Not Present in Weight-Matched C57BL/6J Mice Fed a Western Diet. In: *Journal of diabetes research* 2017. DOI: 10.1155/2017/8503754.
- Chan, Annie; Duker, Jay S.; Ko, Tony H.; Fujimoto, James G.; Schuman, Joel S. (2006): Normal macular thickness measurements in healthy eyes using Stratus optical coherence tomography. In: *Archives of ophthalmology (Chicago, Ill. : 1960)* 124 (2), p. 193–198. DOI: 10.1001/archophth.124.2.193.
- Chen, H.; Charlat, O.; Tartaglia, L. A.; Woolf, E. A.; Weng, X.; Ellis, S. J. et al. (1996): Evidence that the diabetes gene encodes the leptin receptor. Identification of a mutation in the leptin receptor gene in db/db mice. In: *Cell* 84 (3), p. 491–495. DOI: 10.1016/s0092-8674(00)81294-5.
- Cheung, Alvin K. H.; Fung, Maggie K. L.; Lo, Amy C. Y.; Lam, Terence T. L.; So, Kwok Fai; Chung, Stephen S. M.; Chung, Sookja K. (2005): Aldose reductase deficiency prevents diabetes-induced blood-retinal barrier breakdown, apoptosis, and glial reactivation in the retina of db/db mice. In: *Diabetes* 54 (11), p. 3119–3125. DOI: 10.2337/diabetes.54.11.3119.
- Cheung, Ning; Mitchell, Paul; Wong, Tien Yin (2010): Diabetic retinopathy. In: *Lancet (London, England)* 376 (9735), p. 124–136. DOI: 10.1016/S0140-6736(09)62124-3.
- Cheung, Ning; Wong, Tien Y. (2008): Diabetic retinopathy and systemic vascular complications. In: *Progress in retinal and eye research* 27 (2), p. 161–176. DOI: 10.1016/j.preteyeres.2007.12.001.
- Cho, N. C.; Poulsen, G. L.; Ver Hoeve, J. N.; Nork, T. M. (2000): Selective loss of S-cones in diabetic retinopathy. In: *Archives of ophthalmology (Chicago, Ill. : 1960)* 118 (10), p. 1393–1400. DOI: 10.1001/archophth.118.10.1393.
- Chou, Jonathan C.; Rollins, Stuart D.; Fawzi, Amani A. (2013): Trypsin digest protocol to analyze the retinal vasculature of a mouse model. In: *Journal of visualized experiments : JoVE* (76), e50489. DOI: 10.3791/50489.
- Coleman, D. L.; Hummel, K. P. (1974): Hyperinsulinemia in pre-weaning diabetes (db) mice. In: *Diabetologia* 10 Suppl, p. 607–610. DOI: 10.1007/BF01221993.
- Coughlin, Brandon A.; Feenstra, Derrick J.; Mohr, Susanne (2017): Müller cells and diabetic retinopathy. In: *Vision research* 139, p. 93–100. DOI: 10.1016/j.visres.2017.03.013.
- Das, A.; Stroud, S.; Mehta, A.; Rangasamy, S. (2015): New treatments for diabetic retinopathy. In: *Diabetes, obesity & metabolism* 17 (3), p. 219–230. DOI: 10.1111/dom.12384.
- Dauletbekov, Daniyar; Bartz-Schmidt, K. Ulrich; Fischer, M. Dominik (2018): Subretinal and Intravitreal Retinal Injections in Monkeys. In: *Methods in molecular biology (Clifton, N.J.)* 1715, p. 251–257. DOI: 10.1007/978-1-4939-7522-8\_18.
- Davis, Carrie A.; Hitz, Benjamin C.; Sloan, Cricket A.; Chan, Esther T.; Davidson, Jean M.; Gabdank, Idan et al. (2018): The Encyclopedia of DNA elements (ENCODE): data portal update. In: *Nucleic acids research* 46 (D1), D794–D801. DOI: 10.1093/nar/gkx1081.

- Diabetic Retinopathy Vitrectomy Study Research Group (1985): Early vitrectomy for severe vitreous hemorrhage in diabetic retinopathy. Two-year results of a randomized trial. Diabetic Retinopathy Vitrectomy Study report 2. The Diabetic Retinopathy Vitrectomy Study Research Group. In: *Archives of ophthalmology (Chicago, Ill. : 1960)* 103 (11), p. 1644–1652.
- Erickson, Rebecca L.; Browne, Caroline A.; Lucki, Irwin (2017): Hair corticosterone measurement in mouse models of type 1 and type 2 diabetes mellitus. In: *Physiology & behavior* 178, p. 166–171. DOI: 10.1016/j.physbeh.2017.01.018.
- Fan, Baoyan; Liu, Xian Shuang; Szalad, Alexandra; Wang, Lei; Zhang, Ruilan; Chopp, Michael; Zhang, Zheng Gang (2018): Influence of Sex on Cognition and Peripheral Neurovascular Function in Diabetic Mice. In: *Frontiers in neuroscience* 12, p. 795. DOI: 10.3389/fnins.2018.00795.
- Fong, Donald S.; Girach, Aniz; Boney, April (2007): Visual side effects of successful scatter laser photocoagulation surgery for proliferative diabetic retinopathy: a literature review. In: *Retina (Philadelphia, Pa.)* 27 (7), p. 816–824. DOI: 10.1097/IAE.0b013e318042d32c.
- Fu, Shuhua; Dong, Shuqian; Zhu, Meili; Sherry, David M.; Wang, Changyun; You, Zhipeng et al. (2015): Müller Glia Are a Major Cellular Source of Survival Signals for Retinal Neurons in Diabetes. In: *Diabetes* 64 (10), p. 3554–3563. DOI: 10.2337/db15-0180.
- Gallina, Donika; Zelinka, Christopher; Fischer, Andy J. (2014): Glucocorticoid receptors in the retina, Müller glia and the formation of Müller glia-derived progenitors. In: *Development (Cambridge, England)* 141 (17), p. 3340–3351. DOI: 10.1242/dev.109835.
- Gallina, Donika; Zelinka, Christopher Paul; Cebulla, Colleen M.; Fischer, Andy J. (2015): Activation of glucocorticoid receptors in Müller glia is protective to retinal neurons and suppresses microglial reactivity. In: *Experimental neurology* 273, p. 114–125. DOI: 10.1016/j.expneurol.2015.08.007.
- Gaucher, David; Chiappore, Jean-Armand; Pâques, Michel; Simonutti, Manuel; Boitard, Christian; Sahel, José A. et al. (2007): Microglial changes occur without neural cell death in diabetic retinopathy. In: *Vision research* 47 (5), p. 612–623. DOI: 10.1016/j.visres.2006.11.017.
- Ghaseminejad, Farhad; Kaplan, Lew; Pfaller, Anna M.; Hauck, Stefanie M.; Grosche, Antje (2020): The role of Müller cell glucocorticoid signaling in diabetic retinopathy. In: *Graefes archive for clinical and experimental ophthalmology* 258 (2), p. 221–230. DOI: 10.1007/s00417-019-04521-w.
- Giove, Thomas J.; Sena-Esteves, Miguel; Eldred, William D. (2010): Transduction of the inner mouse retina using AAVrh8 and AAVrh10 via intravitreal injection. In: *Experimental eye research* 91 (5), p. 652–659. DOI: 10.1016/j.exer.2010.08.011.
- Gjerstad, Julia K.; Lightman, Stafford L.; Spiga, Francesca (2018): Role of glucocorticoid negative feedback in the regulation of HPA axis pulsatility. In: *Stress (Amsterdam, Netherlands)* 21 (5), p. 403–416. DOI: 10.1080/10253890.2018.1470238.
- Gong, Shuai; Miao, Yi-Long; Jiao, Guang-Zhong; Sun, Ming-Ju; Li, Hong; Lin, Juan et al. (2015): Dynamics and correlation of serum cortisol and corticosterone under different physiological or stressful conditions in mice. In: *PLoS one* 10 (2), e0117503. DOI: 10.1371/journal.pone.0117503.

- Gorovits, R.; Avidan, N.; Avisar, N.; Shaked, I.; Vardimon, L. (1997): Glutamine synthetase protects against neuronal degeneration in injured retinal tissue. In: *Proceedings of the National Academy of Sciences of the United States of America* 94 (13), p. 7024–7029. DOI: 10.1073/pnas.94.13.7024.
- Grant, Maria B.; Afzal, Aqeela; Spoerri, Polyxenie; Pan, Hao; Shaw, Lynn C.; Mames, Robert N. (2004): The role of growth factors in the pathogenesis of diabetic retinopathy. In: *Expert opinion on investigational drugs* 13 (10), p. 1275–1293. DOI: 10.1517/13543784.13.10.1275.
- Griffin, Michael J.; Zhou, Yiming; Kang, Sona; Zhang, Xiaolan; Mikkelsen, Tarjei S.; Rosen, Evan D. (2013): Early B-cell factor-1 (EBF1) is a key regulator of metabolic and inflammatory signaling pathways in mature adipocytes. In: *The Journal of biological chemistry* 288 (50), p. 35925–35939. DOI: 10.1074/jbc.M113.491936.
- Grosche, Antje; Hauser, Alexandra; Lepper, Marlen Franziska; Mayo, Rebecca; Toerne, Christine von; Merl-Pham, Juliane; Hauck, Stefanie M. (2016): The Proteome of Native Adult Müller Glial Cells From Murine Retina. In: *Molecular & cellular proteomics: MCP* 15 (2), p. 462–480. DOI: 10.1074/mcp.M115.052183.
- Ho Sui, Shannan J.; Mortimer, James R.; Arenillas, David J.; Brumm, Jochen; Walsh, Christopher J.; Kennedy, Brian P.; Wasserman, Wyeth W. (2005): oPOSSUM: identification of over-represented transcription factor binding sites in co-expressed genes. In: *Nucleic acids research* 33 (10), p. 3154–3164. DOI: 10.1093/nar/gki624.
- Huberman, Andrew D.; Niell, Cristopher M. (2011): What can mice tell us about how vision works? In: *Trends in neurosciences* 34 (9), p. 464–473. DOI: 10.1016/j.tins.2011.07.002.
- Hummel, K. P.; Dickie, M. M.; Coleman, D. L. (1966): Diabetes, a new mutation in the mouse. In: *Science (New York, N. Y.)* 153 (3740), p. 1127–1128. DOI: 10.1126/science.153.3740.1127.
- Itakura, Hirotaka; Akiyama, Hideo; Hagimura, Norikazu; Doi, Hiroshi; Tanaka, Toru; Kishi, Shoji; Kurabayashi, Masahiko (2006): Triamcinolone acetonide suppresses interleukin-1 beta-mediated increase in vascular endothelial growth factor expression in cultured rat Müller cells. In: *Graefes' archive for clinical and experimental ophthalmology* (2), p. 226–231. DOI: 10.1007/s00417-005-0052-1.
- Jeon, C. J.; Strettoi, E.; Masland, R. H. (1998): The major cell populations of the mouse retina. In: *The Journal of neuroscience: the official journal of the Society for Neuroscience* 18 (21), p. 8936–8946.
- Joseph, S. Iwin Thanakumar; Sravanthi, Tatiparthi; Karunakaran, V.; Priyadharsini, C. (2020): Investigation of Machine Learning Methodologies in Microaneurysms Discernment. In: S. Smys, João Manuel R. S. Tavares, Valentina Emilia Balas and Abdullah M. Iliyasa (Hg.): *Computational Vision and Bio-Inspired Computing*, Bd. 1108. Cham: Springer International Publishing (Advances in Intelligent Systems and Computing), p. 1327–1334.
- Kadmiel, Mahita; Ramamoorthy, Sivapriya; Cidlowski, John (2015): Glucocorticoid Receptor Role in the Mouse Retina. In: *Invest. Ophthalmol. Vis. Sci.* 56 (7), p. 887.
- Kandpal, Raj P.; Rajasimha, Harsha K.; Brooks, Matthew J.; Nellissery, Jacob; Wan, Jun; Qian, Jiang et al. (2012): Transcriptome analysis using next generation sequencing reveals molecular signatures of diabetic retinopathy and efficacy of candidate drugs. In: *Molecular vision* 18, p. 1123–1146.

- Kassambara, Alboukadel; Mundt, Fabian (2020): factoextra: Extract and Visualize the Results of Multivariate Data Analyses. Version: 1.0.7. Online available: <https://CRAN.R-project.org/package=factoextra>.
- Kern, Timothy S.; Berkowitz, Bruce A. (2015): Photoreceptors in diabetic retinopathy. In: *Journal of Diabetes Investigation* 6 (4), p. 371–380. DOI: 10.1111/jdi.12312.
- Kinuthia, Urbanus Muthai; Wolf, Anne; Langmann, Thomas (2020): Microglia and Inflammatory Responses in Diabetic Retinopathy. In: *Frontiers in Immunology* 11. DOI: 10.3389/fimmu.2020.564077.
- Kolde, Raivo (2019): pheatmap: Pretty Heatmaps. Version: 1.0.12. Online available: <https://CRAN.R-project.org/package=pheatmap>.
- Koskela, U. E.; Kuusisto, S. M.; Nissinen, A. E.; Savolainen, M. J.; Liinamaa, M. J. (2013): High vitreous concentration of IL-6 and IL-8, but not of adhesion molecules in relation to plasma concentrations in proliferative diabetic retinopathy. In: *Ophthalmic research* 49 (2), p. 108–114. DOI: 10.1159/000342977.
- Kumar, Ashok; Pandey, Rajeev K.; Miller, Lindsay J.; Singh, Pawan K.; Kanwar, Mamta (2013): Muller glia in retinal innate immunity: a perspective on their roles in endophthalmitis. In: *Critical reviews in immunology* 33 (2), p. 119–135. DOI: 10.1615/critrevimmunol.2013006618.
- Le, Yun-Zheng (2017): VEGF production and signaling in Müller glia are critical to modulating vascular function and neuronal integrity in diabetic retinopathy and hypoxic retinal vascular diseases. In: *Vision research* 139, p. 108–114. DOI: 10.1016/j.visres.2017.05.005.
- Lee, Eun-Shil; Lee, Jea-Young; Jeon, Chang-Jin (2010): Types and density of calretinin-containing retinal ganglion cells in mouse. In: *Neuroscience research* 66 (2), p. 141–150. DOI: 10.1016/j.neures.2009.10.008.
- Lee, Jia Hui; Wang, Jiang-Hui; Chen, Jinying; Li, Fan; Edwards, Thomas L.; Hewitt, Alex W.; Liu, Guei-Sheung (2019): Gene therapy for visual loss: Opportunities and concerns. In: *Progress in retinal and eye research* 68, p. 31–53. DOI: 10.1016/j.preteyeres.2018.08.003.
- Lee, Sammy C. S.; Weltzien, Felix; Madigan, Michele C.; Martin, Paul R.; Grünert, Ulrike (2016): Identification of A II amacrine, displaced amacrine, and bistratified ganglion cell types in human retina with antibodies against calretinin. In: *The Journal of comparative neurology* 524 (1), p. 39–53. DOI: 10.1002/cne.23821.
- Len, Alice C. L.; Powner, Michael B.; Zhu, Ling; Hageman, Gregory S.; Song, Xiaomin; Fruttiger, Marcus; Gillies, Mark C. (2012): Pilot application of iTRAQ to the retinal disease Macular Telangiectasia. In: *Journal of proteome research* 11 (2), p. 537–553. DOI: 10.1021/pr200889t.
- Li, Bing; Sheng, Minjie; Xie, Liqi; Liu, Feng; Yan, Guoquan; Wang, Weifang et al. (2014): Tear proteomic analysis of patients with type 2 diabetes and dry eye syndrome by two-dimensional nano-liquid chromatography coupled with tandem mass spectrometry. In: *Invest. Ophthalmol. Vis. Sci.* 55 (1), p. 177–186. DOI: 10.1167/iovs.13-12080.
- Li, Qing; Puro, Donald G. (2002): Diabetes-induced dysfunction of the glutamate transporter in retinal Müller cells. In: *Investigative ophthalmology & visual science* 43 (9), p. 3109–3116.

- Lieth, E.; LaNoue, K. F.; Antonetti, D. A.; Ratz, M. (2000): Diabetes reduces glutamate oxidation and glutamine synthesis in the retina. The Penn State Retina Research Group. In: *Experimental eye research* 70 (6), p. 723–730. DOI: 10.1006/exer.2000.0840.
- Liu, Bing; Zhang, Tie-Ning; Knight, Jessica K.; Goodwin, Julie E. (2019): The Glucocorticoid Receptor in Cardiovascular Health and Disease. In: *Cells* 8 (10). DOI: 10.3390/cells8101227.
- Liu, Chi-Hsiu; Sun, Ye; SanGiovanni, John Paul; Evans, Lucy; Tian, Katherine; Stahl, Andreas et al. (2016a): Nuclear receptor ROR $\alpha$  regulates retinal inflammation and neovascularization in retinopathy through SOCS3. In: *Invest. Ophthalmol. Vis. Sci.* 57 (12), p. 3630.
- Liu, Yansheng; Beyer, Andreas; Aebersold, Ruedi (2016b): On the Dependency of Cellular Protein Levels on mRNA Abundance. In: *Cell* 165 (3), p. 535–550. DOI: 10.1016/j.cell.2016.03.014.
- Ly, Alice; Scheerer, Markus F.; Zukunft, Sven; Muschet, Caroline; Merl, Juliane; Adamski, Jerzy et al. (2014): Retinal proteome alterations in a mouse model of type 2 diabetes. In: *Diabetologia* 57 (1), p. 192–203. DOI: 10.1007/s00125-013-3070-2.
- Macosko, Evan Z.; Basu, Anindita; Satija, Rahul; Nemesh, James; Shekhar, Karthik; Goldman, Melissa et al. (2015): Highly Parallel Genome-wide Expression Profiling of Individual Cells Using Nanoliter Droplets. In: *Cell* 161 (5), p. 1202–1214. DOI: 10.1016/j.cell.2015.05.002.
- Majumdar, Gipsy; Wright, Jeremiah; Markowitz, Paul; Martinez-Hernandez, Antonio; Raghov, Rajendra; Solomon, Solomon S. (2004): Insulin stimulates and diabetes inhibits O-linked N-acetylglucosamine transferase and O-glycosylation of Sp1. In: *Diabetes* 53 (12), p. 3184–3192. DOI: 10.2337/diabetes.53.12.3184.
- Martinho, A.; Gonçalves, I.; Santos, C. R. (2013): Glucocorticoids regulate metallothionein-1/2 expression in rat choroid plexus: effects on apoptosis. In: *Molecular and cellular biochemistry* 376 (1-2), p. 41–51. DOI: 10.1007/s11010-012-1547-9.
- Mathelier, Anthony; Zhao, Xiaobei; Zhang, Allen W.; Parcy, François; Worsley-Hunt, Rebecca; Arenillas, David J. et al. (2014): JASPAR 2014: an extensively expanded and updated open-access database of transcription factor binding profiles. In: *Nucleic acids research* 42 (Database issue), D142-7. DOI: 10.1093/nar/gkt997.
- McAnany, J. Jason; Park, Jason C. (2019): Cone Photoreceptor Dysfunction in Early-Stage Diabetic Retinopathy: Association Between the Activation Phase of Cone Phototransduction and the Flicker Electretinogram. In: *Invest. Ophthalmol. Vis. Sci.* 60 (1), p. 64–72. DOI: 10.1167/iops.18-25946.
- Miano, Joseph M. (2010): Role of serum response factor in the pathogenesis of disease. In: *Laboratory investigation; a journal of technical methods and pathology* 90 (9), p. 1274–1284. DOI: 10.1038/labinvest.2010.104.
- Midena, E.; Segato, T.; Radin, S.; Di Giorgio, G.; Meneghini, F.; Piermarocchi, S.; Belloni, A. S. (1989): Studies on the retina of the diabetic db/db mouse. I. Endothelial cell-pericyte ratio. In: *Ophthalmic research* 21 (2), p. 106–111. DOI: 10.1159/000266787.
- Moore, Nicholas A.; Morral, Nuria; Ciulla, Thomas A.; Bracha, Peter (2018): Gene therapy for inherited retinal and optic nerve degenerations. In: *Expert opinion on biological therapy* 18 (1), p. 37–49. DOI: 10.1080/14712598.2018.1389886.

- Oakley, Robert H.; Cidlowski, John A. (2013): The biology of the glucocorticoid receptor: new signaling mechanisms in health and disease. In: *The Journal of allergy and clinical immunology* 132 (5), p. 1033–1044. DOI: 10.1016/j.jaci.2013.09.007.
- Ozawa, Glen Y.; Bearnse, Marcus A.; Adams, Anthony J. (2015): Male-female differences in diabetic retinopathy? In: *Current eye research* 40 (2), p. 234–246. DOI: 10.3109/02713683.2014.958500.
- Pannicke, Thomas; Iandiev, Ianors; Wurm, Antje; Uckermann, Ortrud; vom Hagen, Franziska; Reichenbach, Andreas et al. (2006): Diabetes alters osmotic swelling characteristics and membrane conductance of glial cells in rat retina. In: *Diabetes* 55 (3), p. 633–639. DOI: 10.2337/diabetes.55.03.06.db05-1349.
- Pauly, Diana; Agarwal, Divyansh; Dana, Nicholas; Schäfer, Nicole; Biber, Josef; Wunderlich, Kirsten A. et al. (2019): Cell-Type-Specific Complement Expression in the Healthy and Diseased Retina. In: *Cell reports* 29 (9), 2835-2848.e4. DOI: 10.1016/j.celrep.2019.10.084.
- Pazdro, Robert; Burgess, John R. (2010): The role of vitamin E and oxidative stress in diabetes complications. In: *Mechanisms of ageing and development* 131 (4), p. 276–286. DOI: 10.1016/j.mad.2010.03.005.
- Pellissier, Lucie P.; Hoek, Robert M.; Vos, Rogier M.; Aartsen, Wendy M.; Klimczak, Ryan R.; Hoyng, Stefan A. et al. (2014): Specific tools for targeting and expression in Müller glial cells. In: *Molecular therapy. Methods & clinical development* 1. DOI: 10.1038/mtm.2014.9.
- Peng, Bao-yu; Wang, Qiang; Luo, Yan-hong; He, Jian-feng; Tan, Tao; Zhu, Hua (2018): A novel and quick PCR-based method to genotype mice with a leptin receptor mutation (db/db mice). In: *Acta Pharmacologica Sinica* 39 (1), p. 117–123. DOI: 10.1038/aps.2017.52.
- Picard, Emilie; Daruich, Alejandra; Youale, Jenny; Courtois, Yves; Behar-Cohen, Francine (2020): From Rust to Quantum Biology: The Role of Iron in Retina Physiopathology. In: *Cells* 9 (3). DOI: 10.3390/cells9030705.
- Quin, Godfrey J.; Len, Alice C. L.; Billson, Frank A.; Gillies, Mark C. (2007): Proteome map of normal rat retina and comparison with the proteome of diabetic rat retina: new insight in the pathogenesis of diabetic retinopathy. In: *Proteomics* 7 (15), p. 2636–2650. DOI: 10.1002/pmic.200600486.
- R Core Team (2014): R: A language and environment for statistical computing. R Foundation for Statistical Computing, Vienna, Austria. Online available: <http://www.R-project.org/>.
- Ramamoorthy, Sivapriya; Cidlowski, John A. (2016): Corticosteroids: Mechanisms of Action in Health and Disease. In: *Rheumatic diseases clinics of North America* 42 (1), 15-31. DOI: 10.1016/j.rdc.2015.08.002.
- Rashid, Khalid; Akhtar-Schaefer, Isha; Langmann, Thomas (2019): Microglia in Retinal Degeneration. In: *Frontiers in Immunology* 10, p. 1975. DOI: 10.3389/fimmu.2019.01975.
- Reichenbach, Andreas; Bringmann, Andreas (2013): New functions of Müller cells. In: *Glia* 61 (5), p. 651–678. DOI: 10.1002/glia.22477.
- Rodieck, Robert W. (1998): The first steps in seeing. Sunderland, Massachusetts: Sinauer Associates, Inc.

- Roesch, Karin; Jadhav, Ashutosh P.; Trimarchi, Jeffrey M.; Stadler, Michael B.; Roska, Botond; Sun, Ben B.; Cepko, Constance L. (2008): The transcriptome of retinal Müller glial cells. In: *The Journal of comparative neurology* 509 (2), p. 225–238. DOI: 10.1002/cne.21730.
- Rojas, Modesto; Zhang, Wenbo; Lee, Dexter L.; Romero, Maritza J.; Nguyen, Doan T.; Al-Shabraway, Mohamed et al. (2010): Role of IL-6 in angiotensin II-induced retinal vascular inflammation. In: *Investigative ophthalmology & visual science* 51 (3), p. 1709–1718. DOI: 10.1167/iovs.09-3375.
- Rouillard, Andrew D.; Gundersen, Gregory W.; Fernandez, Nicolas F.; Wang, Zichen; Monteiro, Caroline D.; McDermott, Michael G.; Ma'ayan, Avi (2016): The harmonizome: a collection of processed datasets gathered to serve and mine knowledge about genes and proteins. In: *Database: the journal of biological databases and curation* 2016. DOI: 10.1093/database/baw100.
- Roy, Monique S.; Roy, Alec; Brown, Stafford (1998): Increased Urinary-Free Cortisol Outputs in Diabetic Patients. In: *Journal of Diabetes and its Complications* 12 (1), p. 24–27. DOI: 10.1016/S1056-8727(97)00006-8.
- Ruebsam, Anne; Dulle, Jennifer E.; Myers, Angela M.; Sakrikar, Dhananjay; Green, Katelyn M.; Khan, Naheed W. et al. (2018): A specific phosphorylation regulates the protective role of  $\alpha$ A-crystallin in diabetes. In: *JCI insight* 3 (4). DOI: 10.1172/jci.insight.97919.
- Sappington, Rebecca M.; Chan, Matilda; Calkins, David J. (2006): Interleukin-6 protects retinal ganglion cells from pressure-induced death. In: *Investigative ophthalmology & visual science* 47 (7), p. 2932–2942. DOI: 10.1167/iovs.05-1407.
- Sataranatarajan, Kavithalakshmi; Ikeno, Yuji; Bokov, Alex; Feliars, Denis; Yalamanchili, Himabindu; Lee, Hak Joo et al. (2016): Rapamycin Increases Mortality in db/db Mice, a Mouse Model of Type 2 Diabetes. In: *The journals of gerontology. Series A, Biological sciences and medical sciences* 71 (7), p. 850–857. DOI: 10.1093/gerona/glv170.
- Schindelin, Johannes; Arganda-Carreras, Ignacio; Frise, Erwin; Kaynig, Verena; Longair, Mark; Pietzsch, Tobias et al. (2012): Fiji: an open-source platform for biological-image analysis. In: *Nature methods* 9 (7), p. 676–682. DOI: 10.1038/nmeth.2019.
- Shen, Weiyong; Fruttiger, Marcus; Zhu, Ling; Chung, Sook H.; Barnett, Nigel L.; Kirk, Joshua K. et al. (2012): Conditional Müllercell ablation causes independent neuronal and vascular pathologies in a novel transgenic model. In: *The Journal of neuroscience: the official journal of the Society for Neuroscience* 32 (45), p. 15715–15727. DOI: 10.1523/JNEUROSCI.2841-12.2012.
- Shin, Eui Seok; Sorenson, Christine M.; Sheibani, Nader (2014): Diabetes and retinal vascular dysfunction. In: *Journal of ophthalmic & vision research* 9 (3), p. 362–373. DOI: 10.4103/2008-322X.143378.
- Suemori, Shinsuke; Shimazawa, Masamitsu; Kawase, Kazuhide; Satoh, Masahiko; Nagase, Hisamitsu; Yamamoto, Tetsuya; Hara, Hideaki (2006): Metallothionein, an endogenous antioxidant, protects against retinal neuron damage in mice. In: *Investigative ophthalmology & visual science* 47 (9), p. 3975–3982. DOI: 10.1167/iovs.06-0275.
- Sulaiman, Rania S.; Kadmiel, Mahita; Cidlowski, John A. (2018): Glucocorticoid receptor signaling in the eye. In: *Steroids* 133, p. 60–66. DOI: 10.1016/j.steroids.2017.11.002.

- Tang, Ling; Zhang, Yunong; Jiang, Yu; Willard, Lloyd; Ortiz, Edlin; Wark, Logan et al. (2011): Dietary wolfberry ameliorates retinal structure abnormalities in db/db mice at the early stage of diabetes. In: *Experimental biology and medicine (Maywood, N.J.)* 236 (9), p. 1051–1063. DOI: 10.1258/ebm.2011.010400.
- Tarr, Joanna M.; Kaul, Kirti; Chopra, Mohit; Kohner, Eva M.; Chibber, Rakesh (2013): Pathophysiology of diabetic retinopathy. In: *ISRN ophthalmology* 2013. DOI: 10.1155/2013/343560.
- Thomas, Paul D.; Campbell, Michael J.; Kejariwal, Anish; Mi, Huaiyu; Karlak, Brian; Daverman, Robin et al. (2003): PANTHER: a library of protein families and subfamilies indexed by function. In: *Genome research* 13 (9), p. 2129–2141. DOI: 10.1101/gr.772403.
- Toops, Kimberly A.; Berlinicke, Cynthia; Zack, Donald J.; Nickells, Robert W. (2012): Hydrocortisone stimulates neurite outgrowth from mouse retinal explants by modulating macroglial activity. In: *Invest. Ophthalmol. Vis. Sci.* 53 (4), p. 2046–2061. DOI: 10.1167/iovs.11-8646.
- Tsai, Wen-Chi; Bhattacharyya, Nisan; Han, Li-Ying; Hanover, John A.; Rechler, Matthew M. (2003): Insulin inhibition of transcription stimulated by the forkhead protein Foxo1 is not solely due to nuclear exclusion. In: *Endocrinology* 144 (12), p. 5615–5622. DOI: 10.1210/en.2003-0481.
- Van Hove, Inge; Groef, Lies de; Boeckx, Bram; Modave, Elodie; Hu, Tjing-Tjing; Beets, Karen et al. (2020): Single-cell transcriptome analysis of the Akimba mouse retina reveals cell-type-specific insights into the pathobiology of diabetic retinopathy. In: *Diabetologia* 63 (10), p. 2235–2248. DOI: 10.1007/s00125-020-05218-0.
- Vandevyver, Sofie; Dejager, Lien; Libert, Claude (2014): Comprehensive overview of the structure and regulation of the glucocorticoid receptor. In: *Endocrine reviews* 35 (4), p. 671–693. DOI: 10.1210/er.2014-1010.
- Veleri, Shobi; Lazar, Csilla H.; Chang, Bo; Sieving, Paul A.; Banin, Eyal; Swaroop, Anand (2015): Biology and therapy of inherited retinal degenerative disease: insights from mouse models. In: *Disease models & mechanisms* 8 (2), p. 109–129. DOI: 10.1242/dmm.017913.
- Vujosevic, Stela; Martini, Ferdinando; Convento, Enrica; Longhin, Evelyn; Kotsafti, Olympia; Parrozzani, Raffaele; Midena, Edoardo (2013): Subthreshold laser therapy for diabetic macular edema: metabolic and safety issues. In: *Current medicinal chemistry* 20 (26), p. 3267–3271. DOI: 10.2174/09298673113209990030.
- Wang, An-Guor; Chen, Chu-Hsuan; Yang, Chu-Wen; Yen, May-Yung; Hsu, Wen-Ming; Liu, Jorn-Hon; Fann, Ming-Ji (2002): Change of gene expression profiles in the retina following optic nerve injury. In: *Brain research. Molecular brain research* 101 (1-2), p. 82–92. DOI: 10.1016/s0169-328x(02)00171-7.
- Wang, Jiang-Hui; Roberts, Georgina Eloise; Liu, Guei-Sheung (2020): Updates on Gene Therapy for Diabetic Retinopathy. In: *Current diabetes reports* 20 (7), p. 22. DOI: 10.1007/s11892-020-01308-w.
- Wang, Juanjuan; Xu, Xueliang; Elliott, Michael H.; Zhu, Meili; Le, Yun-Zheng (2010): Müller cell-derived VEGF is essential for diabetes-induced retinal inflammation and vascular leakage. In: *Diabetes* 59 (9), p. 2297–2305. DOI: 10.2337/db09-1420.
- Wang, Wei; Lo, Amy C. Y. (2018): Diabetic Retinopathy: Pathophysiology and Treatments. In: *International journal of molecular sciences* 19 (6). DOI: 10.3390/ijms19061816.

- Wirostko, Barbara; Wong, Tien Y.; Simó, Rafael (2008): Vascular endothelial growth factor and diabetic complications. In: *Progress in retinal and eye research* 27 (6), p. 608–621. DOI: 10.1016/j.preteyeres.2008.09.002.
- Wong, Tien Y.; Cheung, Chui Ming Gemmy; Larsen, Michael; Sharma, Sanjay; Simó, Rafael (2016): Diabetic retinopathy. In: *Nature reviews. Disease primers* 2. DOI: 10.1038/nrdp.2016.12.
- Wu, Yuxin; Pan, Quan; Yan, Hui; Zhang, Kebin; Guo, Xiaoqin; Xu, Zihui et al. (2018): Novel Mechanism of Foxo1 Phosphorylation in Glucagon Signaling in Control of Glucose Homeostasis. In: *Diabetes* 67 (11), p. 2167–2182. DOI: 10.2337/db18-0674.
- Yang, Zhenglin; Alvarez, Bernardo V.; Chakarova, Christina; Jiang, Li; Karan, Goutam; Frederick, Jeanne M. et al. (2005): Mutant carbonic anhydrase 4 impairs pH regulation and causes retinal photoreceptor degeneration. In: *Human molecular genetics* 14 (2), p. 255–265. DOI: 10.1093/hmg/ddi023.
- Yego, E. Chepchumba K.; Vincent, Jason A.; Sarthy, Vijay; Busik, Julia V.; Mohr, Susanne (2009): Differential regulation of high glucose-induced glyceraldehyde-3-phosphate dehydrogenase nuclear accumulation in Müller cells by IL-1beta and IL-6. In: *Investigative ophthalmology & visual science* 50 (4), p. 1920–1928. DOI: 10.1167/iovs.08-2082.
- Yoshida, S.; Sotozono, C.; Ikeda, T.; Kinoshita, S. (2001): Interleukin-6 (IL-6) production by cytokine-stimulated human Müller cells. In: *Current eye research* 22 (5), p. 341–347. DOI: 10.1076/ceyr.22.5.341.5498.

### 13. *ACKNOWLEDGEMENTS*

First of all, I would like to thank Prof. Dr. Antje Grosche for giving me the chance to be a part of her amazing team. I always had a lot of fun and I am very grateful that I had an excellent scientist with a great personality as my supervisor.

Our common journey started at the Institute of Human Genetics in Regensburg, where I spent the first year of my PhD. The friendly and helpful colleagues helped me a lot and it was always a great pleasure to work with them. Many thanks to Anni, Lina, Christina, Lisa and Dirkje for their active support in all situations.

After our move to the Institute of Physiological Genomics in Munich, many unique and wonderful colleagues joined the team. Many thanks to the entire GroKo: Gabi, Lew, Josef, Nundi, Oli, Kirsten, Farhad, Susanne, Jacqueline, Tobi, Moni and Michelle. It was an honor to work with you guys.

In addition, I would like to thank Prof. Dr. Ernst Tamm (TAC member), Prof. Dr. Astrid Limb (reviewer), Prof. Dr. Diana Pauly (examination committee) and Prof. Dr. Stylianos Michalakis (examination committee) for their support. Special thanks go to Dr. Stefanie Hauck for her support during the PhD thesis in various administrative positions (reviewer, TAC and examination committee), as well as for many other supporting activities (proteomics, internship).

Thanks to GSN and the team for the great support during my PhD and the possibility to be part of their community.

Very big thanks to my parents as well as to my siblings, Sophie and Paul, who always support me and have an open ear.

Many thanks to my friends who supported me in all things and always gave me helpful advices.

Many thanks to Moritz, who supported me in all matters. Thank you for the motivating words and your infinite patience.

**14. PUBLICATION LIST**

- 11/2019                    Ghaseminejad F., Kaplan L., Pfaller A. M., Hauck S. M., & Grosche A.  
The role of Müller cell glucocorticoid signaling in diabetic retinopathy.  
Graefe's archive for clinical and experimental ophthalmology, 258(2),  
221–230.  
Doi: 10.1007/s00417-019-04521-w.
- 01/2021                    Díaz-Lezama N., Wolf A., Koch S., Pfaller A. M., Biber J., Guillonneau  
X., Langmann T., Grosche A.  
PDGF Receptor Alpha Signaling Is Key for Müller Cell Homeostasis  
Functions.  
International journal of molecular sciences vol. 22,3 1174.  
Doi:10.3390/ijms22031174.

## 15. *EIDESSTATTLICHE VERSICHERUNG/ AFFIDAVIT*

Hiermit versichere ich an Eides statt, dass ich die vorliegende Dissertation „Targeting Müller cells in diabetic retinopathy“ selbstständig angefertigt habe, mich außer der angegebenen keiner weiteren Hilfsmittel bedient und alle Erkenntnisse, die aus dem Schrifttum ganz oder annähernd übernommen sind, als solche kenntlich gemacht und nach ihrer Herkunft unter Bezeichnung der Fundstelle einzeln nachgewiesen habe.

I hereby confirm that the dissertation „Targeting Müller cells in diabetic retinopathy“ is the result of my own work and that I have only used sources or materials listed and specified in the dissertation.

München, den 25.02.2021

Anna Pfaller

**16. *DECLARATION OF AUTHORS CONTRIBUTION***

Prof Dr. Antje Grosche designed and supervised the project. Statistical analysis and bioinformatics were performed by Lew Kaplan and Dr. Felix Grassmann. AAV administrations, explant cultivations and the retinal trypsin digest were performed in collaboration with Dr. Nundehui Diaz-Lezama. ERG recordings were performed in cooperation with Prof. Dr. Susanne Koch. Farhad Ghaseminejad assisted with the Western blot and cortisol experiments. Dr. Kirsten Wunderlich did the STED imaging. Dirkje Felder and Gabriela Jäger supported with their daily work as TA including mouse genotyping. The proteome analysis were performed by the Research Unit Protein Science under the direction of Dr. Stefanie Hauck.

Anna Pfaller

Prof. Dr. Antje Grosche